PFC/JA-86-45

COMPTON AND RAMAN FREE ELECTRON LASER STABILITY PROPERTIES FOR A WARM ELECTRON BEAM PROPAGATING THROUGH A HELICAL MAGNETIC WIGGLER

John A. Davies
Clark University, Worcester, MA 01610

Ronald C. Davidson and George L. Johnston
Plasma Fusion Center
Massachusetts Institute of Technology
Cambridge, MA 02139

July, 1986

This work was supported in part by the Office of Naval Research and in part by the National Science Foundation.

Submitted for publication in: Journal of Plasma Physics.

COMPTON AND RAMAN FREE ELECTRON LASER STABILITY PROPERTIES FOR A WARM ELECTRON BEAM PROPAGATING THROUGH A HELICAL MAGNETIC WIGGLER

John A. Davies
Clark University
Worcester, MA 01610

and

Ronald C. Davidson and George L. Johnston
Plasma Fusion Center
Massachusetts Institute of Technology
Cambridge, MA 02139

ABSTRACT

This paper gives an extensive analytical and numerical characterization of the growth rate curves (imaginary frequency versus wavenumber) derived from the free electron laser dispersion relation for a warm relativistic electron beam propagating through a constant-amplitude helical magnetic wiggler field. The electron beam is treated as infinite in transverse extent. A detailed mathematical analysis is given of the exact dispersion relation and its Compton approximation for the case of a waterbag equilibrium distribution function (uniform distribution in axial momentum p_z). Applicability of the waterbag results to the case of a Gaussian equilibrium distribution in p_z is tested numerically. One result of the waterbag analysis is a set of validity conditions for the Compton approximation. Numerical and analytical results indicate that these conditions are applicable to the Gaussian case far outside the parameter range where the individual waterbag and corresponding Gaussian growth rate curves agree.

1. INTRODUCTION AND SUMMARY

Davidson and Uhm (1980, hereafter referred to as I) developed a fully self-consistent, linearized treatment of the free electron laser instability based on the Vlasov-Maxwell equations. Their analysis treats an intense relativistic electron beam, with uniform cross-section, propagating through an idealized helical wiggler magnetic field. The beam is assumed cold in the transverse directions, so that the distribution function (2) is a product of delta funtions of the transverse components of canonical momentum and the longitudinal distribution $G(z,p_z,t)$. Equilibrium self fields are neglected. No further approximations (other than linearization) are made in deriving the dispersion relation (19), which is referred to as the full dispersion relation (FDR). In particular, no higher-order couplings are neglected in the matrix dispersion relation (9). Because of its completeness, the FDR is useful both for identifying important physical mechanisms and for determining the ranges of validity of commonly used approximate disperion relations.

The full Compton dispersion relation (20), referred to as the CDR, is derived in the same manner as the FDR, but with the neglect of longitudinal perturbations. [See Dimos and Davidson (1985) for a quasilinear analysis of the warm-beam CDR.] The comparison of FDR and CDR stability behavior [such as growth rate curves, i.e., curves of $Im(\hat{\omega})$ vs. $\hat{k}$] gives a direct indication of the consequences of neglecting the longitudinal electric field.

In a recent calculation, Davies, Davidson and Johnston (1985, hereafter referred to as II) analyzed properties of the cold-beam FDR and CDR. The purpose of the present analysis is to determine the influence of thermal effects on the stability results in II.

Two equilibrium distribution functions $G_0\,(p_z)$ are employed. The first is the waterbag distribution (35) (which corresponds to a uniform distribution in axial momentum p_z) from which the waterbag FDR (50) and the waterbag CDR (51)are obtained. These dispersion relations can be treated analytically by a simple extension of techniques used in II for the analysis of the cold-beam FDR and CDR. The second equilibrium distribution function employed is a narrow Gaussian distribution in p_z (45). The resulting Gaussian FDR and CDR are obtained by substituting (46), (47), and (28) – (31) into the FDR (19) and the CDR (20). Analytical results obtained using the waterbag dispersion relations are

compared with numerical results obtained using the Gaussian dispersion relations.

The analysis of I is briefly reviewed in §2 in order to introduce equations and definitions used later in this paper. The waterbag and Gaussian dispersion relations are derived in §3. By requiring that the mean value $\langle (p_z - p_0)^2 \rangle$ be the same for the waterbag and the Gaussian distributions, we relate the widths of the waterbag and Gaussian distributions in (49).

A graphical method of analyzing the nature of the roots of the waterbag FDR (similar to that used in II for the cold-beam FDR) is intoduced in §4. This construct serves as a basis for much of the analysis in later sections. Use of this method gives rigorous upper ($\hat{k}_{ub}$) and lower ($\hat{k}_{lb}$) bounds (62) in the FEL growth interval $[Im(\hat{\omega}) > 0]$ corresponding to positive wavenumber $\hat{k}$.

In II, a sufficient condition that the cold-beam FDR be stable for all $\hat{k}$ was derived. The condition holds for beams with sufficiently high density and sufficiently low energy γ_0. In §5, we derive the corresponding stability condition (70) for the waterbag FDR. It is shown that increasing the longitudinal temperature reduces the density required for stability. However, this reduction is small for typical FEL beam temperatures.

The graphical method of analyzing the nature of the roots of the waterbag CDR is introduced in §6. In II it was noted that the CDR upshifted growth rate curve $[Im(\hat{\omega})$ vs. $\hat{k}]$ does not terminate as $\hat{k} \longrightarrow \infty$. Thus, the cold-beam CDR can never be used to approximate the shape of the FDR growth rate curve. We show that the waterbag CDR growth rate curve (at nonzero temperature) terminates beyond some finite value of $\hat{k}$ and determine the upper ($\hat{k}'_{ub}$) and lower ($\hat{k}'_{lb}$) bounds (75) on the growth interval of wavenumber $\hat{k}$. A sufficient condition that the waterbag CDR be stable for all $\hat{k}$ is derived. However, it can be satisfied only for very low-γ_b beams, regardless of the longitudinal temperature. It is shown that the waterbag CDR has at most one branch exhibiting growth for each $\hat{k}$. This section also contains a discussion of the shape of the waterbag CDR downshifted growth rate curve.

In II, it was shown that some cold-beam FDR growth rate curves exhibit a tail extending from the upshifted growth maximum towards larger values of $\hat{k}$. The tail occurs in cold-beam systems for which the Compton approximation is valid at the upshifted growth

maximum. It is produced by the coupling of the positive- and negative-energy longitudinal modes by the wiggler and radiation fields. In §7, we show that the waterbag FDR tails shorten and eventually disappear with increasing temperature. The waterbag CDR may also exhibit a tail region. Here, the tail is produced by the coupling of the Doppler-shifted beam oscillations by the wiggler and radiation fields. A condition (91) for the existence of a CDR tail is derived. As the temperature is reduced, all CDR systems develop tails which approach infinite length as the temperature approaches zero. This fact acounts for the infinite length of the cold-beam CDR upshifted growth rate curves.

In §8, we discuss the Raman approximation [referred to as the longitudinal-transverse (LT) approximation in this paper]. For the waterbag FDR, the coupling in this approximation (95) is between the negative-energy, electrostatic mode and the forward-propagating, left-hand-polarized radiation mode. At sufficiently high temperatures, the LT-approximation (98) applies to the waterbag CDR. The coupling is between the lower-frequency, Doppler-shifted beam oscillation and the forward-propagating, left-hand-circularly polarized radiation mode. Validity criteria (96) and (102) are given for the LT approximation to the waterbag FDR and CDR, respectively.

Using the results of previous sections based on the waterbag distribution in axial momentum p_z, we analyze the validity of the Compton approximation in §9. The Compton approximation is considered valid only if the waterbag CDR upshifted growth rate curve $[Im(\hat{\omega})$ vs $\hat{k}]$ adequately approximates both the maximum value and shape of the waterbag FDR upshifted growth rate curve. Conditions for validity of the Compton approximation are developed. They are based on the three conditions (104), (106) and (109). The Compton approximation is valid if (104) and either one of (106) or (109) are satisfied. Alternatively, it is valid if both (106) and (109) are satisfied.

The principal results of this paper concerning the waterbag dispersion relations are compared in §10 with numerical computations based on the Gaussian dispersion relations. Results of these comparisons indicate that the validity condition for the Compton approximation developed in §9 are also applicable to the Gaussian dispersion relations even in parameter regions where significant discrepancies exist between the individual waterbag and corresponding Gaussian growth rate curves. It is shown analytically that the valid-

ity conditions developed in §9 extend into the resonant, warm-Compton region for the case of a Gaussian equilibrium distribution function in axial momentum p_z. In particular, it is shown that the Compton approximation validity conditions of §9.3, when satisfied sufficiently strongly, imply the condition (119) for validity of the Compton approximation in the resonance region. It is also shown that the validity condition for the resonant warm-Compton regime is included in the conditions developed in §9.

2. THEORETICAL MODEL

In this section we give a brief summary of the Davidson and Uhm stability analysis (I), with emphasis on those equations and results which are used in this work. The relativistic electron beam propagates axially through the ideal helical wiggler field

$$\underset{\sim}{B}_0(z) = -B_0 \cos k_0 z \, \hat{\underset{\sim}{e}}_x - B_0 \sin k_0 z \, \hat{\underset{\sim}{e}}_y, \tag{1}$$

with corresponding vector potential

$$\underset{\sim}{A}_0(z) = \frac{B_0}{k_0} \cos k_0 z \, \hat{\underset{\sim}{e}}_x + \frac{B_0}{k_0} \sin k_0 z \, \hat{\underset{\sim}{e}}_y.$$

Here, $B_0 = \text{const.}$ is the wiggler amplitude, and $\lambda_0 = 2\pi/k_0 = \text{const.}$ is the wiggler wavelength. It is assumed that spatial variations are only in the beam direction ($\partial/\partial x = \partial/\partial y = 0$). The beam is cold in the transverse directions with distribution function given by

$$f(z, \underset{\sim}{p}, t) = n_0 \delta \left(p_x - \frac{eA_x}{c} \right) \delta \left(p_y - \frac{eA_y}{c} \right) G(z, p_z, t). \tag{2}$$

Here, $A_x(z,t)$ and $A_y(z,t)$ are the $x-$ and $y-$ components of the total vector potential. The distribution function $G(z, p_z, t)$ is normalized such that

$$n_0 \int dp_z G(z, p_z, t) = n(z,t),$$

where $n_0 = \text{const.}$ is the average number density, and $n(z,t)$ is the (varying) number density.

The distribution function $G(z, p_z, t)$ satisfies the one-dimensional Vlasov equation

$$\left[\frac{\partial}{\partial t} + v_z \frac{\partial}{\partial z} - \frac{\partial}{\partial z} H(z, p_z, t) \frac{\partial}{\partial p_z} \right] G(z, p_z, t) = 0, \tag{3}$$

where the effective potential $H(z, p_z, t)$ is defined by

$$H(z, p_z, t) = \gamma_T mc^2 - e\delta\phi(z,t).$$

The quantity $\delta\phi$ is the electrostatic potential, and the total particle energy $\gamma_T mc^2$ is defined by

$$\gamma_T mc^2 = \left[m^2c^4 + p_z^2c^2 + \epsilon^2\left(A_x^2 + A_y^2\right)\right]^{1/2}. \tag{4}$$

Maxwell's equations (with the choice of Coulomb gauge) can be expresssed as

$$\left(\frac{1}{c^2}\frac{\partial^2}{\partial t^2} - \frac{\partial^2}{\partial z^2}\right)\delta A_x = -\frac{4\pi n_0 \epsilon^2}{mc^2}\left[A_x\int\frac{dp_z}{\gamma_T}G(z,p_z,t) - A_{0x}\int\frac{dp_z}{\gamma}G_0(p_z)\right], \tag{5}$$

$$\left(\frac{1}{c^2}\frac{\partial^2}{\partial t^2} - \frac{\partial^2}{\partial z^2}\right)\delta A_y = -\frac{4\pi n_0 \epsilon^2}{mc^2}\left[A_y\int\frac{dp_z}{\gamma_T}G(z,p_z,t) - A_{0y}\int\frac{dp_z}{\gamma}G_0(p_z)\right], \tag{6}$$

and

$$\frac{\partial^2\delta\phi}{\partial z^2} = 4\pi e(n - n_0). \tag{7}$$

In the above equations, $\delta A_x \equiv A_x - A_{0x}$, $\delta A_y \equiv A_y - A_{0y}$, $G_0(p_z)$ is the equilibrium distribution function, and γmc^2 is the equilibrium particle energy defined by

$$\gamma mc^2 = \left[m^2c^4 + p_z^2c^2 + \epsilon^2 B_0^2/k_0^2\right]^{1/2}. \tag{8}$$

By linearizing (3) and (5) - (7) for small-amplitude perturbations δA_x, δA_y, $\delta\phi$ and $\delta G = G - G_0$ about the equilibrium state, Davidson and Uhm obtain the following matrix equation relating the field perturbations:

$$\begin{pmatrix} \hat{D}^t\left(\hat{k}+1,\hat{\omega}\right) + \hat{g}\left(\hat{k},\hat{\omega}\right), & \hat{g}\left(\hat{k},\hat{\omega}\right), & -\hat{\omega}_c\hat{\chi}^{(1)}\left(\hat{k},\hat{\omega}\right) \\ \hat{g}\left(\hat{k},\hat{\omega}\right), & \hat{D}^t\left(\hat{k}-1,\hat{\omega}\right) + \hat{g}\left(\hat{k},\hat{\omega}\right), & -\hat{\omega}_c\hat{\chi}^{(1)}\left(\hat{k},\hat{\omega}\right) \\ -\hat{\omega}_c\hat{\chi}^{(1)}\left(\hat{k},\hat{\omega}\right), & -\hat{\omega}_c\hat{\chi}^{(1)}\left(\hat{k},\hat{\omega}\right), & 2\hat{D}^l\left(\hat{k},\hat{\omega}\right) \end{pmatrix} \begin{pmatrix} \delta A^+\left(\hat{k}+1,\hat{\omega}\right) \\ \delta A^-\left(\hat{k}-1,\hat{\omega}\right) \\ \delta\phi\left(\hat{k},\hat{\omega}\right) \end{pmatrix}$$

$$= \begin{pmatrix} 0 \\ 0 \\ 0 \end{pmatrix}, \tag{9}$$

where

$$\hat{g}\left(\hat{k},\hat{\omega}\right) = \frac{1}{2}\hat{\omega}_c^2\left[\alpha_3\hat{\omega}_p^2 + \hat{\chi}^{(2)}\left(\hat{k},\hat{\omega}\right)\right].$$

In (9), we have introduced the complex vector potential amplitudes, δA^+ and δA^-, corresponding to right- and left-circular polarization respectively. These are given by

$$\delta A^{\pm} = \delta A_x \pm i\delta A_y. \tag{10}$$

Other quantities appearing in (9) include the dimensionless wavenumber and frequency,

$$\hat{k} = k/k_0, \tag{11}$$

$$\hat{\omega} = \omega/ck_0, \tag{12}$$

the dimensionless susceptibilities,

$$\hat{\chi}^{(n)}(\hat{k},\hat{\omega}) = \gamma_0^{n+1} mc\hat{\omega}_p^2 \int \frac{dp_z}{\gamma^n} \frac{\hat{k}\partial G_0/\partial p_z}{\hat{\omega} - \hat{k}v_z/c}, \tag{13}$$

the longitudinal and transverse dielectric functions,

$$\hat{D}^l(\hat{k},\hat{\omega}) = \hat{k}^2 + \hat{\chi}^{(0)}(\hat{k},\hat{\omega}), \tag{14}$$

$$\hat{D}^t(\hat{k},\hat{\omega}) = \hat{\omega}^2 - \hat{k}^2 - \alpha_1\hat{\omega}_p^2, \tag{15}$$

and the coefficients

$$\alpha_n = \gamma_0^n \int \frac{dp_z}{\gamma^n} G_0(p_z). \tag{16}$$

Finally, (9) also contains the normalized relativistic cylotron frequency defined by

$$\hat{\omega}_c = \omega_c/ck_0, \tag{17}$$

where

$$\omega_c = \epsilon B_0/\gamma_0 mc,$$

and the normalized relativistic plasma frequency-squared defined by

$$\hat{\omega}_p^2 = \omega_p^2/(ck_0)^2, \tag{18}$$

where

$$\omega_p^2 = 4\pi n_0 e^2/\gamma_0 m.$$

The quantity $\gamma_0 mc^2$ is the average particle energy, which will be defined explicitly later.

We refer to the dispersion relation obtained by setting the determinant in (9) equal to zero as the full dispersion relation (FDR). The FDR is given by

$$\begin{aligned} &\hat{D}^l(\hat{k},\hat{\omega})\hat{D}^t(\hat{k}-1,\hat{\omega})\hat{D}^t(\hat{k}+1,\hat{\omega}) \\ &\quad = \frac{\hat{\omega}_c^2}{2}\left[\hat{D}^t(\hat{k}+1,\hat{\omega}) + \hat{D}^t(\hat{k}-1,\hat{\omega})\right] \\ &\quad \times \left\{\left[\hat{\chi}^{(1)}(\hat{k},\hat{\omega})\right]^2 - \hat{D}^l(\hat{k},\hat{\omega})\left[\alpha_3\hat{\omega}_p^2 + \hat{\chi}^{(2)}(\hat{k},\hat{\omega})\right]\right\}. \end{aligned} \tag{19}$$

If the longitudinal perturbation $\delta\hat{\phi}$ is neglected in the above derivation, the resulting two-by-two matrix equation corresponds to the upper left-hand portion of (9). We refer to the corresponding dispersion relation as the Compton dispersion relation (CDR). The CDR is given by

$$\hat{D}^t(\hat{k}-1,\hat{\omega})\hat{D}^t(\hat{k}+1,\hat{\omega}) = -\frac{\hat{\omega}_c^2}{2}\left[\hat{D}^t(\hat{k}-1,\hat{\omega}) + \hat{D}^t(\hat{k}+1,\hat{\omega})\right]\left[\alpha_3\hat{\omega}_p^2 + \hat{\chi}^{(2)}(\hat{k},\hat{\omega})\right]. \tag{20}$$

3. DISPERSION RELATION FOR NARROW MOMENTUM SPREAD

We assume that $G_0(p_z)$ has a maximum at $p_z = p_0$ and is symmetric about $p_z = p_0$. Let Δ denote the characteristic width of $G_0(p_z)$ in momentum space. We define the quantity γ_0, which appears in (13), (16), (17) and (18) by

$$\gamma_0 mc^2 = \left[m^2c^4 + p_0^2c^2 + e^2B_0^2/k_0^2\right]^{1/2}. \tag{21}$$

That is, $\gamma_0 mc^2$ is the equilibrium electron energy (8) evaluated at $p_z = p_0$. We now assume that $G_0(p_z)$ has a narrow momentum spread with

$$\hat{\Delta} = \frac{\Delta}{\gamma_0 mc} \ll 1. \tag{22}$$

Therefore, γ and v_z, which appear in the integrands of (13) and (16), are expanded to first order in $(p_z - p_0)$. We obtain

$$\frac{1}{\gamma^n} = \frac{1}{\gamma_0^n} - \frac{n}{\gamma_0^n}\beta_b\frac{(p_z - p_0)}{\gamma_0 mc}, \tag{23}$$

and

$$\frac{v_z}{c} = \frac{p_z}{\gamma mc} = \beta_b + \frac{(p_z - p_0)}{\gamma_b^2\gamma_0 mc}. \tag{24}$$

In the above equations, β_b and γ_b are defined by

$$\beta_b = p_0/\gamma_0 mc, \tag{25}$$

and

$$\gamma_b = (1 - \beta_b^2)^{-1/2}. \tag{26}$$

From (17), (21), (25) and (26), a useful relation between γ_0 and γ_b is given by

$$\frac{1}{\gamma_b^2} = \frac{1}{\gamma_0^2} + \hat{\omega}_c^2. \tag{27}$$

Making use of the expansions (23) and (24), and assuming that $G_0(p_z)$ is symmetric about $p_z = p_0$, the following expressions are obtained for the quantities (13) and (16) appearing in the FDR (19) and the CDR (20):

$$\hat{\chi}^{(0)}(\hat{k},\hat{\omega}) = \gamma_0 mc\hat{\omega}_p^2 \frac{\gamma_b^2}{\hat{\Delta}} \int d\xi \frac{\partial G_0/\partial\xi}{\zeta - \xi}, \tag{28}$$

$$\hat{\chi}^{(1)}(\hat{k},\hat{\omega}) = (1 - \beta_b\hat{\Delta}\zeta)\hat{\chi}^{(0)}(\hat{k},\hat{\omega}), \tag{29}$$

$$\hat{\chi}^{(2)}(\hat{k},\hat{\omega}) = (1 - 2\beta_b\hat{\Delta}\zeta)\hat{\chi}^{(0)}(\hat{k},\hat{\omega}), \tag{30}$$

and

$$\alpha_n = 1. \tag{31}$$

In the above equations ζ and ξ are defined by

$$\zeta = \frac{\gamma_b^2(\hat{\omega} - \hat{k}\beta_b)}{\hat{k}\hat{\Delta}}, \tag{32}$$

and

$$\xi = \frac{(p_z - p_0)}{\Delta}. \tag{33}$$

The fractional energy spread $\Delta\gamma/\gamma_0$ is related to the normalized momentum spread $\hat{\Delta} = \Delta/\gamma_0 mc$ by

$$\frac{\Delta\gamma}{\gamma_0} = \beta_b\hat{\Delta}. \tag{34}$$

Two equilibrium distribution functions will be used to study the influence of thermal effects on the stability results in II. To obtain a dispersion relation which is easily analyzed, we choose a "waterbag" equilibrium distribution, which corresponds to a uniform distribution in axial momentum p_z. Results obtained using this distribution function are then compared numerically with those obtained using a Gaussian distribution function with narrow momentum spread.

The waterbag distribution in p_z is defined by

$$G_0(p_z) = \begin{cases} \frac{1}{2\delta}, & |p_z - p_0| \leq \delta \\ 0, & \text{otherwise.} \end{cases} \tag{35}$$

For present purposes, we identify

$$\hat{\delta} = \delta/\gamma_0 mc$$

with $\hat{\Delta}$ in the formulas presented earlier in this section. Substituting (35) into (28) gives

$$\hat{\chi}^{(0)}(\hat{k},\hat{\omega}) = \hat{\omega}_p^2 \frac{\gamma_b^2}{\hat{\delta}^2} \left[1 - \frac{\gamma_b^4(\hat{\omega} - \hat{k}\beta_b)^2}{\hat{\delta}^2\hat{k}^2}\right]^{-1}. \tag{36}$$

Moveover, substituting (28) – (31) and (36) into the FDR (19) yields the dispersion relation

$$\begin{aligned} &\left[(\hat{\omega} - \hat{k}\beta_b)^2 - \frac{\hat{\delta}^2\hat{k}^2}{\gamma_b^4} - \frac{\hat{\omega}_p^2}{\gamma_b^2}\right]\left[\hat{\omega}^2 - (\hat{k}-1)^2 - \hat{\omega}_p^2\right]\left[\hat{\omega}^2 - (\hat{k}+1)^2 - \hat{\omega}_p^2\right] \\ &= -\hat{\omega}_c^2\hat{\omega}_p^2\left[\hat{\omega}^2 - \hat{k}^2 - 1 - \hat{\omega}_p^2\right]\left\{\left[\hat{\omega}^2 - \hat{k}^2\left(1 + \frac{\hat{\delta}^2}{\gamma_b^4}\right) - \hat{\omega}_p^2\right] - \epsilon(\hat{k},\hat{\omega})\right\}, \end{aligned} \tag{37}$$

where

$$\epsilon(\hat{k},\hat{\omega}) = \frac{\beta_b^2\hat{\omega}_p^2\hat{\delta}^2\hat{k}^2}{\gamma_b^4}\left[(\hat{\omega} - \hat{k}\beta_b)^2 - \frac{\hat{\delta}^2\hat{k}^2}{\gamma_b^4}\right]^{-1}. \tag{38}$$

For future reference, we introduce the following frequencies which are solutions to the individual dielectric factors on the left-hand side of (37). These are the positive- ($\hat{\omega}_u$) and negative- ($\hat{\omega}_l$) energy longitudinal frequencies defined by

$$\left.\begin{matrix}\hat{\omega}_u \\ \hat{\omega}_l\end{matrix}\right\} = \hat{k}\beta_b \pm \left(\frac{\hat{\omega}_p^2}{\gamma_b^2} + \frac{\hat{\delta}^2\hat{k}^2}{\gamma_b^4}\right)^{1/2}, \tag{39}$$

and the left- ($\hat{\omega}_-$) and right- ($\hat{\omega}_+$) hand circularly-polarized radiation frequencies defined by

$$\hat{\omega}_{\pm} = \left[(\hat{k} \pm 1)^2 + \hat{\omega}_p^2\right]^{1/2}. \tag{40}$$

For the wiggler field in (1), it is the radiative mode with left-hand polarization which couples with the longitudinal modes to produce growth.

Equation (37) is an eighth-degree polynomial for the complex oscillation frequency $\hat{\omega}$, whereas the cold-beam FDR analyzed in II is a sixth-degree polynomial. We reduce (37) to a sixth-degree polynomial for $\hat{\omega}$ by showing that the term $\epsilon(\hat{k}, \hat{\omega})$ can be neglected. We estimate the ratio of terms on the right-hand side of (37) defined by

$$r(\hat{k}, \hat{\omega}) = \frac{|\epsilon(\hat{k}, \hat{\omega})|}{|\hat{\omega}^2 - \hat{k}^2\left(1 + \frac{\hat{\delta}^2}{\gamma_b^4}\right) - \hat{\omega}_p^2|}. \tag{41}$$

Approximating the numerator in (41) by setting $\hat{\omega} = \hat{\omega}_l$, approximating the denominator by setting $\hat{\omega} = \hat{\omega}_-$ (see I), and neglecting the termin the denominator proportional to $\hat{\delta}^2$, we obtain

$$r(\hat{k}, \hat{\omega}) \simeq \beta_b^2 \left(\frac{\hat{k}}{\gamma_b^2}\right) \frac{\hat{k}}{|2\hat{k} - 1|} \hat{\delta}^2. \tag{42}$$

In both the neighborhoods of the upshifted growth rate maximum where $\hat{k} \simeq 1/(1 - \beta_b)$ and the downshifted growth rate maximum where $\hat{k} \simeq 1/(1 + \beta_b)$, (see I), we find that (42) reduces to

$$r(\hat{k}, \hat{\omega}) \simeq \beta_b^2 \hat{\delta}^2.$$

Typical values of $\hat{\delta}^2$ considered in the present analysis are less than 10^{-2}. Thus, in what follows, we neglect $\epsilon(\hat{k}, \hat{\omega})$ in (37). We also neglect the term $\hat{\delta}^2/\gamma_b^4$ appearing on the right-hand side of (37). Thus, the waterbag FDR (37) is approximated by

$$\left[(\hat{\omega} - \hat{k}\beta_b)^2 - \frac{\hat{\delta}^2\hat{k}^2}{\gamma_b^4} - \frac{\hat{\omega}_p^2}{\gamma_b^2}\right]\left[\hat{\omega}^2 - (\hat{k} - 1)^2 - \hat{\omega}_p^2\right]\left[\hat{\omega}^2 - (\hat{k} + 1)^2 - \hat{\omega}_p^2\right]$$

$$= -\hat{\omega}_c^2\hat{\omega}_p^2\left(\hat{\omega}^2 - \hat{k}^2 - 1 - \hat{\omega}_p^2\right)\left(\hat{\omega}^2 - \hat{k}^2 - \hat{\omega}_p^2\right). \tag{43}$$

The waterbag FDR differs from the cold-beam FDR of II only through the addition of the thermal correction term appearing in the electrostatic dielectric function on the left-hand side of (43).

The derivation of the waterbag CDR from (20) is straightforward because we are not required to neglect any term analogous to $\epsilon(\hat{k},\hat{\omega})$. Again making the approximation $(1+\hat{\delta}^2/\gamma_b^4)\simeq 1$ on the right-hand side, we obtain the waterbag CDR

$$\left[(\hat{\omega}-\hat{k}\beta_b)^2-\frac{\hat{k}^2\hat{\delta}^2}{\gamma_b^4}\right]\left[\hat{\omega}^2-(\hat{k}-1)^2-\hat{\omega}_p^2\right]\left[\hat{\omega}^2-(\hat{k}+1)^2-\hat{\omega}_p^2\right] \tag{44}$$
$$=-\hat{\omega}_c^2\hat{\omega}_p^2\left(\hat{\omega}^2-\hat{k}^2-1-\hat{\omega}_p^2\right)\left(\hat{\omega}^2-\hat{k}^2\right).$$

In §10, we will check numerically to determine the conditions for the conclusions based on the waterbag distribution to remain valid when a Gaussian distribution in p_z is used. For comparison purposes, we choose $G_0(p_z)$ to be a narrow Gaussian of the form

$$G_0(p_z)=\frac{1}{\sqrt{\pi}\Delta}\exp\left[-\frac{(p_z-p_0)^2}{\Delta^2}\right]. \tag{45}$$

Then (28) reduces to

$$\hat{\chi}^{(0)}(\hat{k},\hat{\omega})=\frac{\hat{\omega}_p^2\gamma_b^2}{\hat{\Delta}^2}2\left[1+\zeta Z(\zeta)\right]=-\frac{\hat{\omega}_p^2\gamma_b^2}{\hat{\Delta}^2}Z'(\zeta), \tag{46}$$

where $Z(\zeta)$ is the plasma dispersion function defined by (for $Im\hat{\omega}>0$)

$$Z(\zeta)=\frac{1}{\sqrt{\pi}}\int d\xi\frac{\exp(-\xi^2)}{(\xi-\zeta)}, \tag{47}$$

and $\zeta=\gamma_b^2(\hat{\omega}-\hat{k}\beta_b)/\hat{k}\hat{\Delta}$ [see (32)]. The FDR for a narrow Gaussian is obtained by substituting (46) and (28) – (31) into the FDR (19). The narrow Gaussian CDR is obtained by substituting (46), (28), (30) and (31) into the CDR (20). Since these dispersion relations are used only for purposes of comparing numerical results, they are not presented explicitly here.

Finally, we relate the momentum spread of the waterbag distribution ($\hat{\delta}$) to that of the Gaussian ($\hat{\Delta}$). This relation is defined by requiring that both distribution functions give the same mean value $\langle (p_z - p_0)^2 \rangle$. Using (35) and (45), we obtain

$$\langle (p_z - p_0)^2 \rangle_{\text{waterbag}} = \frac{\delta^2}{3},$$

and

$$\langle (p_z - p_0)^2 \rangle_{\text{Gaussian}} = \frac{\Delta^2}{2}. \tag{48}$$

Comparing the above expressions, we find

$$\hat{\delta}^2 = \frac{3}{2}\hat{\Delta}^2. \tag{49}$$

Therefore, expressed in terms of the effective $\hat{\Delta}$ for a Gaussian, the waterbag FDR (43) becomes

$$\begin{aligned} &\left[(\hat{\omega} - \hat{k}\beta_b)^2 - \frac{3}{2}\frac{\hat{\Delta}^2\hat{k}^2}{\gamma_b^4} - \frac{\hat{\omega}_p^2}{\gamma_b^2}\right]\left[\hat{\omega}^2 - (\hat{k}-1)^2 - \hat{\omega}_p^2\right]\left[\hat{\omega}^2 - (\hat{k}+1)^2 - \hat{\omega}_p^2\right] \\ &\qquad = -\hat{\omega}_c^2\hat{\omega}_p^2\left(\hat{\omega}^2 - \hat{k}^2 - 1 - \hat{\omega}_p^2\right)\left(\hat{\omega}^2 - \hat{k}^2 - \hat{\omega}_p^2\right). \end{aligned} \tag{50}$$

Similarly, the waterbag CDR (44) is given by

$$\begin{aligned} &\left[(\hat{\omega} - \hat{k}\beta_b)^2 - \frac{3}{2}\frac{\hat{\Delta}^2\hat{k}^2}{\gamma_b^4}\right]\left[\hat{\omega} - (\hat{k}-1)^2 - \hat{\omega}_p^2\right]\left[\hat{\omega}^2 - (\hat{k}+1)^2 - \hat{\omega}_p^2\right] \\ &\qquad = -\hat{\omega}_c^2\hat{\omega}_p^2\left(\hat{\omega}^2 - \hat{k}^2 - 1 - \hat{\omega}_p^2\right)\left(\hat{\omega}^2 - \hat{k}^2\right). \end{aligned} \tag{51}$$

We remark that (50) and (51) can also be derived from fluid equations obtained from the zeroth- and p_z-moments of the one-dimensional Vlasov equation (2), together with an

assumed equation of state $Pn^{-3} = \text{const.}$, where P is the longitudinal pressure. With the neglect of terms of order $\hat{\Delta}^2$ in the coupling term, the resulting fluid dispersion relation is the same as the waterbag dispersion relation.

4. INFLUENCE OF THERMAL EFFECTS ON PROPERTIES OF THE FULL DISPERSION RELATION

In II, general properties of the cold-beam FDR were analyzed by means of a graphical construction. A similar construction can be applied to the waterbag FDR in order to study the influence of thermal effects on the stability results in II. We express the waterbag FDR (50) in the form

$$LHS(\hat{k},\hat{\omega}) = RHS(\hat{k},\hat{\omega}) \tag{52}$$

where

$$LHS(\hat{k},\hat{\omega}) = (\hat{\omega} - \hat{k}\beta_b)^2 - \frac{\hat{\omega}_p^2}{\gamma_b^2} - \frac{3}{2}\frac{\hat{\Delta}^2\hat{k}^2}{\gamma_b^4}, \tag{53}$$

and

$$RHS(\hat{k},\hat{\omega}) = -\hat{\omega}_c^2\hat{\omega}_p^2\frac{(\hat{\omega}^2 - \hat{\omega}_2^2)(\hat{\omega}^2 - \hat{\omega}_1^2)}{(\hat{\omega}^2 - \hat{\omega}_+^2)(\hat{\omega}^2 - \hat{\omega}_-^2)}. \tag{54}$$

In the above equations, $\hat{\omega}_+$, $\hat{\omega}_-$, $\hat{\omega}_1$ and $\hat{\omega}_2$ are defined by

$$\hat{\omega}_+ = \left[(\hat{k}+1)^2 + \hat{\omega}_p^2\right]^{1/2}, \tag{55}$$

$$\hat{\omega}_- = \left[(\hat{k}-1)^2 + \hat{\omega}_p^2\right]^{1/2}, \tag{56}$$

$$\hat{\omega}_1 = \left(\hat{k}^2 + \hat{\omega}_p^2\right)^{1/2}, \tag{57}$$

and

$$\hat{\omega}_2 = \left(\hat{k}^2 + 1 + \hat{\omega}_p^2\right)^{1/2}. \tag{58}$$

These frequencies have the following orderings for $\hat{k} > 0$:

$$\hat{\omega}_1 < \hat{\omega}_- < \hat{\omega}_2 < \hat{\omega}_+, \text{ if } 0 < \hat{k} < \frac{1}{2}, \tag{59}$$

5. SUFFICIENT CONDITION FOR STABILITY

In II, we derived a sufficient condition that a cold electron beam be stable for all values of $\hat{k}$. If (66) has no real solutions ($b^2 - 4c < 0$), then $\hat{k}_{ub}$ and $\hat{k}_{lb}$ do not exist and the system is stable. The cold-beam stability criterion can be expressed as

$$\hat{\omega}_p^2 \geq \gamma_0^2 + \frac{1}{16\gamma_0^2} + \frac{1}{16}\frac{\gamma_0^2}{\gamma_b^4} - \frac{1}{2}\left(1 + \frac{\gamma_0^2}{\gamma_b^2} + \frac{1}{4\gamma_b^2}\right) \equiv [\hat{\omega}_p^2]_{\min}. \tag{69}$$

That is, for given values of γ_0 and γ_b, a cold electron beam is stable for all values of $\hat{k}$ provided $\hat{\omega}_p^2 > [\hat{\omega}_p^2]_{\min}$.

The corresponding stability criterion for $\hat{\Delta} > 0$ is obtained from (62) and properties of the cubic equation. The waterbag FDR (50) exhibits no FEL instability if

$$\frac{B^2}{4} + \frac{A^3}{27} > 0, \tag{70}$$

where A and B are defined by

$$A = \frac{1}{3}\left(3q - p^2\right),$$

and

$$B = \frac{1}{27}\left(2p^3 - 9pq + 27r\right).$$

The quantities p, q and r are defined in (63) - (65).

In terms of the graphical construct of the previous section, stability for all values of $\hat{k}$ occurs when the LHS parabola in figure 1b fails to become detached from the RHS (in the interval $0 < \hat{\omega} < \hat{\omega}_-$), as the parabola shifts first to the right and then to the left with increasing $\hat{k}$. The sufficiency condition (70) is satisfied if the minimum of the parabola fails to intersect the LHS for all values of $\hat{k}$. The only effect of increasing $\hat{\Delta}$ in the graphs in figure 1b is to shift the LHS parabola downward. The RHS curve is temperature independent. Thus, increasing the temperature reduces the value of $\hat{\omega}_p^2$ actually required for stability. Furthermore, it reduces the minimum value of $\hat{\omega}_p^2$ defined in (70) which is sufficient for stability.

For given values of γ_0, γ_b and $\hat{\Delta}$, the corresponding value of $[\hat{\omega}_p^2]_{\min}$ is readily obtained numerically from (70). In agreement with the discussion in the previous paragraph, the value of $[\hat{\omega}_p^2]_{\min}$ decreases with increasing $\hat{\Delta}$. Nevertheless, for typical FEL beam temperatures, there is little difference between the density limits imposed by (69) and (70). Figure 5 shows contours of $[\hat{\omega}_p^2]_{\min}$ in a plot of γ_0 vs γ_b for a cold beam, and for (very large) beam temperature corresponding to $\hat{\Delta} = 0.10$. (A beam with given $\hat{\omega}_p^2$ will be stable for all values of γ_0 and γ_b below the corresponding contour in figure 5.) We note that even for high beam temperatures (and moderate densities), the stability condition (70) applies only to systems with relatively low energies.

The approach to stability predicted by the waterbag FDR (50), with increasing $\hat{\omega}_p^2$, is illustrated in figure 6 for the choice of system parameters $\gamma_0 = 1.3$ and $\gamma_b = 1.1$. Two cases corresponding to $\hat{\Delta} = 0$ and $\hat{\Delta} = 0.04$ are shown. The respective values of $[\hat{\omega}_p^2]_{\min}$ are 0.498 and 0.494. A detailed numerical analysis of the dispersion relation (50) shows that FEL instability ceases at $\hat{\omega}_p^2 = 0.37$ for $\hat{\Delta} = 0$, and at $\hat{\omega}_p^2 = 0.365$ for $\hat{\Delta} = 0.04$.

6. INFLUENCE OF THERMAL EFFECTS ON PROPERTIES OF THE COMPTON DISPERSION RELATION

We use a graphical construction analogous to that for the FDR (§4) to analyze the influence of thermal effects on FEL stability behavior for the CDR (51). In this regard, we express the waterbag CDR in the form

$$\mathrm{LHS}'(\hat{k},\hat{\omega}) = \mathrm{RHS}'(\hat{k},\hat{\omega}), \tag{71}$$

where

$$\mathrm{LHS}'(\hat{k},\hat{\omega}) = \left(\hat{\omega} - \hat{k}\beta_b\right)^2 - \frac{3}{2}\frac{\hat{\Delta}^2\hat{k}^2}{\gamma_b^4}, \tag{72}$$

and

$$\mathrm{RHS}'(\hat{k},\hat{\omega}) = -\hat{\omega}_c^2\hat{\omega}_p^2\frac{\left(\hat{\omega}^2-\hat{\omega}_2^2\right)\left(\hat{\omega}^2-\hat{k}^2\right)}{\left(\hat{\omega}^2-\hat{\omega}_+^2\right)\left(\hat{\omega}^2-\hat{\omega}_-^2\right)}. \tag{73}$$

The frequencies in the above equations are defined by equation (55), $\hat{\omega}_+ = \left[\left(\hat{k}+1\right)^2+\hat{\omega}_p^2\right]^{1/2}$, equation (56), $\hat{\omega}_- = \left[\left(\hat{k}-1\right)^2+\hat{\omega}_p^2\right]^{1/2}$, and equation (58), $\hat{\omega}_2 = \left(\hat{k}^2+1+\hat{\omega}_p^2\right)^{1/2}$. Note that these frequencies satisfy the orderings

$$\hat{k} < \hat{\omega}_- < \hat{\omega}_2 < \hat{\omega}_+, \text{ for } 0 < \hat{k} < \left(1+\hat{\omega}_p^2\right)/2,$$

and

$$\hat{\omega}_- < \hat{k} < \hat{\omega}_2 < \hat{\omega}_+, \text{ for } \hat{k} > \left(1+\hat{\omega}_p^2\right)/2.$$

Schematic plots of $\mathrm{RHS}'(\hat{k},\hat{\omega})$ and $\mathrm{LHS}'(\hat{k},\hat{\omega})$ vs $\hat{\omega}$ for the above orderings are illustrated in figures 7a and 7b, respectively. The intersections of the LHS′ parabola with the $\hat{\omega}$-axis are the Doppler-shifted beam oscillation frequencies defined by

$$\left.\begin{matrix}\hat{\omega}_u' \\ \hat{\omega}_l'\end{matrix}\right\} = \hat{k}\beta_b \pm \hat{k}\left(\frac{3\hat{\Delta}^2}{2\gamma_b^4}\right)^{1/2}. \tag{74}$$

The general scheme given in §4 (of growth intervals appearing as the LHS moves to the right relative to the RHS and then back to the left) holds for the CDR (71) when $\hat{\Delta} > 0$. In particular, if the situation analogous to that depicted in figure 3 does not occur, then there will be just one growth rate curve as shown in figure 2a. Otherwise separated downshifted and upshifted growth rate curves will be present as shown in figure 2b. It is easily demonstrated for small $\hat{\Delta}$ that the waterbag CDR has at most one pair of complex conjugate roots $\hat{\omega}(\hat{k})$ for each $\hat{k}$. Referring to figures 7a and 7b, we note that at least four of the six roots $\hat{\omega}(\hat{k})$ must be real if $\hat{\omega}'_u \leq \hat{k}$ for all $\hat{k}$. From (74), we find that this condition is satisfied provided $\hat{\Delta} \leq (2/3)^{1/2}(1+\beta_b)^{-1} \gtrsim 0.41$, an inequality which is readily satisfied in practical FEL applications.

In II, we discussed the fact that the cold-beam CDR upshifted growth rate curve never adequately approximates the shape of the cold-beam FDR upshifted growth curve. That is, if $\hat{\Delta} = 0$, then the minimum of the LHS$'$ parabola (71) for the CDR always lies on the $\hat{\omega}$-axis in figures 7a and 7b. Thus, it cannot link with the RHS$'$ curve in the interval $0 < \hat{\omega} < \hat{\omega}_-$ to terminate the instability at large $\hat{k}$. In fact, it was shown in II that $Im(\hat{\omega}) \longrightarrow \hat{\omega}_c\hat{\omega}_p$ as $\hat{k} \longrightarrow \infty$ for the cold-beam CDR.

For $\hat{\Delta} > 0$, the CDR behavior is qualitatively different, because the minimum of the LHS$'$ parabola moves downward in figure 7b with increasing $\hat{k}$. In this case, there exists some value of $\hat{k}$ above which instability ceases. In particular, if $\hat{k}$ is sufficiently large, then the minimum of the LHS$'$ parabola (72) lies in the interval $0 < \hat{\omega} < \hat{\omega}_-$ of figure 7b. From (73), it follows that

$$\lim_{\hat{k}\to\infty} \mathrm{RHS}'\left(\hat{k}, \hat{\omega} = \hat{k}\beta_b\right) = \hat{\omega}_c^2\hat{\omega}_p^2,$$

whereas from (72) we obtain

$$\lim_{\hat{k}\to\infty} \mathrm{LHS}'\left(\hat{k}, \hat{\omega} = \hat{k}\beta_b\right) = -\infty \text{ for } \hat{\Delta} > 0.$$

Nevertheless, the width of the Compton upshifted growth rate curve may greatly exceed the width of the FDR growth rate curve for some system parameters with $\hat{\Delta} > 0$, even

when there is good agreement between the values of the maximum growth rates. We discuss this property in §9.

Upper and lower bounds on the waterbag CDR growth interval in $\hat{k}$-space are determined by setting $\hat{\omega} = \hat{k}\beta_b$ in the CDR (51) and solving for $\hat{k}$. (See the corresponding discussion for the FDR in §4.) One solution is $\hat{k} = 0$. This root merely shows that when $\hat{k} = 0$ the LHS′ and RHS′ are tangent at $\hat{\omega} = 0$ in figure 7a. The remaining solutions, which correspond to the bounds, are given by

$$\left.\begin{matrix} \hat{k}'^2_{ub} \\ \hat{k}'^2_{lb} \end{matrix}\right\} = \frac{1}{2a}\left[-b \pm \left(b^2 - 4ac\right)^{1/2}\right], \tag{75}$$

where a, b and c are defined by

$$a = \frac{3\hat{\Delta}^2}{2\gamma_b^6},$$

$$b = -\frac{3\hat{\Delta}^2}{\gamma_b^2}\left[2 - \frac{(1+\hat{\omega}_p^2)}{\gamma_b^2}\right] - \frac{\hat{\omega}_c^2\hat{\omega}_p^2}{\gamma_b^2},$$

$$c = \frac{3\hat{\Delta}^2}{2\gamma_b^2}\left[1+\hat{\omega}_p^2\right]^2 - \hat{\omega}_c^2\hat{\omega}_p^2\left(1+\hat{\omega}_p^2\right),$$

and

$$b^2 - 4ac = -16\left(\frac{3\hat{\Delta}^2}{2\gamma_b^2}\right)^2\frac{(1+\hat{\omega}_p^2)}{\gamma_b^2} + \left[4\left(\frac{3\hat{\Delta}^2}{2\gamma_b^2}\right) + \frac{\hat{\omega}_c^2\hat{\omega}_p^2}{\gamma_b^2}\right]^2. \tag{76}$$

Solutions with real $\hat{k}'_{lb} > 0$ do not exist unless $c > 0$, i.e.,

$$\frac{3\hat{\Delta}^2}{2\gamma_b^2} > \frac{\hat{\omega}_c^2\hat{\omega}_p^2}{(1+\hat{\omega}_p^2)}. \tag{77}$$

A sufficient condition that the waterbag CDR (51) gives stable solutions for all values of $\hat{k}$ is $b^2 - 4ac < 0$. Using (76), we express this sufficiency criterion as two conditions

$$1 + \hat{\omega}_p^2 > \gamma_b^2, \tag{78}$$

and

$$\frac{3\hat{\Delta}^2}{2\gamma_b^2} > \frac{\hat{\omega}_c^2\hat{\omega}_p^2}{4\left[\gamma_b\left(1+\hat{\omega}_p^2\right)^{1/2}-\gamma_b^2\right]}.$$

For moderate beam density with $\hat{\omega}_p^2 \lesssim 1$, the sufficiency condition is satisfied only for systems of small γ_b, regardless of the value of $\hat{\Delta}$.

In II, we showed in the case of a cold beam that the shape of the CDR downshifted growth rate curve differs qualitatively from that of the FDR even when there is good agreement between the maximum growth rates. It is evident from figure 7a and (72) that, for $\hat{\Delta} = 0$, the CDR downshifted growth region begins at $\hat{k} = 0$. In contrast, the left edge of the FDR downshifted growth curve lies above $\hat{k} = 1/2$. (This type of behavior is illustrated schematically in figure 2b.) We now investigate the influence of thermal effects on this small-$\hat{k}$ behavior using the waterbag CDR. We first consider figure 7a. When $\hat{k} = 0$, the LHS′ parabola and the RHS′ curve are tangent at the origin. For sufficiently small $\hat{\Delta}$, the LHS′ will not move downward and to the right rapidly enough (with increasing $\hat{k}$) to link immediately with the RHS′ curve near the origin. Then the CDR downshifted growth rate curve begins at $\hat{k} = 0$ as in the cold-beam case. Solving the waterbag CDR (51) for $\hat{\omega} \simeq 0$ as a function of $\hat{k} \simeq 0$, we obtain the first-order result

$$\begin{aligned}\hat{\omega} = {} & \frac{\hat{k}\beta_b\left(1+\hat{\omega}_p^2\right)}{\left[\left(1+\hat{\omega}_p^2\right)-\hat{\omega}_c^2\hat{\omega}_p^2\right]} \\ & \pm i\frac{\hat{k}}{\left[\left(1+\hat{\omega}_p^2\right)-\hat{\omega}_c^2\hat{\omega}_p^2\right]}\left\{\hat{\omega}_c^2\hat{\omega}_p^2\left[\frac{1}{\gamma_b^2}+\frac{\hat{\omega}_p^2}{\gamma_0^2}\right]\right. \\ & \left.-\frac{3}{2}\frac{\hat{\Delta}^2}{\gamma_b^2}\left[\left(1+\hat{\omega}_p^2\right)-\hat{\omega}_c^2\hat{\omega}_p^2\right]\left[\frac{1}{\gamma_b^2}+\frac{\hat{\omega}_p^2}{\gamma_b^2}\right]\right\}^{1/2}.\end{aligned} \tag{79}$$

Therefore, a sufficient condition that the waterbag CDR downshifted growth region begins at $\hat{k} = 0$ is given by

$$\frac{3\hat{\Delta}^2}{2\gamma_b^2} < \frac{\hat{\omega}_c^2\hat{\omega}_p^2}{\left[\left(1+\hat{\omega}_p^2\right)-\hat{\omega}_c^2\hat{\omega}_p^2\right]}\left[\frac{1}{\gamma_b^2}+\frac{\hat{\omega}_p^2}{\gamma_0^2}\right]\left[\frac{1}{\gamma_b^2}+\frac{\hat{\omega}_p^2}{\gamma_b^2}\right]^{-1}. \tag{80}$$

However, the above is not a necessary condition because second-order imaginary terms may have been neglected in the derivation of (79).

A sufficient condition for stability in the immediate neighborhood of $\hat{k} = 0$ is the existence of $\hat{k}'_{lb} > 0$ [see (75)]. Therefore, (77) is a sufficient condition that the downshifted growth does not begin at $\hat{k} = 0$. In figure 8, we illustrate this behavior of the waterbag CDR downshifted growth rate curve for a system with parameters $\gamma_0 = 10$, $\hat{\omega}_c = 0.05$ and $\hat{\omega}_p^2 = 0.01$. In this example, the sufficient condition (77) for stability in the immediate neighborhood of $\hat{k} = 0$ is satisfied by $\hat{\Delta} > 0.037$.

7. COUPLED LONGITUDINAL OSCILLATIONS

In II, we discussed the existence of tails in $\hat{k}$-space, which occur in some cold-beam FDR growth rate curves, extending from the upshifted growth maximum to larger values of $\hat{k}$. It was shown that the instability in the tail region is due to a coupling of the negative- and positive-energy, longitudinal modes by the radiation and wiggler fields. A combination of numerical and analytical results showed that the cold-beam systems possessing an FDR tail region are those systems whose FDR and CDR upshifted growth rate curves agree closely in the region of maximum growth. [See §9 of II.] The condition for close agreement between cold-beam FDR and CDR stability properties at maximum growth is given by

$$\frac{4\beta_b\left(1-\beta_b\right)\hat{\omega}_p}{\gamma_b\hat{\omega}_c^2} \ll 1. \tag{81}$$

[See equation (62) of II with $\hat{k} = 1/(1-\beta_b)$.] For the cold-beam FDR, such tails were shown to occur when the LHS parabola (see figure 1b), shifting to the left, relinks with the RHS (in the interval $0 < \hat{\omega} < \hat{\omega}_-$) at a point where their common slope is very small. Then, $\hat{\omega} \simeq \hat{k}\beta_b$ in some $\hat{k}$-interval in the right-most region of the upshifted growth rate curve, and both $|\hat{\omega}-\hat{\omega}_l|$ and $|\hat{\omega}-\hat{\omega}_u|$ may be simultaneously small. [See (61) with $\hat{\Delta}=0$.] If in addition $|\hat{\omega}-\hat{\omega}_u| \ll |\hat{\omega}-\hat{\omega}_-|$, then the interval is a tail region. In II, we refer to the approximation to the FDR, valid in the tail region, as the longitudinal-longitudinal (LL) approximation.

In order to investigate the influence of thermal effects on stability properties in the tail region, we derive the longitudinal-longitudinal approximation to the waterbag FDR. Assuming that $|\hat{\omega}-\hat{\omega}_u| \gg |\hat{\omega}-\hat{\omega}_-|$ and that $\hat{\omega} \simeq \hat{k}\beta_b$, we approximate the waterbag FDR (50) by

$$\left(\hat{\omega}-\hat{\omega}_l\right)\left(\hat{\omega}-\hat{\omega}_u\right) = \mathrm{RHS}\left(\hat{k}, \hat{\omega}=\hat{k}\beta_b\right), \tag{82}$$

where $\mathrm{RHS}\left(\hat{k},\hat{\omega}\right)$ is defined in (54), and $\hat{\omega}_l$ and $\hat{\omega}_u$ are defined in (61). Solving (82) for the unstable root, we obtain the approximate result

$$\hat{\omega} = \hat{k}\beta_b + i\left\{\hat{\omega}_c^2\hat{\omega}_p^2\frac{\left[\hat{\omega}_2^2 - \hat{k}^2\beta_b^2\right]\left[\hat{\omega}_1^2 - \hat{k}^2\beta_b^2\right]}{\left[\hat{\omega}_+^2 - \hat{k}^2\beta_b^2\right]\left[\hat{\omega}_-^2 - \hat{k}^2\beta_b^2\right]} - \frac{1}{\gamma_b^2}\left[\hat{\omega}_p^2 + \frac{3\hat{\Delta}^2}{2\gamma_b^2}\hat{k}^2\right]\right\}^{1/2}, \qquad (83)$$

where $\hat{\omega}_+$, $\hat{\omega}_-$, and $\hat{\omega}_2$ are defined in (55) - (58). With decreasing $\hat{k}$, the instability in (83) begins at $\hat{k} = \hat{k}_{ub}$ [equation (62)]. The growth rate approaches infinity as the value of $\hat{k}$ satisfying $\hat{k}\beta_b = \hat{\omega}_-$ is approached from above. Below this value of $\hat{k}$ and in the interval of the upshifted growth rate curve, the growth rate in (83) is zero.

For the sake of definiteness, we define the tail region of a waterbag FDR growth rate curve as that portion of the curve which is approximated closely by (83). If no part of the curve is approximated closely by (83), then no tail region exists.

Because an increase in beam temperature shifts the LHS parabola downward in figure 1b, we expect that increasing the beam temperature will shorten and finally eliminate the tail region. In figures 9 and 10, are shown typical growth rate curves calculated from the waterbag FDR (50) for a system with parameters $\gamma_0 = 7.6$, $\hat{\omega}_c = 0.363$ and $\hat{\omega}_p^2 = 0.0157$. Henceforth we refer to this case as System C, since its FDR and CDR upshifted growth maxima agree closely when $\hat{\Delta} = 0$. [The values of γ_0 and $\hat{\omega}_c$ in figures 9 and 10 correspond to parameters cited by Orzechowski, et al., (1985). The value of $\hat{\omega}_p^2$ corresponds to a beam current of 1000A instead of the 500A cited by these authors.] LL-FDR growth rate curves are shown in figure 9 for $\hat{\Delta} = 0.005$ and 0.02 (dashed curves), and in figure 10 for $\hat{\Delta} = 0.04$. With increasing $\hat{\Delta}$, the length of the tail region (and the range of validity of the LL-FDR) decrease. For $\hat{\Delta} = 0.04$ (figure 10), there is no tail region because the LL approximation is not valid. Graphs of the frequency mismatches including $|\hat{\omega} - \hat{k}\beta_b|$, $|\hat{\omega} - \hat{\omega}_-|$, $|\hat{\omega} - \hat{\omega}_l|$ and $|\hat{\omega} - \hat{\omega}_u|$ are shown in figures 11 and 12 for $\hat{\Delta} = 0.005$ and $\hat{\Delta} = 0.04$, respectively. At the lower value, $\hat{\Delta} = 0.005$, the relations $|\hat{\omega} - \hat{k}\beta_b| \ll |\hat{\omega} - \hat{\omega}_l| \simeq |\hat{\omega} - \hat{\omega}_u| \ll |\hat{\omega} - \hat{\omega}_-|$, which are characteristic of a tail region, hold over much of the upshifted growth interval. At the higher value, $\hat{\Delta} = 0.04$, these relations are not valid anywhere in the growth interval.

The growth rate curves for the CDR (51) may also exhibit tail regions. In this case the tail is produced by a coupling of the Doppler-shifted beam oscillations by the radiative and wiggler fields. The graphical explanation based on figure 7b is similar to that for the

FDR tail region. The corresponding longitudinal-longitudinal approximation for the CDR (LL-CDR) for the waterbag distribution is obtained from the approximation

$$(\hat{\omega} - \hat{\omega}_l')(\hat{\omega} - \hat{\omega}_u') = \mathrm{RHS}'\left(\hat{k}, \hat{\omega} = \hat{k}\beta_b\right)$$

where $\mathrm{RHS}'\left(\hat{k}, \hat{\omega}\right)$ is defined in (73), and $\hat{\omega}_l'$ and $\hat{\omega}_u'$ are defined in (74). Solving the above equation for $\hat{\omega}$, we obtain

$$\hat{\omega} = \hat{k}\beta_b + i\left[\hat{\omega}_c^2\hat{\omega}_p^2 \frac{\left(\hat{\omega}_2^2 - \hat{k}^2\beta_b^2\right)\left(\hat{k}^2 - \hat{k}^2\beta_b^2\right)}{\left(\hat{\omega}_+^2 - \hat{k}^2\beta_b^2\right)\left(\hat{\omega}_-^2 - \hat{k}^2\beta_b^2\right)} - \frac{3\hat{\Delta}^2\hat{k}^2}{2\gamma_b^4}\right]^{1/2}, \tag{84}$$

for the unstable branch. With decreasing $\hat{k}$, the instability in (84) begins at $\hat{k} = \hat{k}_{ub}$ [equation (75)]. The growth rate approaches infinity as the value of $\hat{k}$ satisfying $\hat{\omega}_- = \hat{k}\beta_b$ is approached from above. Below this value of $\hat{k}$ and in the upshifted growth interval, the growth rate in (84) is zero. We define the tail region of a waterbag CDR growth rate curve as that portion of the curve which is approximated closely by (84).

All growth rate curves obtained from the cold-beam CDR possess a tail which does not vanish as $\hat{k} \to \infty$. Substituting $\hat{\Delta} = 0$ into (84) yields $Im(\hat{\omega}) \to \hat{\omega}_c\hat{\omega}_p$ as $\hat{k} \to \infty$. As a result, the cold-beam CDR never provides an adequate approximation of the shape of the upshifted growth rate curve for the cold-beam FDR.

In figures 13 and 14, we show the growth rate curves calculated from the waterbag CDR (51) for System C ($\gamma_0 = 7.6$, $\hat{\omega}_c = 0.363$, $\hat{\omega}_p^2 = 0.0157$). Comparing figures 9 and 13, we note that these lower temperature CDR tails (although finite in length) are much longer than those obtained from the FDR (50). From figure 14, it is clear that no CDR tail region is present when $\hat{\Delta} = 0.04$. At this temperature, the shape of the CDR growth rate curve is a good approximation to the shape of the FDR growth curve. (Compare figures 10 and 14.)

We now derive a condition for the existence of a waterbag CDR tail region, assuming that $\gamma_b^2 \gg 1$. The first requirement for a waterbag CDR tail region is the existance of an interval of $\hat{k}$ where the frequency mismatches of the modes that are coupled, $|\hat{\omega} - \hat{\omega}_u'|$ and $|\hat{\omega} - \hat{\omega}_l'|$, are simultaneously small. From (74), we recall that $\hat{\omega}_l' = \hat{k}\beta_b - \left(3\hat{\Delta}^2/2\gamma_b^2\right)^{1/2}\hat{k}/\gamma_b$

and $\hat{\omega}'_u = \hat{k}\beta_b + \left(3\hat{\Delta}^2/2\gamma_b^2\right)^{1/2}\hat{k}/\gamma_b$. Thus the requirement of small frequency mismatch is satisfied provided

$$|\hat{\omega} - \hat{k}\beta_b| \ll \frac{\hat{k}}{\gamma_b}\left(\frac{3\hat{\Delta}^2}{2\gamma_b^2}\right)^{1/2} \tag{85}$$

at the right edge of the upshifted growth rate curve. The inequality in (85) is satisfied if the common slope of the LHS′ parabola (72) and the RHS′ curve (73) is very small at the point where they relink in the interval $0 < \hat{\omega} < \hat{\omega}_-$ shown in figure 7b. Since the magnitude of the slope of the parabola (at relinking) is $2|\hat{\omega} - \hat{k}\beta_b|$, the condition in (85) can be expressed as

$$\left|\frac{\partial \mathrm{RHS}'\left(\hat{k}'_{ub}, \hat{\omega}\right)}{\partial \hat{\omega}}\right|_{\hat{\omega}=\hat{k}'_{ub}\beta_b} \ll \frac{2\hat{k}'_{ub}}{\gamma_b}\left(\frac{3\hat{\Delta}^2}{2\gamma_b^2}\right)^{1/2}, \tag{86}$$

where we have approximated the upper boundary of the growth curve by the upper bound on the growth interval $\hat{k}'_{ub}$ [equation (75)]. Differentiating (73) and assuming $\hat{k}'_{ub} > \gamma_b^2 \gg 1$ (because $2\gamma_b^2 \simeq \hat{k}$ at the maximum), we reduce the inequality in (86) to

$$16\hat{\omega}_c^2\hat{\omega}_p^2\left[\frac{\hat{k}'^2_{ub}}{\gamma_b^4} - 4\right]^{-1} \ll \left(\frac{3\hat{\Delta}^2}{2}\right)^{1/2}. \tag{87}$$

Making use of (76) and assuming that $\hat{k}'_{ub} > \gamma_b^2 \gg 1$, $\hat{\Delta}^2 \ll 1$, and $\hat{\omega}_p^2 \lesssim 1$, we approximate (75) by

$$\hat{k}'^2_{ub} = 4\gamma_b^4\left[1 + \frac{\hat{\omega}_c^2\hat{\omega}_p^2}{6\hat{\Delta}^2}\right]. \tag{88}$$

Substituting (88) into (87) yields the first validity condition for the existence of a waterbag CDR tail region, i.e.,

$$\left(3\hat{\Delta}^2\right)^{3/2} \ll \frac{\hat{\omega}_c^2\hat{\omega}_p^2}{4\sqrt{2}}. \tag{89}$$

The second requirement for existence of a tail region is that

$$|\hat{\omega} - \hat{\omega}'_u| \ll |\hat{\omega} - \hat{\omega}_-|. \tag{90}$$

Making the same approximations as those used to derive (89) [including (88)], we reduce (90) to the condition

$$\left(6\hat{\Delta}^2\right)^{1/2} \ll 1 - \left[1 + \frac{\hat{\omega}_c^2\hat{\omega}_p^2}{6\hat{\Delta}^2}\right]^{-1/2}. \tag{91}$$

It is easily shown that (91) is the stronger condition for the existence of a tail region. If $\hat{\omega}_c^2\hat{\omega}_p^2/6\hat{\Delta}^2 \ll 1$, then (91) reduces to (89).

As a numerical example, we again consider System C ($\gamma_0 = 7.6,$, $\hat{\omega}_c = 0.363$, $\hat{\omega}_p^2 = 0.0157$). Reference to figure 14 shows that no CDR tail region is present when $\hat{\Delta} = 0.04$. Substituting these parameters into (91) yields the incorrect result $9.80 \times 10^{-2} \ll 9.30 \times 10^{-2}$. Reference to figure 13 shows that a tail region is present when $\hat{\Delta}$ is reduced to the value of 0.01. In this case, condition (91) is satisfied with $2.45 \times 10^{-2} \ll 5.26 \times 10^{-1}$.

We have not derived a condition for the existence of an FDR tail region. However, from an examination of numerical examples, we find that the condition (91) together with condition (81) for the existence of a cold-beam FDR tail region are useful for predicting the existence of FDR tail regions.

Finally, we note that both the FDR and CDR downshifted growth rate curves may possess a tail region (due to coupled longitudinal oscillations), extending from the downshifted maximum towards lower values of $\hat{k}$. Equation (83) for the FDR, and (84) for the CDR are also applicable to these downshifted tails. The waterbag FDR tail must terminate above $\hat{k} = 1/2$. On the other hand, it is the CDR downshifted tail which causes the left edge of the CDR downshifted growth rate curve to be located at $\hat{k} = 0$ for lower temperatures. [See figure 8 and the discussion at the end of §6.] Equation (84) can be used to estimate the values of $\hat{\Delta}$ required to shift the left edge of the CDR downshifted tail above $\hat{k} = 0$, and the result is the same as (77).

8. THE RAMAN APPROXIMATION

If $|\hat{\omega} - \hat{\omega}_l| \simeq |\hat{\omega} - \hat{\omega}_-| \ll |\hat{\omega} - \hat{\omega}_u|$ in an interval of the FDR growth rate curve, then the coupling producing growth in the interval is between the left-hand-circularly polarized radiative mode and the negative energy longitudinal mode. We refer to this approximation as the longitudinal-transverse approximation to the FDR (LT-FDR). This approximation is also referred to as the Raman approximation. The waterbag LT-FDR is obtained by approximating the waterbag FDR (50) by

$$(\hat{\omega} - \hat{\omega}_l)(\hat{\omega} - \hat{\omega}_-) = -\frac{R\left(\hat{k}, \hat{\omega} = \hat{\omega}_-\right)}{2L},$$

where

$$L = \left(\frac{\hat{\omega}_p^2}{\gamma_b^2} + \frac{3\hat{k}^2\hat{\Delta}^2}{2\gamma_b^4}\right)^{1/2}, \tag{92}$$

$$R\left(\hat{k}, \hat{\omega} = \hat{\omega}_-\right) = \frac{\hat{\omega}_c^2\hat{\omega}_p^2}{4\hat{\omega}_-}\left(2\hat{k} - 1\right), \tag{93}$$

From (92) and (61),

$$\left.\begin{matrix}\hat{\omega}_l \\ \hat{\omega}_u\end{matrix}\right\} = \hat{k}\beta_b \mp L,$$

and from (56), $\hat{\omega}_- = \left[\left(\hat{k} - 1\right)^2 + \hat{\omega}_p^2\right]^{1/2}$. In the above, we have assumed that

$$\hat{\omega} \simeq \hat{\omega}_l \simeq \hat{\omega}_-,$$

and

$$\hat{\omega} - \hat{\omega}_u \simeq \hat{\omega}_l - \hat{\omega}_u = -2L. \tag{94}$$

Solving for the unstable mode, we obtain

$$\hat{\omega} = \hat{\omega}_l + \frac{1}{2}\left[(\hat{\omega}_l - \hat{\omega}_-)^2 - \frac{2R}{L}\right]^{1/2}. \tag{95}$$

[Kwan, Dawson and Lin (1977) used a procedure similar to the above in order to obtain the Raman approximation to the warm-fluid FEL dispersion relation.]

A condition for the validity of (95) at the upshifted growth maximum is obtained by requiring that (94) and (95), with $\hat{\omega}_l = \hat{\omega}_-$, be consistent. The validity condition is

$$[2R/L]^{1/2} \ll 4L. \tag{96}$$

In order to apply (96), we approximate the wavenumber by $\hat{k} = 1/(1-\beta_b)$. For systems with $\gamma_b^2 \gg 1$, $\hat{k} \simeq 2\gamma_b^2$ and $\hat{\Delta}^2 \ll 1$, the inequality (96) reduces to

$$\hat{\omega}_c \hat{\omega}_p \ll 4\left[\frac{\hat{\omega}_p^2}{\gamma_b^2} + 6\hat{\Delta}^2\right]^{3/4}. \tag{97}$$

As numerical examples, we consider the cases in figure 9 (System C with parameters $\gamma_0 = 7.6$, $\hat{\omega}_c = 0.363$, and $\hat{\omega}_p^2 = 0.0157$). The case with $\hat{\Delta} = 0.01$ does not satisfy (97) since substitution of the parameters yields $0.045 \ll 0.051$. For the case where $\hat{\Delta} = 0.02$, the inequality in (97) is satisfied only marginally with $0.045 \ll 0..072$. On the other hand, if $\hat{\Delta}$ is increased to the value 0.04, then (97) is readily satisfied with $0.045 \ll 0.144$. Referring to figure 10, we note that in this case the upshifted growth rate curved obtained from the LT-FDR (95) provides a good approximation to that of the FDR (50).

The cold-beam CDR must be approximated by a cubic equation because growth is produced by a coupling of two free-streaming modes and the forward-propagating, left-hand-polarized, electromagnetic mode. However, with a sufficient increase in $\hat{\Delta}$, the primary coupling is between the lower-frequency Doppler-shifted beam oscillation and the electromagnetic mode. Then the longitudinal-transverse approximation becomes valid for the CDR. A procedure analogous to that for the FDR is used to derive the LT-CDR for the waterbag distribution. Using (51), we obtain the LT-CDR approximate result

$$\hat{\omega} = \hat{\omega}_l' + \frac{1}{2}\left[(\hat{\omega}_l' - \hat{\omega}_-)^2 - \frac{2R'}{L'}\right]^{1/2}, \tag{98}$$

where

$$R' = \frac{\hat{\omega}_c^2 \hat{\omega}_p^2}{4\hat{\omega}_-} \left(2\hat{k} - 1 - \hat{\omega}_p^2 \right), \tag{99}$$

$$L' = \frac{\hat{k}}{\gamma_b} \left(\frac{3\hat{\Delta}^2}{2\gamma_b^2} \right)^{1/2}, \tag{100}$$

From (74), the beam oscillation frequencies are

$$\left.\begin{matrix} \hat{\omega}'_l \\ \hat{\omega}'_u \end{matrix}\right\} = \hat{k}\beta_b \mp L'.$$

The assumptions made in the derivation of (98) are

$$\hat{\omega} \simeq \hat{\omega}'_l \simeq \hat{\omega}'_-,$$

and

$$\hat{\omega} - \hat{\omega}'_u \simeq \hat{\omega}'_l - \hat{\omega}'_u = -2L'. \tag{101}$$

Requiring that (98) and (101) be consistent at the growth curve maximum ($\hat{\omega}'_l = \hat{\omega}_-$) leads to the validity condition

$$(2R'/L')^{1/2} \ll 4L', \tag{102}$$

where we approximate $\hat{k}$ by $1/(1-\beta_b)$. If $\gamma_b^2 \gg 1$, $\hat{k} \simeq 2\gamma_b^2$, and $\hat{\Delta}^2 \ll 1$, then the above validity condition becomes

$$\hat{\omega}_c \hat{\omega}_p \ll 4 \left(6\hat{\Delta}^2 \right)^{3/4}. \tag{103}$$

Note that (102) and (103) cannot be satisfied by a cold beam with $\hat{\Delta} = 0$.

Apart from numerical factors, the square of (102) or (103) is the converse of the weaker condition (89) for the existence of a CDR (51) tail region. Furthermore, the weaker condition (89) may be used in place of the stronger condition (91) when $\hat{\omega}_c^2 \hat{\omega}_p^2 / 6\hat{\Delta}^2 \ll 1$,

i.e., when $\hat{\Delta}^3 \gg \hat{\omega}_c^2 \hat{\omega}_p^2 \hat{\Delta}/6$. Therefore, we also consider (102) or (103) as the condition which assures that no CDR tail region exists.

Substituting the parameters for System C ($\gamma_0 = 7.6$, $\hat{\omega}_c = 0.363$, $\hat{\omega}_p^2 = 0.0157$) with $\hat{\Delta} = 0.04$ into (103) yields $0.045 \ll 0.123$. For this system, figure 14 shows that the waterbag LT-CDR (98) growth rate curve provides a good approximation to that of the waterbag CDR (51). Also note that the CDR (51) growth rate curve has no tail region when $\hat{\Delta} = 0.04$. Figure 15 shows the frequency mismatches obtained from (51) as functions of $\hat{k}$ in the CDR growth region for this system. The assumptions made in the LT-CDR derivation ($|\hat{\omega} - \hat{\omega}_l'| \simeq |\hat{\omega} - \hat{\omega}_-| \ll |\hat{\omega} - \hat{\omega}_u'|$) are valid over most of the growth rate curve.

Finally, we emphasize that the validity condition (102) or (103) for the LT-CDR indicates that the LT-CDR is a valid approximation to the waterbag CDR (51). It does not necessarily indicate that the LT-CDR is a valid approximation to the waterbag FDR (50).

9. RANGE OF VALIDITY OF THE COMPTON APPROXIMATION

In this section, we obtain conditions for the validity of the Compton approximation. The Compton approximation is considered to be valid if the CDR adequately approximates both the shape of the FDR upshifted growth rate curve and its maximum value. The validity conditions obtained in this section are based upon an analysis of the waterbag FDR (50) and CDR (51). The numerical and analytical results presented in §10 indicate that these validity conditions are also applicable when a Gaussian equilibrium distribution in p_z is assumed.

Two conditions for validity of the Compton approximation are derived below. If the system parameters satisfy either condition, then the Compton approximation is valid. The condition derived in §9.1 assures validity of the Compton approximation for systems whose cold-beam CDR and FDR upshifted maximum growth rates closely agree. The condition derived in §9.2 assures validity of the Compton approximation even if the cold-beam CDRand FDR maximum growth rates do not agree.

9.1 First Validity Condition

For cold beams, the condition that the CDR be valid at the upshifted growth curve maximum is derived in II using the cubic approximation to the CDR. This condition [see (81)] is given by

$$\frac{4\beta_b\left(1-\beta_b\right)\hat{\omega}_p}{\gamma_b\hat{\omega}_c^2} \ll 1. \tag{104}$$

For $\gamma_b^2 \gg 1$, the inequality in (104) reduces to

$$\frac{2\hat{\omega}_p}{\gamma_b^3\hat{\omega}_c^2} \ll 1. \tag{105}$$

Our numerical computations indicate that increasing the temperature ($\hat{\Delta}$) improves the agreement between the CDR and FDR at the growth rate maximum. Therefore, we assume that (104) is sufficient for validity of the CDR at the growth rate maximum for all values of $\hat{\Delta}$.

Numerical results indicate that if the CDR and FDR upshifted maxima are in close agreement, then the shapes of the growth rate curves are also in close agreement provided no CDR tail region exists. However, when a CDR tail is present, the shape of the CDR growth curve may differ greatly from that of the FDR.

In II, it was noted that the cold-beam ($\hat{\Delta} = 0$) CDR never adequately approximates the shape of the corresponding FDR upshifted growth rate curve. The reason for this is that the CDR growth rate in the tail region [given by (84) with $\hat{\Delta} = 0$] approaches the value $\hat{\omega}_c\hat{\omega}_p$ as $\hat{k}$ approaches infinity, whereas the FDR instability terminates after some finite maximum value of $\hat{k}$. We compare the cold-beam ($\hat{\Delta} = 0$) growth rate curve in figure 9 with the corresponding CDR growth rate curve in figure 13. With the exception of a relatively small interval of $\hat{k}$ just to the right of the maximum, the CDR growth rate curve provides an extremely poor approximation to that of the FDR over the interval of the FDR tail. This behavior is typical of all cold-beam systems for which we have obtained numerical results.

If $\hat{\Delta} > 0$, then the CDR growth rate curve vanishes beyond some finite value of $\hat{k}$. [The waterbag CDR growth curve is bounded above by $\hat{k}'_{ub}$ in (75).] Nevertheless, at sufficiently low beam temperatures the CDR tail will be much too long to provide an adequate approximation to the shape of the FDR growth curve. For example, compare the FDR (50) growth rate curves in figure 9 with the corresponding CDR (51) growth rate curves in figure 13 for $\hat{\Delta} > 0$.

To summarize, if the shapes of the FDR and CDR growth rate curves are not to disagree in shape because of an excessively long CDR tail, it is necessary either that the temperature be sufficiently high that no CDR tail exists, or that it be sufficiently high that the CDR tail provides an adequate approximation to the FDR tail if an FDR tail exists. (For some systems, we will show below that the tails cease to exist before the CDR tail adequately approximates the FDR tail.)

Recall from §8 that the condition which insures that no CDR tail exists is also the validity condition for the LT-CDR (102). Thus, the condition that the temperature is sufficiently high that no CDR tail remains is given by

$$4L' \gg \left[\frac{2R'}{L'}\right]^{1/2}, \tag{106}$$

where $R' = \hat{\omega}_c^2\hat{\omega}_p^2\left(2\hat{k} - 1 - \hat{\omega}_p^2\right)/4\hat{\omega}_-$ [equation (99)], $L' = \left(3\hat{\Delta}^2\hat{k}^2/2\gamma_b^4\right)^{1/2}$ [equation (100)] and $\hat{k} = 1/(1-\beta_b)$. If $\gamma_b^2 \gg 1$, $\hat{k} \simeq 2\gamma_b^2$ and $\hat{\Delta}^2 \ll 1$, then (106) reduces to (103). That is, the condition becomes

$$4\left(6\hat{\Delta}^2\right)^{3/4} \gg \hat{\omega}_c\hat{\omega}_p. \tag{107}$$

The condition which insures that the temperature is sufficiently high that the waterbag CDR is an adequate approximation to the waterbag FDR in the tail region is obtained by comparing the LL-FDR (83) and the LL-CDR (84). The condition is given by

$$\frac{3\hat{\Delta}^2\hat{k}^2}{2\gamma_b^2} \gg \hat{\omega}_p^2. \tag{108}$$

In contrast to the relative behavior of the CDR and FDR in the regions of maximum growth, approximating the waterbag FDR by the CDR at any fixed $\hat{k}$ in the tail region becomes less adequate with increasing temperature. [In Appendix A, we show that at any fixed $\hat{k}$ (within both the FDR and CDR tails) the relative error of the CDR growth rate (relative to that of the FDR) increases with increasing temperature.] As a result, as $\hat{\Delta}$ increases, the CDR and FDR tails agree only if the tails shrink into a region of $\hat{k}$ for which there is good agreement between the cold-beam tails. [Recall that the numerical computations sometimes show a relatively small interval of the tail, just to the right of the growth curve maximum, where the cold-beam CDR and FDR growth rates agree closely.] Therefore, we can approximate $\hat{k}$ in (108) by $1/(1-\beta_b)$, its value near maximum growth. Then, the condition that the FDR and CDR tails agree can be expressed as

$$\frac{3\hat{\Delta}^2(1+\beta_b)}{2(1-\beta_b)} \gg \hat{\omega}_p^2. \tag{109}$$

For $\gamma_b^2 \gg 1$, this inequality reduces to

$$6\hat{\Delta}^2 \gg \frac{\hat{\omega}_p^2}{\gamma_b^2}. \tag{110}$$

Equation (109) is the condition for agreement of the FDR and CDR tail remnants, if indeed the tails still exist at a given value of $\hat{\Delta}$. Equation (106) is the condition that the CDR tail no longer exists. Therefore, we can state the first condition for validity of the Compton approximation. That is, if (104) [(105)] is satisfied and either one of (106) [(107)] or (109) [(110)] is satisfied, then the Compton approximation is valid.

9.2 Second Validity Condition

Systems whose cold-beam CDR and FDR upshifted growth maxima differ significantly do not satisfy (104). Furthermore, such systems do not possess FDR tail regions. Therefore, only (106) can be used to assure agreement between the shapes of the CDR and FDR growth rate curves. If (106) is satisfied, then validity of the Compton approximation also requires that the CDR growth maximum closely approximates the FDR growth maximum. Recall that (106) is also the validity condition for the LT-CDR. Comparing conditions (96) and (102), we see that validity of the LT-CDR (98) [with respect to the CDR (51)] implies validity of the LT-FDR (95) [with respect to the FDR (50)]. Therefore, comparing (95) and (98), at the growth maxima, we find that the condition assuring that the CDR (51) adequately approximates the FDR (50) growth rate maximum is

$$\frac{3\hat{\Delta}^2\,(1+\beta_b)}{2\,(1-\beta_b)} \gg \hat{\omega}_p^2. \tag{111}$$

[To obtain (111), we have assumed that $2\hat{k}-1 \gg \hat{\omega}_p^2$ at the growth maximum, i.e. $(1+\beta_b)\,/\,(1-\beta_b) \gg \hat{\omega}_p^2$. This condition is readily satisfied in all practical FEL applications.] The inequality in (111) is identical to condition (109).

On the basis of the preceding analysis, we state the second validity condition. That is, if both (106) [(107)] and (109) [(110)] are satisfied, then the Compton approximation is valid.

9.3 Summary of Validity Conditions

We summarize here the validity conditions obtained in §9.1 and §9.2. If (104) [(105)] is satsified and either one of (106) [(107)] or (109) [(110)] is satisfied, then the Compton approximation is valid. Alternatively, if both (106) [(107)] and (109) [(110)] are satisfied,

then the Compton approximation is valid.

Inequalities in (104) and (109) (in the second condition) pertain to the validity of the CDR at the growth maximum. Inequality (104) is temperature-independent and is satisfied by increasing the strength of the wiggler field, reducing the beam density, and increasing the beam energy. (It is also satisfied as β_b approaches zero.) Inequality (109) is satisfied by increasing the beam temperature, reducing the beam density, and increasing the beam energy. Inequalities in (106) and (109) (in the first condition) pertain to the validity of the shape of the CDR growth rate curve. Inequality (106) is satisfied by increasing the temperature and reducing the dimensionless coupling constant $\hat{\omega}_c\hat{\omega}_p$.

Finally, we point out that the dimensionless momentum spread $\hat{\Delta}$ used in the above inequalities is related to the beam energy spread $\Delta\gamma/\gamma$ by (34), i.e., $\Delta\gamma/\gamma = \beta_b\hat{\Delta}$.

9.4 Numerical Examples

As a numerical example, we compare figures 10 and 14. We note that the waterbag CDR (51) provides a good approximation to the corresponding FDR (50) upshifted growth rate curve in both its shape and maximum value for System C ($\gamma_0 = 7.6$, $\hat{\omega}_c = 0.363$, $\hat{\omega}_p^2 = 0.0157$) when $\hat{\Delta} = 0.04$. Substituting these parameters into (104), the validity condition for the cold-beam CDR at the growth maximum, becomes $0.105 \ll 1$. Substituting the parameters into (106), the condition that no CDR tail exists, becomes $0.38 \gg 0.15$. Substituting the parameters into (109), the condition for agreement of the FDR and CDR tails, becomes $0.060 \gg 0.0157$. If $\hat{\Delta}$ is reduced to 0.01, neither (106) nor (109) is satisfied. (Substituting the parameters yields the erroneous results $0.094 \gg 0.30$ and $0.0037 \gg 0.157$, respectively.) Referring to figures 9 and 13, we find that the CDR does not provide an adequate approximation of the FDR growth curve shape in this case.

As a second example, we consider a system with parameters $\gamma_0 = 50$, $\hat{\omega}_c = 0.015$ and $\hat{\omega}_p^2 = 3.6 \times 10^{-5}$. These parameters approximate those of the Stanford beam experiment [Elias, et al. (1976)]. The numerical results in figure 16 show that when $\hat{\Delta} = 0.0002$ the waterbag CDR maximum adequately approximates that of the FDR even though the remnant of a tail region still exists. (The cold-beam growth rate curve for this system is shown in II, figure 18.) Substituting the parameters into (105) yields $8.3 \times 10^{-4} \ll 1$.

Thus, the condition for agreement of the cold-beam CDR and FDR at the growth maxima is strongly satisfied. Substituting the parameters into (107) yields the incorrect result $4.34 \times 10^{-5} \gg 9.00 \times 10^{-5}$. Thus, $\hat{\Delta}$ is not sufficiently large to assure that there is no CDR tail. On the other hand, substituting the parameters into (110) yields $2.4 \times 10^{-7} \gg 2.25 \times 10^{-8}$, indicating that the CDR and FDR tail remnants agree and that the Compton approximation is valid.

As a final example, we consider a system with parameters $\gamma_0 = 1.3$, $\hat{\omega}_c = 0.236$ and $\hat{\omega}_p^2 = 0.0039$ [Fajans and Bekefi (1986)]. We refer to this system as System R because the Raman approximation is valid at $\hat{\Delta} = 0$. [That is, the LT-FDR (95) provides a good approximation of the FDR (50) upshifted growth rate curve when $\hat{\Delta} = 0$.] This system does not satisfy (104), because a substitution of parameters yields $0.87 \ll 1$. Therefore, the conditions for the validity of the Compton approximation are given by (106) and (109). The FDR (50) and CDR (51) growth rate curves for $\hat{\Delta} = 0$ and $\hat{\Delta} = 0.02$ are plotted in figure 17. The CDR is seen to provide a poor approximation to the FDR growth curve when $\hat{\Delta} = 0.02$. In this case, substituting the parameters shows that (106) is satisfied marginally with $0.156 \gg 0.086$. Substitution of the parameters into (109) leads to the incorrect result $2.4 \times 10^{-3} \gg 3.9 \times 10^{-3}$. The FDR and CDR growth rate curves for $\hat{\Delta} = 0.04$ and $\hat{\Delta} = 0.06$ are shown in figure 18. When $\hat{\Delta} = 0.04$, the CDR is seen to provide a fair approximation to the FDR growth curve. Substituting the parameters shows that (106) is satisfied with $0.312 \gg 0.0610$, and that (109) is maginally satisfied with $9.4 \times 10^{-3} \gg 3.9 \times 10^{-3}$. Finally, the FDR and CDR growth curves are found to agree well when $\hat{\Delta} = 0.06$. Condition (106) is satisfied with $0.468 \gg 0.0498$. Condition (109) is satisfied with $2.1 \times 10^{-2} \gg 3.9 \times 10^{-3}$.

10. COMPARISON WITH THE DISPERSION RELATION FOR A GAUSSIAN DISTRIBUTION

We have not carried out an extensive analytical study of the FDR and CDR for a narrow Gaussian distribution in p_z developed in §3. [The FDR and CDR for a narrow Gaussian distribution are obtained by substituting (46), (47) and (28) – (31) into the FDR (19) and CDR (20), respectively.] Nevertheless, by using a combination of numerical and analytical techniques, it is possible to obtain an understanding of how well the stability results based on the waterbag distribution correspond to the stability results based on the Gaussian distribution.

10.1 Condition For the Growth Rate to Be Insensitive to the Form of $G_0(p_z)$

For the case of a narrow, equilibrium distribution function,symmetric in p_z, the susceptibilities appearing in the exact FDR (19) and CDR (20) are given by (28) – (30). [The only remaining $G_0(p_z)$-dependence in (19) and (20) is in the constants, α_1 and α_3, which are approximated by unity for a narrow, symmetric equilibrium distribution. [See (16) and (31).] Therefore, both (19) and (20) depend upon $G_0(p_z)$ only through the integral

$$I = \frac{1}{\Delta}\int d\xi \frac{\partial G_0/\partial \xi}{\zeta - \xi} = -\frac{1}{\Delta}\int d\xi \frac{G_0(\xi)}{(\xi-\zeta)^2}. \tag{112}$$

In the above equation, $\xi = (p_z - p_0)/\Delta$ [equation (33)], and $\zeta = \gamma_b^2\left(\hat{\omega} - \hat{k}\beta_b\right)/\hat{k}\hat{\Delta}$ [equation (32)].

It follows that $G_0(\xi)$ is a function which is relatively large over the interval $\Delta\xi = 1$ centered at $\xi = 0$. If the relative change of $(\xi-\zeta)^{-2}$ is small over the interval $\Delta\xi = 1$, i.e.,

$$|\frac{\partial}{\partial\xi}(\xi-\zeta)^{-2}\,||_{\xi=0}\Delta\xi \ll |\,(\xi-\zeta)^{-2}\,||_{\xi=0}, \tag{113}$$

then the integral in (112) can be approximated by

$$I \simeq -\frac{1}{\Delta^2\zeta^2} - \frac{3}{\Delta^4\zeta^4}\int dp_z\,(p_z-p_0)^2\,G_0(p_z).$$

Here, the product $\Delta\zeta$ is independent of Δ. In this case, the susceptibilities occurring in (19) and (20) depend only on the mean value of $(p_z - p_0)^2$ and not on the detailed form of $G_0(p_z)$. Then, from (32), (33) and (113), we find that the dispersion relations are insensitive to the specific form of $G_0(p_z)$ provided the mean value of $(p_z - p_0)^2$ is the same and

$$|\zeta| = \frac{\gamma_b^2 |\hat{\omega} - \hat{k}\beta_b|}{\hat{k}\hat{\Delta}} \gg 2. \tag{114}$$

Referring to (48) and (49), we note that (114) is the condition for agreement between the waterbag and Gaussian dispersion relations, and therefore the corresponding stability properties.

However, failure to satisfy (114) does not necessarily imply that the stability criteria obtained from the waterbag dispersion relation do not apply to the Gaussian dispersion relation. For example, numerical and analytical results in §10.2 and §10.3 indicate that the validity conditions for the Compton approximation (§9.3) are applicable to the Gaussian FDR and CDR growth rate curves even when the details of these curves depend strongly on the shape of $G_0(p_z)$.

10.2 Numerical Comparison of Waterbag and Gaussian Growth Rate Curves

In this section, we compare the waterbag growth rate curves discussed earlier in this paper with the corresponding growth rate curves obtained for a Gaussian $G_0(p_z)$. The purpose of this analysis is to gain a qualitative understanding of how well the previous results (based on the waterbag distribution) apply to the case of a Gaussian distribution.

In §4, we developed a sufficient condition (70) that the waterbag FDR exhibit no FEL instability. For the waterbag, figure 6 shows the onset of stability with increasing density for a system with parameters $\gamma_0 = 1.3$, $\gamma_b = 1.1$ and $\hat{\Delta} = 0.04$. The corresponding graph for the Gaussian FDR is shown in figure 19. Evidently, the two graphs are in close agreement.

In §6, we discussed the behavior of the CDR downshifted growth rate curve. Unlike the cold-beam FDR downshifted growth curve, that of the CDR begins increasing from zero growth rate (with increasing $\hat{k}$) at $\hat{k} = 0$. This behavior is due to the CDR downshifted tail

and

$$\hat{\omega}_- < \hat{\omega}_1 < \hat{\omega}_2 < \hat{\omega}_+, \text{if } \hat{k} > \frac{1}{2}. \tag{60}$$

Plots of LHS$(\hat{k},\hat{\omega})$ and RHS$(\hat{k},\hat{\omega})$ vs real $\hat{\omega}$ at fixed $\hat{k}$ for the cases in (59) and (60) are shown in figures 1a and 1b, respectively. The zeros of the LHS parabola are the positive-energy $\hat{\omega}_u$ and negative-energy $\hat{\omega}_l$ longitudinal frequencies defined by

$$\left.\begin{matrix}\hat{\omega}_u \\ \hat{\omega}_l\end{matrix}\right\} = \hat{k}\beta_b \pm \left(\frac{\hat{\omega}_p^2}{\gamma_b^2} + \frac{3}{2}\frac{\hat{\Delta}^2\hat{k}^2}{\gamma_b^4}\right)^{1/2}. \tag{61}$$

The relative behavior of the LHS parabola and the RHS for the waterbag model is similar to that for the case of a cold beam discussed in II. As $\hat{k}$ increases from zero, the LHS parabola first shifts to the right relative to the RHS, and then shifts back to the left. For example, the quantity $\hat{k}\beta_b - \omega_-$ (where $\hat{\omega} = \hat{k}\beta_b$ is the $\hat{\omega}$-coordinate of the minimum of the parabola) increases from the value $-\left(1+\hat{\omega}_p^2\right)^{1/2}$ at $\hat{k} = 0$ to a maximum value of $\beta_b - \hat{\omega}_p/\gamma_b$ at $\hat{k} = 1 + \beta_b\gamma_b\hat{\omega}_p$, and then approaches $-\infty$ as $\hat{k}$ tends to $+\infty$. Similarly, for small values of $\hat{\Delta}[\hat{\Delta} < 2/3(1+\beta_b)]$, the quantity $\hat{\omega}_u - \hat{\omega}'$ (where $\hat{\omega}' = \hat{\omega}_1$, $\hat{\omega}_2$, $\hat{\omega}_+$ or $\hat{\omega}_-$) at first increases as $\hat{k}$ increases from zero, and then approaches $-\infty$ as $\hat{k}$ tends to $+\infty$.

The occurence of pairs of complex conjugate roots $\hat{\omega}(\hat{k})$, one of which represents growth, is similar to that discussed in II for the case of the cold-beam FDR [equation (50) with $\hat{\Delta} = 0$]. The FEL instability arises if, with increasing $\hat{k}$, the LHS parabola (shifting to the right in figure 1b) becomes detached from the RHS curve in the interval $0 < \hat{\omega} < \hat{\omega}_-$. Then the number of intersections of the LHS and RHS curves is reduced to four, and two complex roots of the waterbag FDR (50) appear. One of these roots represents growth $[Im(\hat{\omega}) > 0]$. If with further increase in $\hat{k}$, the LHS simply shifts back (relatively) and reattaches, then a single growth maximum in $Im\hat{\omega}(\hat{k})$ vs $\hat{k}$ will occur. (See figure 2a.) On the other hand, if the situation depicted in figure 3 develops before the final reattachment in the interval $0 < \hat{\omega} < \hat{\omega}_-$, then an interval of no growth will occur as a function of $\hat{k}$, thereby leading to separated downshifted and upshifted growth rate curves. (See figure 2b.) There is always some finite value of $\hat{k}$ beyond which no growth occurs. This follows because, from (53) and (27),

$$\lim_{\hat{k}\to\infty} \mathrm{LHS}\left(\hat{k}, \hat{\omega} = \hat{k}\beta_b\right) = \begin{cases} -\hat{\omega}_p^2\left(\hat{\omega}_c^2 + \frac{1}{\gamma_0^2}\right), & \hat{\Delta} = 0 \\ -\infty, & \hat{\Delta} > 0\,, \end{cases}$$

whereas from (54)

$$\lim_{\hat{k}\to\infty} \mathrm{RHS}\left(\hat{k}, \hat{\omega} = \hat{k}\beta_b\right) = -\hat{\omega}_c^2\hat{\omega}_p^2.$$

In II, it was shown that the behavior illustrated in figures 4a and 4b does not occur in plots of LHS and RHS vs $\hat{\omega}$ for the cold-beam FDR. We cannot prove that this behavior does not occur for the waterbag FDR (50) for special choices of parameters when $\hat{\Delta} > 0$. Figure 4a would represent the existence of an unstable mode inside the interval $0 < \hat{k} < \frac{1}{2}$. For small $\hat{\Delta}$, the behavior illustrated in figure 4b would represent a second unstable mode over a narrow interval of $\hat{k}$-space above $\hat{k} = 1/2$. However, we find that the possibility of such behavior is very sensitive to corrections of order $\hat{\Delta}^2$ in the coupling term in (50). Such terms were dropped in the approximations made between equations (37) and (43). Furthermore, the second order terms in $\hat{\delta}$ in the coupling term of (37) are incomplete because of our assumption that $G_0(p_z)$ is sufficiently narrow that the expansions (23) and (24) are valid. Carrying out the expansions of (23) and (24) to higher order in $(p_z - p_0)$ would be inappropiate for a distribution function with as little detail as the waterbag distribution. Therefore, we regard the possibility of such unstable modes of the waterbag FDR (50) as spurious and neglect the possibility in the following treatment. [We also note that such modes have never been found in the numerical computations.] If the situation shown in figure 4a does not occur, then instability is not possible for $\hat{k} < \frac{1}{2}$. This follows because it is easily shown that the minimum of the LHS parabola in figure 1a is lower than the minimum of the RHS curve in the interval $0 < \hat{\omega} < \hat{\omega}_1$.

Referring to figure 1b, we now obtain upper ($\hat{k}_{ub}$) and lower ($\hat{k}_{lb}$) bounds on the entire FEL growth region (including both the downshifted and upshifted growth curves). We note that $\hat{\omega} = \hat{k}\beta_b$ will become a root of the waterbag FDR (50) before the LHS parabola, shifting to the right, becomes detached from the RHS in the interval $0 < \hat{\omega} < \hat{\omega}_-$. It becomes a root a second time after the LHS, shifting to the left, reattaches. Thus, $\hat{k}_{ub}$ and

$\hat{k}_{lb}$ are the two positive roots obtained by setting $\hat{\omega} = \hat{k}\beta_b$ in (50) and solving for $\hat{k}$. The result of this substitution is a cubic equation in $\hat{k}^2$, which can be expressed as

$$(\hat{k}^2)^3 + p(\hat{k}^2)^2 + q\hat{k}^2 + r = 0, \tag{62}$$

where

$$p = \frac{2}{3}\frac{\hat{\omega}_p^2}{\hat{\Delta}^2}\frac{\gamma_b^4}{\gamma_0^2} - 2\gamma_b^4\left[2 - \frac{(1+\hat{\omega}_p^2)}{\gamma_b^2}\right], \tag{63}$$

$$q = -\frac{2}{3}\frac{\gamma_b^6}{\hat{\Delta}^2}\hat{\omega}_p^2\left[4 - \frac{2\hat{\omega}_p^2}{\gamma_0^2} - \frac{1}{\gamma_b^2} - \frac{1}{\gamma_0^2}\right] + \gamma_b^4\left(1+\hat{\omega}_p^2\right)^2, \tag{64}$$

and

$$r = \frac{2}{3}\frac{\gamma_b^8}{\hat{\Delta}^2}\hat{\omega}_p^2\left(1+\hat{\omega}_p^2\right)\left[\frac{1}{\gamma_b^2} + \frac{\hat{\omega}_p^2}{\gamma_0^2}\right]. \tag{65}$$

From Descartes' rule of signs, it follows that (62) has either two real, positive solutions or no real, positive solutions for $\hat{k}^2$. Thus, both $\hat{k}_{ub} > 0$ and $\hat{k}_{lb} > 0$ exist or neither exists.

For $\hat{\Delta} \to 0$, equation (62) reduces to the quadratic equation (derived in II) which gives $\hat{k}_{ub}$ and $\hat{k}_{lb}$ in the cold-beam limit, i.e.,

$$\left(\hat{k}^2\right)^2 + b\hat{k}^2 + c = 0, \tag{66}$$

where

$$b = -\left(4\gamma_b^2\gamma_0^2 - 2\gamma_b^2\hat{\omega}_p^2 - \gamma_0^2 - \gamma_b^2\right), \tag{67}$$

and

$$c = \left(1+\hat{\omega}_p^2\right)\gamma_b^2\left(\gamma_0^2 + \hat{\omega}_p^2\gamma_b^2\right). \tag{68}$$

region discussed in §7. Using the waterbag model, we found (for sufficiently large $\hat{\Delta}$) that the left edge of the CDR growth curve is located at $\hat{k} > 0$. For the waterbag distribution, (80) is a sufficient condition that the CDR growth interval begins at $\hat{k} = 0$, and (77) is a sufficient condition that it begins at a larger value of $\hat{k}$. The downshifted waterbag CDR growth curves (for system parameters $\gamma_0 = 10$, $\hat{\omega}_c = 0.05$, $\hat{\omega}_p^2 = 0.01$, and several values of $\hat{\Delta}$) are shown in figure 8. The plots (not shown) obtained for a Gaussian distribution are very similar. However, whereas (77) and (80) predict that growth begins at $\hat{k} > 0$ for all $\hat{\Delta} \gtrsim 0.037$, this does not occur in the Gaussian case until $\hat{\Delta} \gtrsim 0.062$. Therefore at best, (77) and (80) can be used only to make order-of-magnitude estimates for the Gaussian CDR.

The attenuation of the FDR upshifted tail regions with increasing temperature was discussed in §7. A comparison of the tail regions for the waterbag and Gaussian distributions is made by examining figures 9 and 20. These figures refer to System C ($\gamma_0 = 7.6$, $\hat{\omega}_c = 0.363$, $\hat{\omega}_p^2 = 0.0157$). The waterbag (figure 9) and Gaussian (figure 20) graphs are similar except that the Gaussian tails are significantly longer for each temperature. A consideration of the inequality in (114) shows that discrepancies should occur between the waterbag and Gaussian tail regions unless $\hat{\Delta}$ is very close to zero. As the end of the waterbag tail is approached (with increasing $\hat{k}$), $Re(\hat{\omega} - \hat{k}\beta_b)$ becomes very small (see §7) and $Im(\hat{\omega})$ tends to zero. Therefore, the left-hand side of (114) becomes very small. For example, consider the waterbag curve in figure 9 with $\hat{\Delta} = 0.01$. Near maximum growth at $\hat{k} = 13.0$, the numerical computations show that $Re(\hat{\omega}) - \hat{k}\beta_b = -0.0467$ and $Im(\hat{\omega}) = 0.0917$. Substituting the parameters into (114) yields $5.3 \gg 2$. Close to the edge of the tail region at $\hat{k} = 28.1$, we obtain $Re\hat{\omega} - \hat{k}\beta_b = -0.000329$ and $Im(\hat{\omega}) = 0.00328$. Substituting the parameters into (114) yields the incorrect result $0.079 \gg 2$.

A corresponding comparison of the attenuation of the waterbag and Gaussian CDR tails with increasing $\hat{\Delta}$ is made by examining figures 13 and 21. Although the Gaussian CDR tails are shortened with increasing $\hat{\Delta}$, they are much longer than the corresponding waterbag tails.

In §9.4, numerical computations of waterbag FDR and CDR growth rate curves were presented as examples of the application of the validity conditions for the Compton ap-

proximation derived in §9.3. Here, we parallel the examples in (§9.4) for the case of a Gaussian distribution. The inequality (114) is violated in the tail regions at small values of $\hat{\Delta}$ and at the growth maxima for sufficiently large values of $\hat{\Delta}$. Therefore, one might expect that the validity conditions in §9.3, based on an analysis of the waterbag dispersion relation, would have a very limited range of applicability to the Gaussian distribution. Nevertheless, the numerical results, such as those presented below, indicate that the validity conditions are also applicable to the Gaussian growth rate curves even when (114) is violated strongly. However, in some examples, we do find that the inequalities must be stronger in the Gaussian case.

The first example studied in §9.3 corresponded to System C ($\gamma_0 = 7.6$, $\hat{\omega}_c = 0.363$, $\hat{\omega}_p^2 = 0.0157$), which for $\hat{\Delta} = 0.04$ satisfies (104), (106) and (109). Reference to figures 10 and 14 shows that the FDR and CDR upshifted growth rate curves for the waterbag distribution agree closely in both their maximum values and shapes. The corresponding FDR and CDR growth rate curves for the Gaussian are shown in figure 22. The Gaussian CDR is seen to provide a good approximation to the Gaussian FDR growth rate curve in spite of the fact that corresponding waterbag and Gaussian growth rate curves do not agree closely in shape. Numerical results for the waterbag FDR show that at $\hat{k} = 13.8$, near the right edge of the growth curve, the inequality in (114) is disobeyed with $0.54 \gg 2$.

The second example studied in §9.4 corresponded to parameters for the Stanford beam ($\gamma_0 = 50$, $\hat{\omega}_c = 0.015$, $\hat{\omega}_p^2 = 3.6 \times 10^{-5}$). For the waterbag distribution we found that the Compton approximation is valid when $\hat{\Delta} = 0.0002$. At this beam temperature, a remnant of the CDR tail remains. However, the condition in (110) for agreement between the FDR and CDR tails is valid [as well as the condition in (105)]. Both the waterbag and Gaussian FDR and CDR growth rate curves for this system are plotted in figure 16. Note that in spite of the longer tails in the Gaussian case, the relation between the FDR and CDR curves is similar in both cases. The Gaussian CDR growth rate curve provides a good approximation to the Gaussian FDR curve.

The last example given in the previous section corresponded to System R ($\gamma_0 = 1.3$, $\hat{\omega}_c = 0.236$, $\hat{\omega}_p^2 = 0.0039$). From figure 18, we found for the case of the waterbag distribution that there is fair agreement between the FDR and CDR growth rate curves when

$\hat{\Delta} = 0.04$. At this temperature, (106) is satisfied and (109) is satisfied marginally. We also found that there is good agreement between the waterbag FDR and CDR growth curves when $\hat{\Delta} = 0.06$. Then both the inequalities in (106) and (109) are satisfied. The corresponding growth rate curves for the Gaussian case are shown in figure 23. Comparing figures 18 and 23, we find at these temperatures that there are significant differences between the corresponding waterbag and Gaussian growth curves even though there are no tail regions. The waterbag growth curves are higher and narrower than the Gaussian growth curves. However, the qualitative relations between the corresponding FDR and CDR growth curves in the waterbag and Gaussian cases are similar. Clearly, in the Gaussian case, the inequalities in (106) and (109) must be satisfied more strongly than is required in the waterbag case. There is, however, fair agreement between Gaussian CDR and FDR growth rate curves when $\hat{\Delta} = 0.06$.

10.3 The Resonant Warm-Compton Regime

In this section, we show analytically that the applicability of the Compton-approximation validity conditions in §9.3 extends to the resonant, warm-Compton region for the case of a Gaussian equilibrium distribution in p_z. This result (together with the numerical results discussed in §10.2) strongly indicates that the validity conditions in §9.3, which were derived for the case of a waterbag distribution function, can also be applied to the Gaussian case for all parameter regimes of practical interest.

At sufficiently high beam temperatures that $Im(\omega)/k$ is much less than the thermal spread Δv_z in the longitudinal velocity, the CDR (20) predicts that the growth rate as a function of $\hat{k}$ is proportional to $\gamma \partial G_0/\partial p_z$ evaluated at $v_z = Re(\omega)/k$. [Here $G_0(p_z)$ is a smoothly varying function.] If in addition the CDR (20) is a valid approximation to the FDR (19), then this parameter regime is referred to as the resonant, warm-Compton regime. Clearly, the waterbag and Gaussian growth rates cannot agree in this regime.

This regime has been studied by Kroll and McMullin (1978), and more recently by Dimos and Davidson (1985). Using the CDR (20), the latter authors obtained an approximate expression for the growth rate for the case of a Gaussian distribution, i.e.,

$$Im(\hat{\omega}) = \frac{\pi^{1/2}}{2} \frac{\hat{\omega}_p^2 \hat{\omega}_c^2}{\hat{\Delta}^3} \frac{\gamma_b^4 \left(\beta_b - Re(\hat{\omega})/\hat{k}\right)}{Re(\hat{\omega})} \times \exp\left[-\frac{\gamma_b^4 \left(\beta_b - Re(\hat{\omega})/\hat{k}\right)^2}{\hat{\Delta}^2}\right], \tag{115}$$

where $Re\,(\hat{\omega}) = \hat{k} - 1$. We refer to (115) as the warm-Compton growth rate.

From the requirement that $Im(\omega)/k \ll \Delta v_z$ (the condition for strong resonance), Dimos and Davidson obtained the following condition for validity of (115), i.e.,

$$2.63\beta_b \left(1 + \beta_b\right)^2 \hat{\Delta}^3 \gg \hat{\omega}_p^2 \hat{\omega}_c^2. \tag{116}$$

For $\gamma_b^2 \gg 1$, this condition reduces to

$$10.5\hat{\Delta}^3 \gg \hat{\omega}_p^2 \hat{\omega}_c^2. \tag{117}$$

We now obtain a second validity condition for (115) by requiring that the upshifted growth rate curve obtained from the CDR (20) adequately approximates that of the FDR (19) in the region of maximum growth. We compare the FDR (19) with the CDR (20) and also note (for a narrow distribution) that (28) – (30) imply that the susceptibilities $|\hat{\chi}^{(0)}|$, $|\hat{\chi}^{(1)}|$ and $|\hat{\chi}^{(2)}|$ are of similar magnitude. It follows that the CDR (20) adequately approximates the FDR (19) provided $\hat{D}^l\left(\hat{k}, \hat{\omega}\right) = \hat{k}^2 + \hat{\chi}^{(0)}\left(\hat{k}, \hat{\omega}\right) \simeq \hat{k}^2$. That is, we require that

$$|\hat{\chi}^{(0)}\left(\hat{k}, \hat{\omega}\right)| \ll \hat{k}^2. \tag{118}$$

For a narrow Gaussian distribution $\hat{\chi}^{(0)} = 2\hat{\omega}_p^2 \gamma_b^2 \left[1 + \zeta Z\left(\zeta\right)\right]/\hat{\Delta}^2$ [equation (46)], where $\zeta = \gamma_b^2 \left(\hat{\omega} - \hat{k}\beta_b\right)/\hat{k}\hat{\Delta}$[equation (32)]. Evaluating $\hat{\chi}^{(0)}$ at the maximum of the growth rate curve in (115) (i.e., $\zeta = -1/\sqrt{2}$) and substituting the result into (118), we obtain a second condition for validity of the warm-Compton approximation, i.e.,

$$\hat{\Delta}^2 \gg 1.62\frac{\hat{\omega}_p^2\gamma_b^2}{\hat{k}^2}.$$

Finally, we approximate $\hat{k}$ by $1/(1-\beta_b)$ in the above equation and obtain the condition

$$\hat{\Delta}^2 \gg 1.62\frac{(1-\beta_b)}{(1+\beta_b)}\hat{\omega}_p^2. \tag{119}$$

The inequality in (119) assures that the CDR (20) is valid at the upshifted growth maximum. If $\gamma_b^2 \gg 1$, then (119) reduces to

$$\hat{\Delta}^2 \gg \frac{\hat{\omega}_p^2}{2.5\gamma_b^2}. \tag{120}$$

In summary, the inequality in (116) [(117)] assures strong resonance, and the inequality in (119) [(120)] assures that the CDR (20) is valid at the growth maximum. Similar relations were obtained by Kroll and McMullin (1978) for the case where $\gamma_b^2 \gg 1$.

We now demonstrate that the validity conditions for the Compton approximation derived from the waterbag dispersion relations in §9.3 extrapolate to the resonant, warm-Compton regime for the case of a Gaussian distribution. We show that if any one of the validity conditions in §9.3 is satisfied sufficiently strongly for a system in the resonance regime, then (119) (the condition for validity of the Compton approximation in the resonance regime) is satisfied. There are three ways of satisfying a Compton approximation validity conditon in §9.3. A condition is satisfied if both (104) and (109) are true, or if both (106) and (109) are true. Except for numerical coefficients, (109) is the same as (119). The remaining condition in §9.3 is that both (104) and (106) are satisfied. Assuming that $\left(\hat{k}-1\right)^2 \gg \hat{\omega}_p^2$ in the upshifted growth interval of $\hat{k}$-space, and using (99), (100) and (56) with $\hat{k} = 1/(1-\beta_b)$, we express (106) in the form

$$7.67\,(1+\beta_b)\,\beta_b^{1/2}\hat{\Delta}^{3/2} \gg \hat{\omega}_c\hat{\omega}_p. \tag{121}$$

Moreover, combining (121) and (104), we obtain the inequality

$$\left(\hat{\Delta}^2\right)^{3/4} \gg \frac{0.130\hat{\omega}_c\hat{\omega}_p}{\left[(1+\beta_b)\,\beta_b^{1/2}\right]} > 0.261\left[\frac{(1-\beta_b)}{(1+\beta_b)}\hat{\omega}_p^2\right]^{3/4}. \tag{122}$$

Except for numerical coefficients, the 4/3-power of (122) is the same as (119).

Finally we show that the validity condition for the warm-Compton growth rate (115) [i.e., that both (116) and (119) are satisfied] is included in the validity conditions for the Compton approximation in §9.3. If (109) is satisfied sufficiently strongly, then (119) is satisfied. Referring to (121), we find that, except for numerical coefficients, (106) is the same as the square root of (116). Therefore, if (106) is satisfied sufficiently strongly, then (116) is satisfied. It follows that the resonance regime condition is included in the second validity condition for the Compton approximation in §9.3 [i.e., that both (106) and (109) are satisfied].

The above results show analytically that the conditions of §9.3 extrapolate into the warm-Compton regime for a Gaussian equilibrium distribution. Together with the numerical results in §9.2, they show that the conditions in §9.3 are widely applicable to the case of a narrow Gaussian distribution.

11. CONCLUSIONS

In II, we analyzed properties of growth rate curves [$Im(\hat{\omega})$ vs $\hat{k}$] of the FEL instability for the case of a cold beam. In this paper, we have determined the influence of thermal effects on these cold-beam stability results using the FDR (19) and the CDR (20). Two equilibrium distribution functions are employed. These are a simple waterbag distribution (35) in axial momentum p_z and a narrow Gaussian distribution (45). Analytic results are obtained using the waterbag FDR (50) and CDR (51), and their longitudinal-transverse (Raman) and longitudinal-longitudinal (tail region) approximations. The analytical results are compared numerically with both the waterbag dispersion relations and the Gaussian FDR and CDR (§3).

In II, it was shown that (for low beam energies) the cold-beam FEL becomes stable at sufficiently large beam densities [i.e., for the FDR, $Im(\hat{\omega}) = 0$ for all $\hat{k}$ at sufficiently large densities]. Using the waterbag FDR, we find that increasing the longitudinal temperature causes the the FEL instability to stabilize at somewhat lower densities than for the cold-beam case. However, the thermal effects are small for realistic FEL beam temperatures. Numerical results show that the decrease in growth rate with increasing density (near the waterbag stability region) is similar for the waterbag and Gaussian FDR.

In the case of a cold beam (II), we found that for some systems the FDR upshifted growth rate curve possesses a tail of finite length extending from the growth rate maximum towards larger values of $\hat{k}$. The tail occurs in cold-beam systems for which the CDR adequately approximates the FDR upshifted growth rate maximum. The primary coupling producing the tail is between the positive- and negative-energy longitudinal modes. In the present analysis, we find that increasing the beam temperature shortens and finally extinguishes the FDR tail. We also find that the CDR upshifted growth rate curve may exhibit a tail. The coupling producing the CDR tail is between the lower- and higher-frequency Doppler shifted beam oscillations. As the longitudinal temperature is decreased, a CDR tail develops, which approaches infinite length in $\hat{k}$-space as the temperature approaches zero. As a consequence of the infinitely long CDR tail, the cold-beam CDR never adequately approximates the shape of the upshifted FDR growth rate curve.

An important result of this analysis is a set of validity conditions for the Compton approximation. We consider the Compton approximation to be valid if the CDR adequately approximates the FDR upshifted growth rate curve [$Im(\hat{\omega})$ vs $\hat{k}$] both in its maximum value and shape. The validity conditions are that either (106) [(107)] and (109) [(110)] are satisfied, or that (104) [(105)] and either (106) [(107)] or (109) [(110)] are satisfied. These conditions are derived using a waterbag equilibrium distribution function in the CDR and FDR. However, numerical computations indicate that they are also applicable to the case of a Gaussian equilibrium distribution function, even in parameter regions where significant differences exist between corresponding waterbag and Gaussian growth rate curves. We show analytically that the applicability of the validity conditions based on the waterbag distribution extends into the resonant, warm Compton region for the Gaussian case. In particular, it is shown that if the conditions (§9.3) based on the waterbag distribution are satisfied sufficiently strongly, then the condition (119) for validity of the Compton approximation in the resonance region is satisfied. Furthermore, it is shown that the condition for the resonant warm-Compton regime [i.e., that both (116) and (119) are satisfied] is included in the condition in §9.3.

ACKNOWLEDGEMENTS

This research was supported in part by the Office of Naval Research and in part by the National Science Foundation.

REFERENCES

Davidson, R.C. & Uhm, H.S. 1980 *Phys. Fluids*, 23, 2076.

Davies, J.A., Davidson, R.C. & Johnston, G.L. 1985 *J. Plasma Phys.*, 33, 387.

Dimos, A.M. & Davidson, R.C. 1985 *Phys. Fluids*, 28, 677.

Elias, G.R., Fairbank, W.M., Madey, J.M., Schwettman, H.A. & Smith, T.I. 1976 *Phys. Rev. Lett.* 36, 717.

Fajans, J. & Bekefi, G. 1986 MIT Plasma Fusion Center Report No. JA–86–12.

Kwan, T., Dawson, J.M. & Lin, A.T. 1977 *Phys. Fluids*, 20, 581.

Kroll, N.M. & McMullin, W.A. 1978 *Phys. Rev.* A 17, 300.

Orzechowski, T.J., Anderson, B., Fawley, W.M., Prosnitz, D., Scharlemann, E.T., Yarema, S., Hopkins, D., Paul, A.C., Sessler, A.M. & Wurtele, J. 1985 *Phys. Rev. Lett.* 54, 889.

APPENDIX A. RELATIVE ERROR OF THE CDR IN THE TAIL REGION

Consider a value of $\hat{k}$ which is in both the CDR and FDR tail regions. The square of the FDR growth rate $[Im^2(\hat{\omega}_{FDR})]$ and the CDR growth rate $[Im^2(\hat{\omega}_{CDR})]$ appear in the square roots in (83) and (84), respectively. Subtracting with the aid of (55) – (58), we obtain

$$\begin{aligned} & Im^2(\hat{\omega}_{CDR}) - Im^2(\hat{\omega}_{FDR}) \\ & = \frac{\hat{\omega}_p^2}{\gamma_b^2} - \frac{\hat{\omega}_c^2\hat{\omega}_p^4\left(\hat{\omega}_2^2 - \hat{k}^2\beta_b^2\right)}{\left(\hat{\omega}_+^2 - \hat{k}^2\beta_b^2\right)\left(\hat{\omega}_-^2 - \hat{k}^2\beta_b^2\right)} = D. \end{aligned} \tag{A.1}$$

The difference D is independent of $\hat{\Delta}$. The relative error of the waterbag CDR versus the waterbag FDR is

$$\begin{aligned} & \frac{Im(\hat{\omega}_{CDR}) - Im(\hat{\omega}_{FDR})}{Im(\hat{\omega}_{FDR})} \\ & = \frac{D}{Im(\hat{\omega}_{FDR})\left[Im(\hat{\omega}_{FDR}) + Im(\hat{\omega}_{CDR})\right]}. \end{aligned} \tag{A.2}$$

Since D is independent of temperature, and the growth rates decrease with increasing $\hat{\Delta}$, the relative error increases with increasing $\hat{\Delta}$.

FIGURE CAPTIONS

Fig. 1 Schematic plots of LHS (- - -) and RHS (——) vs $\hat{\omega}$ for fixed $\hat{k}$ in the intervals (a) $0 < \hat{k} < 1/2$, and (b) $\hat{k} > 1/2$ [equations (53) and (54)].

Fig. 2 Schematic plots of the FDR (——) and CDR (- - -) growth rate curves for the cases corresponding to: (a) a single growth rate maximum, and (b) two distinct downshifted and upshifted growth rate curves.

Fig. 3 Schematic plot of LHS (- - -) and RHS (——) for $\hat{k}$ in the interval between the upshifted and downshifted growth rate curves [equations (53) and (54)].

Fig. 4 Illustrative plots for spurious instabilities of the waterbag FDR (50) with (a) $0 < \hat{k} < 1/2$, and (b) $\hat{k} > 1/2$.

Fig. 5 Plot showing the sufficient condition for stability of a cold beam (——) and for the waterbag FDR with $\hat{\Delta} = 0.10$ (- - -) [equation (70)].

Fig. 6 Plots of growth rate $Im(\hat{\omega})$ vs $\hat{k}$ obtained numerically from the FDR (50) for several values of $\hat{\omega}_p^2$ for a cold electron beam with $\hat{\Delta} = 0$ (——) and for a warm waterbag distribution with $\hat{\Delta} = 0.04$ (- - -). Other system parameters are $\gamma_0 = 1.3$, and $\gamma_b = 1.1$.

Fig. 7 Schematic plots of LHS$'$ (- - -) and RHS$'$ (——) vs $\hat{\omega}$ for fixed $\hat{k}$ in the intervals (a) $0 < \hat{k} < (1 + \hat{\omega}_p^2)/2$, and (b) $\hat{k} > (1 + \hat{\omega}_p^2)/2$ [equations (72) and (73)].

Fig. 8 Plots of downshifted growth rate $Im(\hat{\omega})$ vs $\hat{k}$,obtained numerically from the CDR (51) for several values of $\hat{\Delta}$. Other system parameters are $\gamma_0 = 10$, $\hat{\omega}_c = 0.05$, and $\hat{\omega}_p^2 = 0.01$.

Fig. 9 Plots of the upshifted growth rate $Im(\hat{\omega})$ vs $\hat{k}$ obtained numerically from the waterbag FDR (50) for several values of $\hat{\Delta}$ (——). The system parameters are $\gamma_0 = 7.6$, $\hat{\omega}_c = 0.363$ and $\hat{\omega}_p^2 = 0.01570$. The growth rate curves (- - -) obtained from the LL-FDR (83) are presented for $\hat{\Delta} = 0.005$ and $\hat{\Delta} = 0.02$.

Fig. 10 Plots of the upshifted growth rate $Im(\hat{\omega})$ vs $\hat{k}$ obtained numerically from (a) the waterbag FDR (50), (b) the LT-FDR (95), and (c) the LL-FDR (83) for system parameters $\gamma_0 = 7.6$, $\hat{\omega}_c = 0.363$, $\hat{\omega}_p^2 = 0.0157$, and $\hat{\Delta} = 0.04$.

Fig. 11 Plots of the frequency mismatches (a) $|\hat{\omega} - \hat{\omega}_+|$, (b) $|\hat{\omega} - \hat{k}\beta_b|$, (c) $|\hat{\omega} - \hat{\omega}_-|$, (d) $|\hat{\omega} - \hat{\omega}_l|$, and (e) $|\hat{\omega} - \hat{\omega}_u|$ versus $\hat{k}$ for system parameters $\gamma_0 = 7.6$, $\hat{\omega}_c = 0.363$, $\hat{\omega}_p^2 = 0.0157$, and $\hat{\Delta} = 0.005$. The complex $\hat{\omega}$ in figure 11 solves the waterbag FDR (50).

Fig. 12 Plots of the frequency mismatches (a) $|\hat{\omega} - \hat{\omega}_+|$, (b) $|\hat{\omega} - \hat{k}\beta_b|$, (c) $|\hat{\omega} - \hat{\omega}_-|$, (d) $|\hat{\omega} - \hat{\omega}_l|$, and (e) $|\hat{\omega} - \hat{\omega}_u|$ versus $\hat{k}$ for system parameters $\gamma_0 = 7.6$, $\hat{\omega}_c = 0.363$, $\hat{\omega}_p^2 = 0.0157$, and $\hat{\Delta} = 0.04$. The complex $\hat{\omega}$ in figure 12 solves the waterbag FDR (50).

Fig. 13 Plots of the upshifted growth rate $Im(\hat{\omega})$ vs $\hat{k}$ obtained numerically from the waterbag CDR (51) (——) for several values of $\hat{\Delta}$. Other system parameters are $\gamma_0 = 7.6$, $\hat{\omega}_c = 0.363$ and $\hat{\omega}_p^2 = 0.0157$. The LL-CDR curves (- - -) obtained from (84) are shown for $\hat{\Delta} = 0.005$, and $\hat{\Delta} = 0.02$.

Fig. 14 Plots of the upshifted growth rate $Im(\hat{\omega})$ vs $\hat{k}$ obtained numerically from (a) the waterbag CDR (50), (b) the LT-CDR (98), and (c) the LL-CDR (84) for system parameters $\gamma_0 = 7.6$, $\hat{\omega}_c = 0.363$, $\hat{\omega}_p^2 = 0.0157$, and $\hat{\Delta} = 0.04$.

Fig. 15 Plots of the frequency mismatches (a) $|\hat{\omega} - \hat{\omega}_+|$, (b) $|\hat{\omega} - \hat{k}\beta_b|$, (c) $|\hat{\omega} - \hat{\omega}_-|$, (d) $|\hat{\omega} - \hat{\omega}_l|$, and (e) $|\hat{\omega} - \hat{\omega}_u|$ versus $\hat{k}$ for the system parameters $\gamma_0 = 7.6$, $\hat{\omega}_c = 0.363$, $\hat{\omega}_p^2 = 0.0157$ and $\hat{\Delta} = 0.04$. The complex $\hat{\omega}$ in figure 15 solves the waterbag CDR (51).

Fig. 16 Plots of the upshifted growth rate $Im(\hat{\omega})$ vs $\hat{k}$ obtained numerically from the waterbag FDR (50) and CDR (51), and from the Gaussian FDR and CDR. The system parameters are $\gamma_0 = 50$, $\hat{\omega}_c = 0.015$, $\hat{\omega}_p^2 = 3.6 \times 10^{-5}$, and $\hat{\Delta} = 0.0002$.

Fig. 17 Plots of the upshifted growth rate $Im(\hat{\omega})$ vs $\hat{k}$ obtained numerically from the waterbag FDR (50) (——) and CDR (51) (- - -) for several values of $\hat{\Delta}$. Other system parameters are $\gamma_0 = 1.3$, $\hat{\omega}_c = 0.236$, and $\hat{\omega}_p^2 = 0.0039$.

Fig. 18 Plots of the upshifted growth rate $Im(\hat{\omega})$ vs $\hat{k}$ obtained numerically from the waterbag FDR (50) (——) and CDR (51) (- - -) for several values of $\hat{\Delta}$. Other system parameters are $\gamma_0 = 1.3$, $\hat{\omega}_c = 0.236$, and $\hat{\omega}_p^2 = 0.0039$.

Fig. 19 Plots of the upshifted growth rate $Im(\hat{\omega})$ vs $\hat{k}$ obtained numerically from the Gaussian FDR for several values of $\hat{\omega}_p^2$. Other system parameters are $\gamma_0 = 1.3$, $\gamma_b = 1.1$, and $\hat{\Delta} = 0.04$.

Fig. 20 Plots of the upshifted growth rate $Im(\hat{\omega})$ vs $\hat{k}$ obtained numerically from the Gaussian FDR for several values of $\hat{\Delta}$. Other system parameters are $\gamma_0 = 7.6$, $\hat{\omega}_c = 0.363$, and $\hat{\omega}_p^2 = 0.0157$.

Fig. 21 Plots of the upshifted growth rate $Im(\hat{\omega})$ vs $\hat{k}$ obtained numerically from the Gaussian CDR for several values of $\hat{\Delta}$. Other system parameters are $\gamma_0 = 7.6$, $\hat{\omega}_c = 0.363$, and $\hat{\omega}_p^2 = 0.0157$.

Fig. 22 Plots of the upshifted growth rate $Im(\hat{\omega})$ vs $\hat{k}$ obtained numerically from the Gaussian (a) FDR and (b) CDR. The system parameters are $\gamma_0 = 7.6$, $\hat{\omega}_c = 0.363$, $\hat{\omega}_p^2 = 0.0157$, and $\hat{\Delta} = 0.04$.

Fig. 23 Plots of the upshifted growth rate $Im(\hat{\omega})$ vs $\hat{k}$ obtained numerically from the Gaussian FDR (——) and the Gaussian CDR(- - -) for several values of $\hat{\Delta}$. Other system parameters are $\gamma_0 = 1.3$, $\hat{\omega}_c = 0.236$, and $\hat{\omega}_p^2 = 0.0039$.

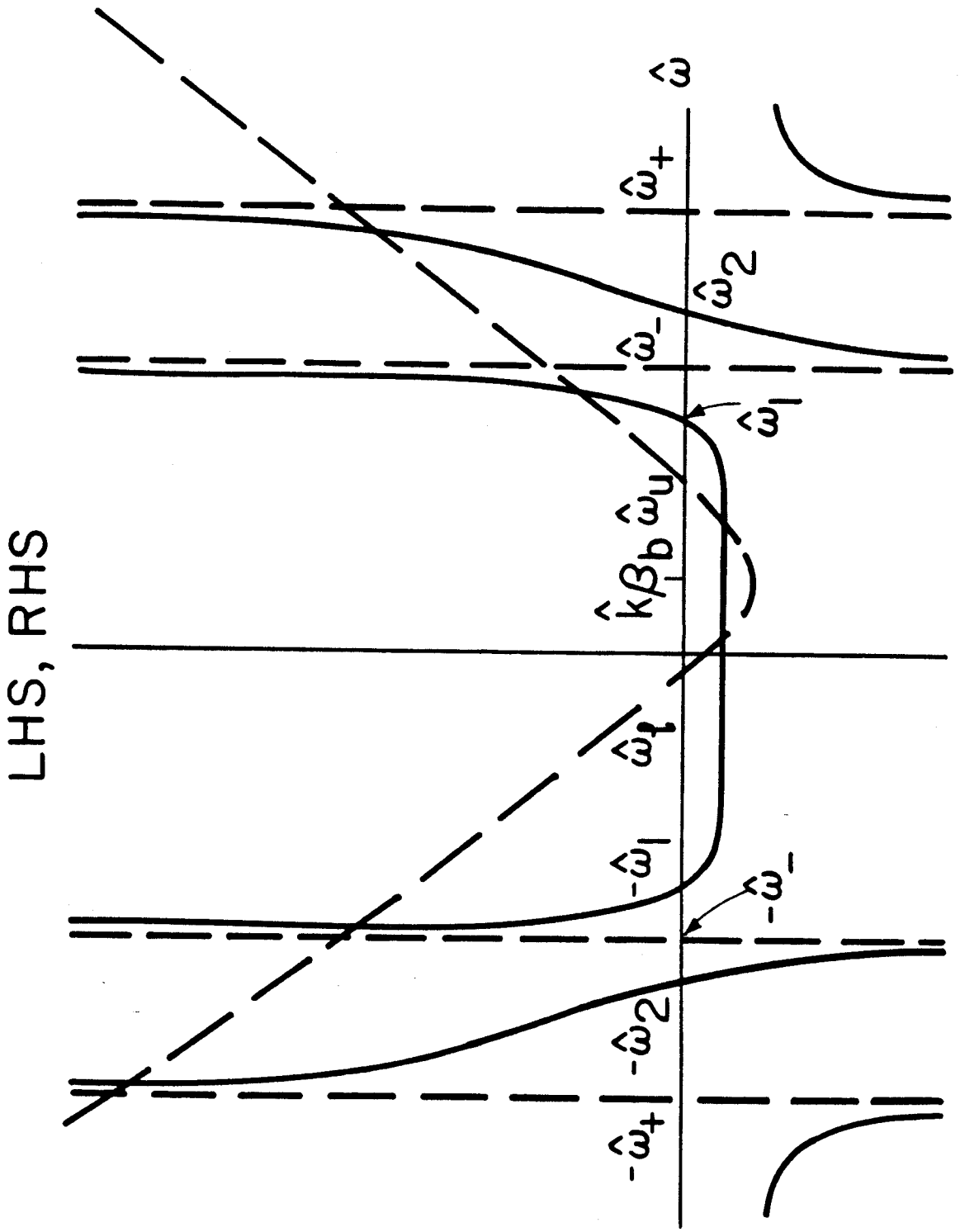
LHS, RHS
$\hat{\omega}$
$\hat{\omega}_+$
$\hat{\omega}_2$
$\hat{\omega}_-$
$\hat{\omega}_1$
$\hat{k}\beta_b\hat{\omega}_u$
$\hat{\omega}_t$
$-\hat{\omega}_1$
$-\hat{\omega}_-$
$-\hat{\omega}_2$
$-\hat{\omega}_+$

Fig. 1(a)

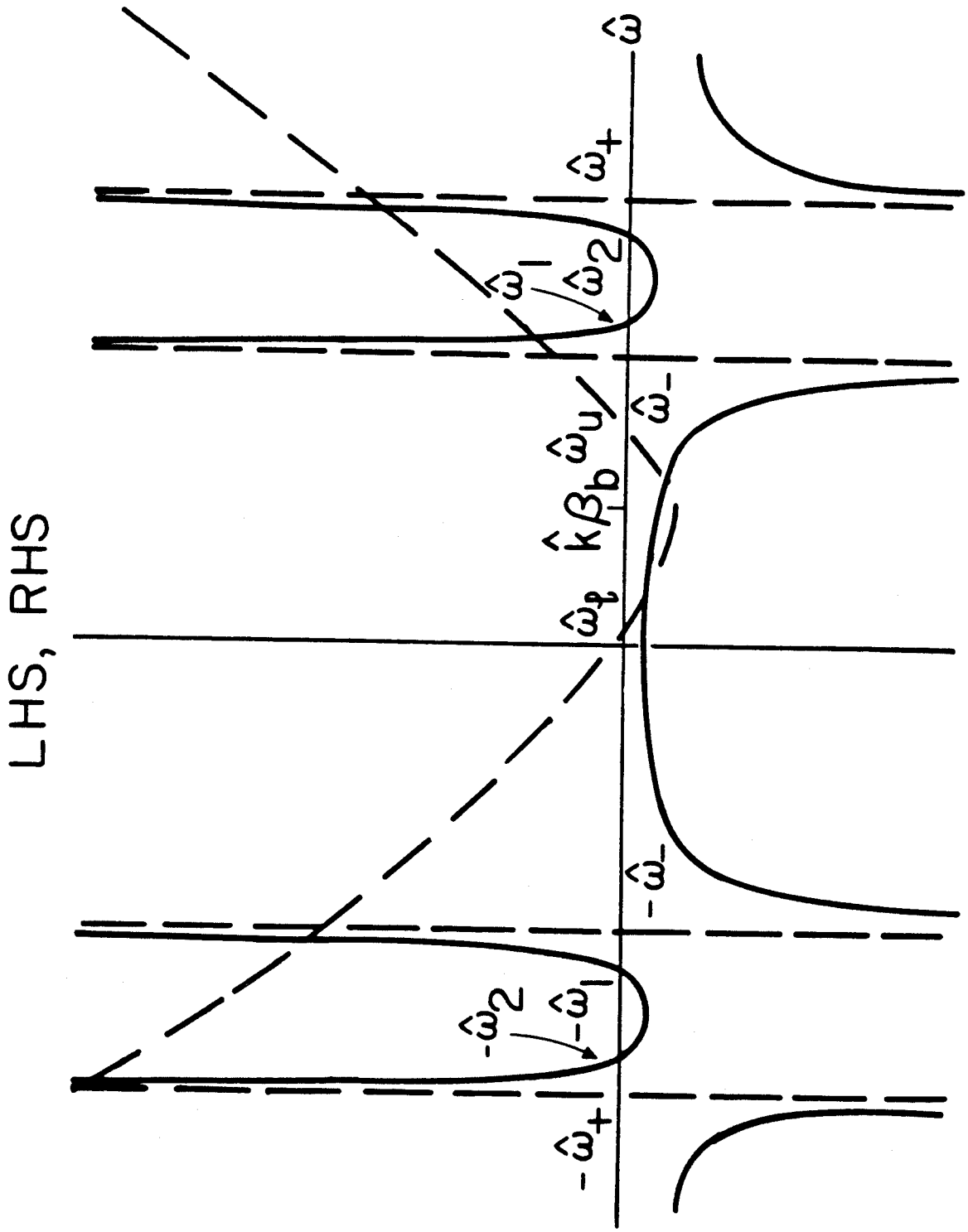
LHS, RHS
$\hat{\omega}$
$\hat{\omega}_+$
$\hat{\omega}_1$
$\hat{\omega}_2$
$\hat{\omega}_-$
$\hat{\omega}_u$
$\hat{k}\beta_b$
$\hat{\omega}_t$
$-\hat{\omega}_-$
$-\hat{\omega}_2$
$-\hat{\omega}_1$
$-\hat{\omega}_+$

Fig. 1(b)

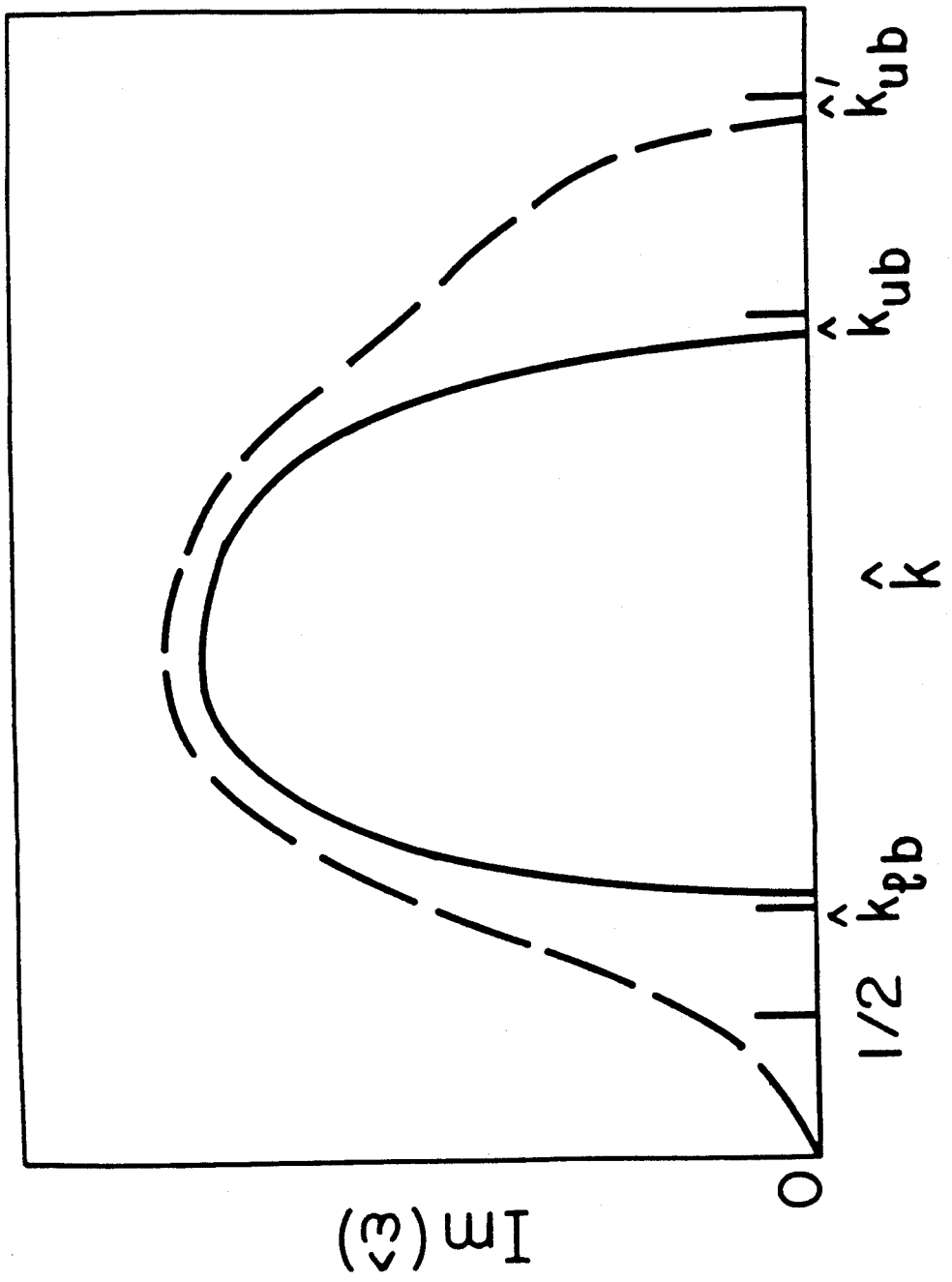

Fig. 2(a)

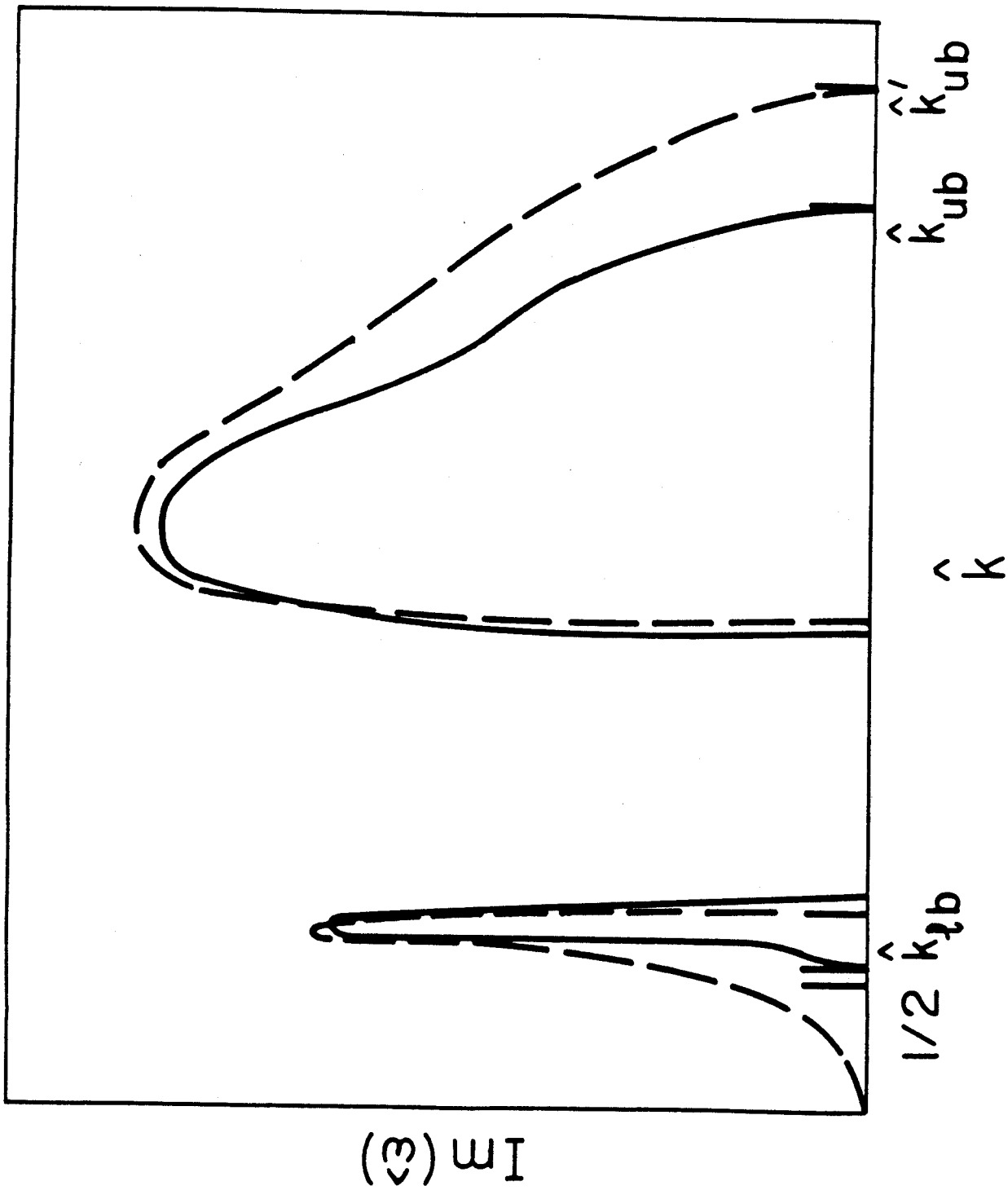

Fig. 2(b)

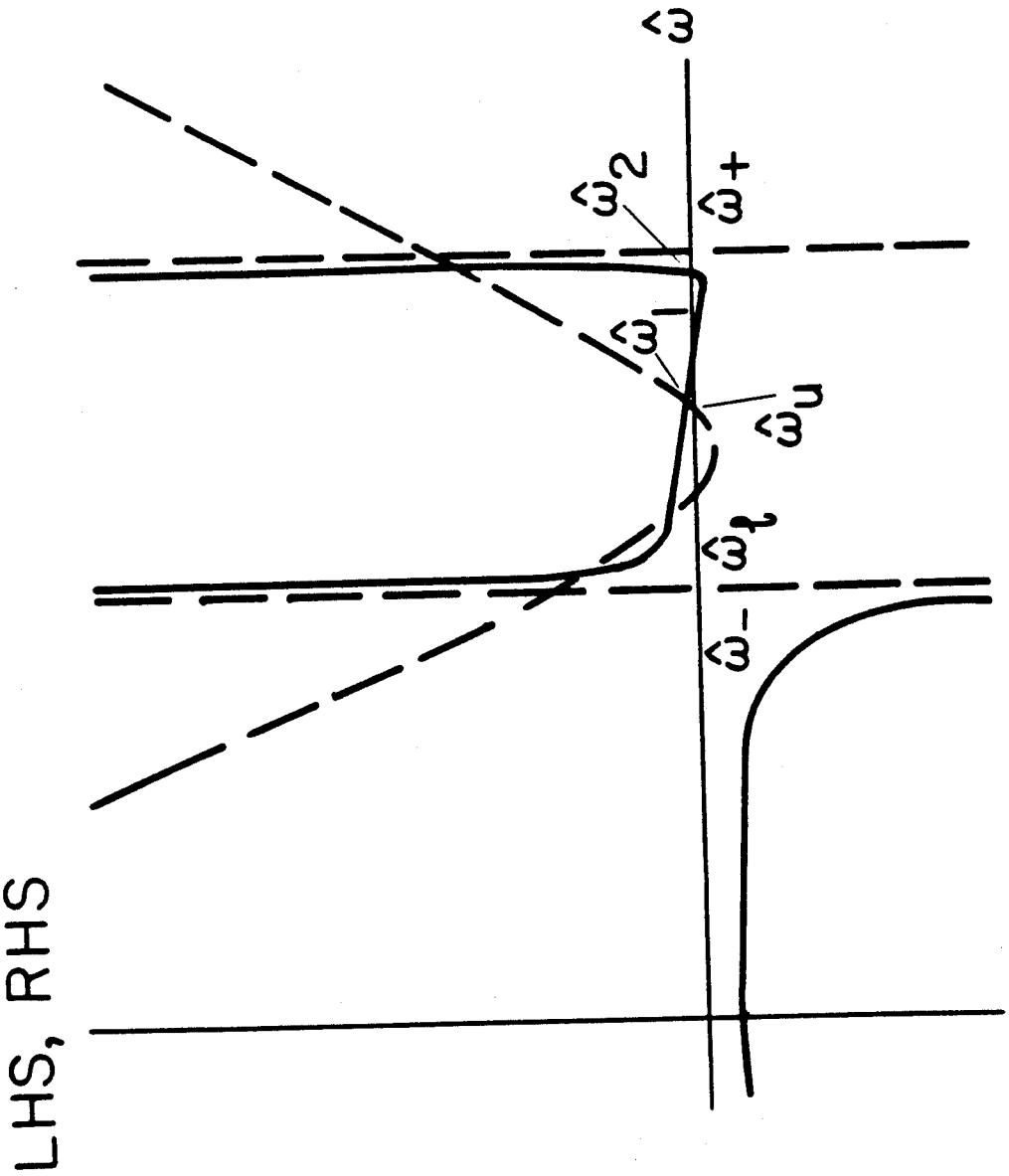

Fig 3

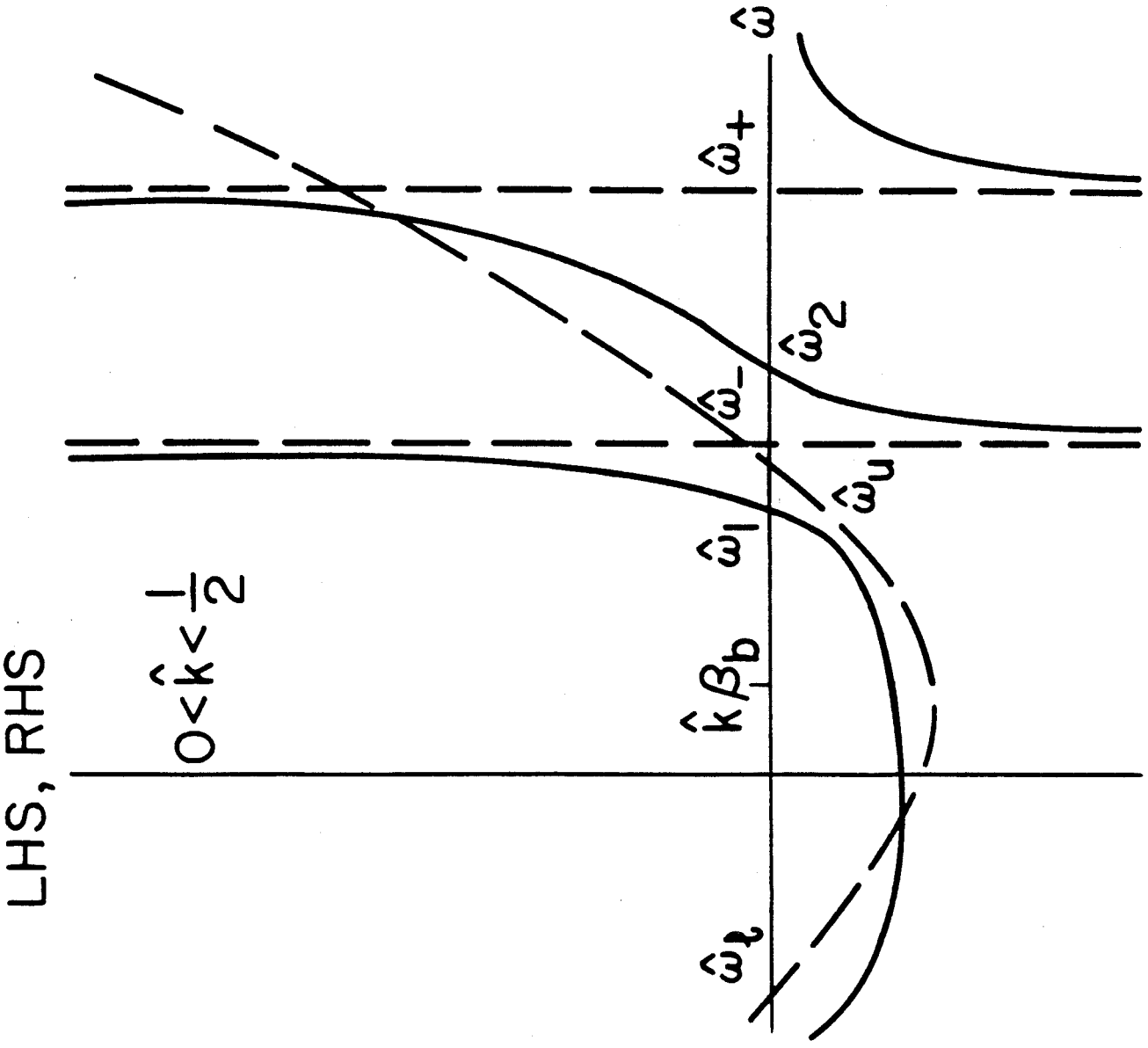
LHS, RHS
$0<\hat{k}<\frac{1}{2}$
$\hat{\omega}$
$\hat{\omega}_+$
$\hat{\omega}_2$
$\hat{\omega}_-$
$\hat{\omega}_u$
$\hat{\omega}_1$
$\hat{k}\beta_b$
$\hat{\omega}_l$

Fig. 4(a)

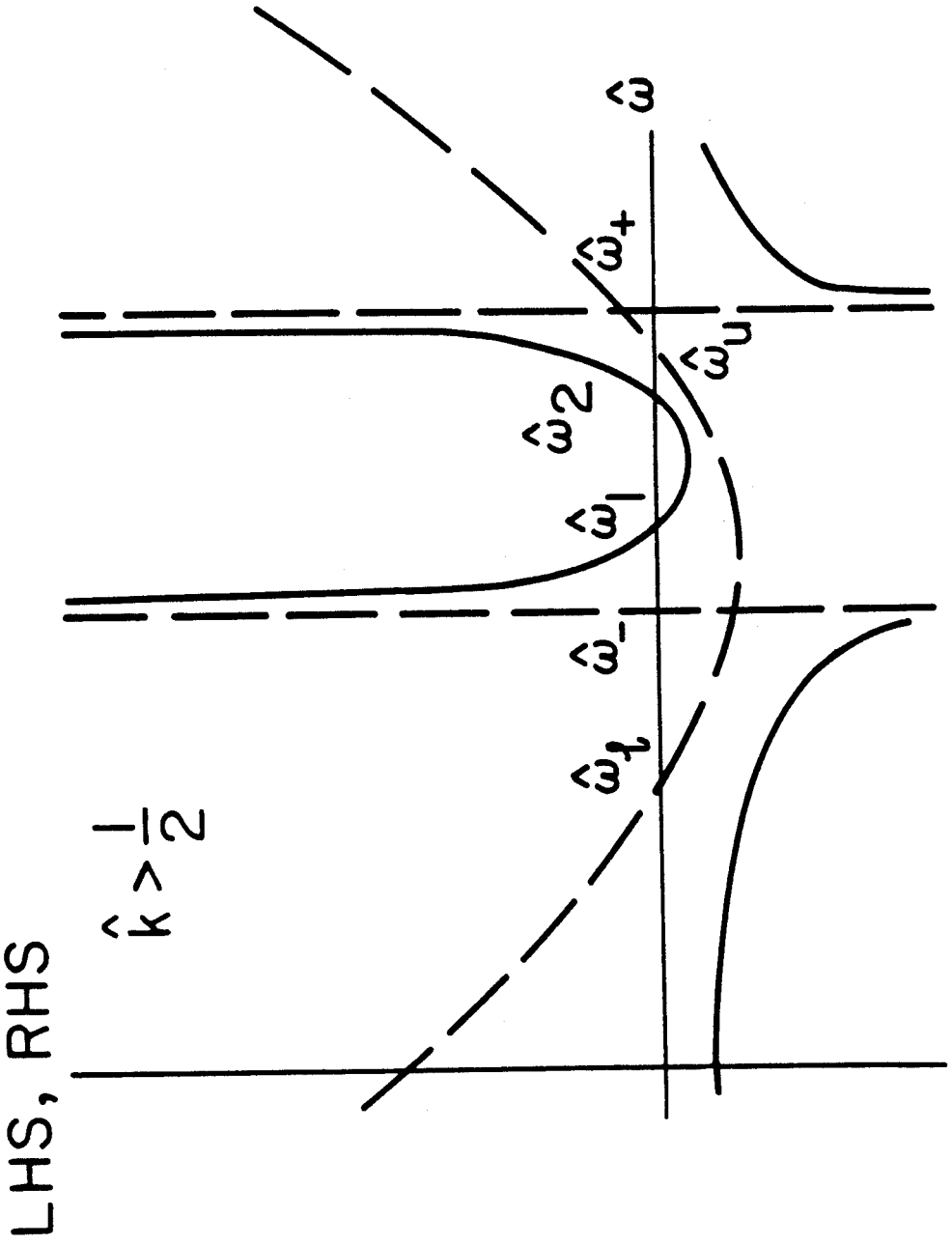
LHS, RHS
$\langle k \rangle \frac{1}{2}$
$\hat{\omega}$
$\hat{\omega}_+$
$\hat{\omega}_u$
$\hat{\omega}_2$
$\hat{\omega}_1$
$\hat{\omega}_-$
$\hat{\omega}_l$

Fig. 4(b)

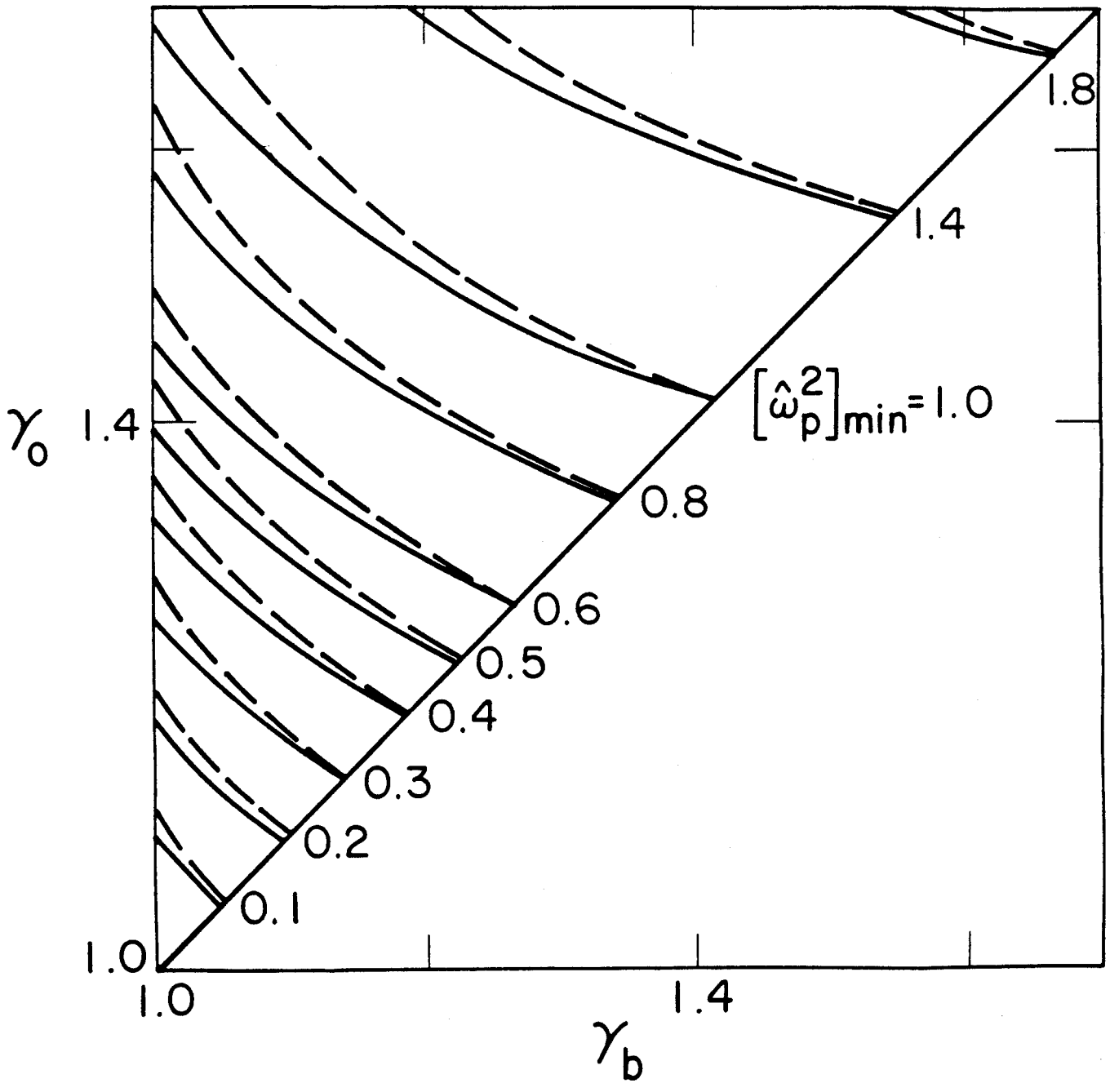
1.8
1.4
$[\hat{\omega}_p^2]_{min}=1.0$
0.8
0.6
0.5
0.4
0.3
0.2
0.1
γ_0
1.4
1.0
1.0
1.4
γ_b

Fig. 5

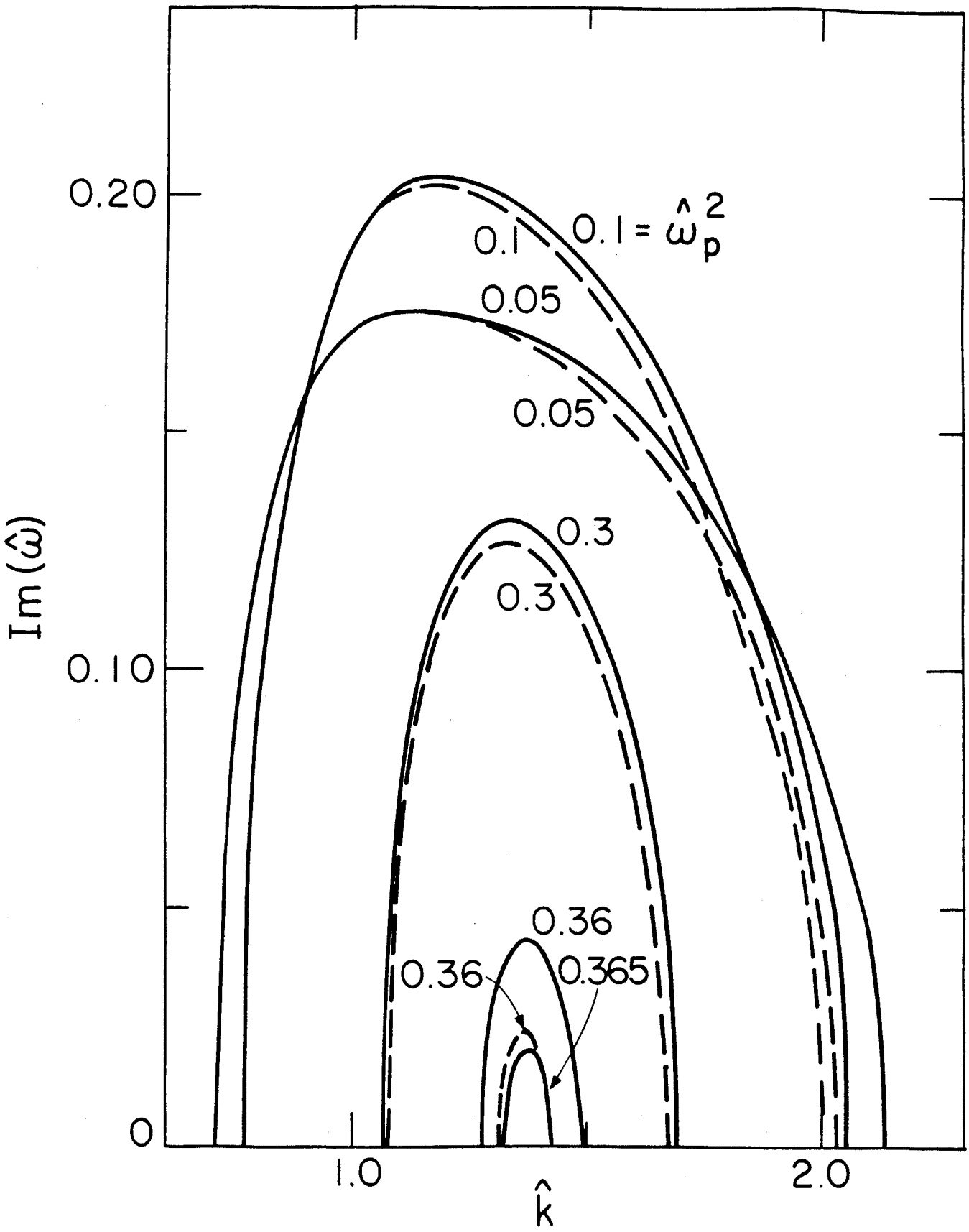

Fig. 6

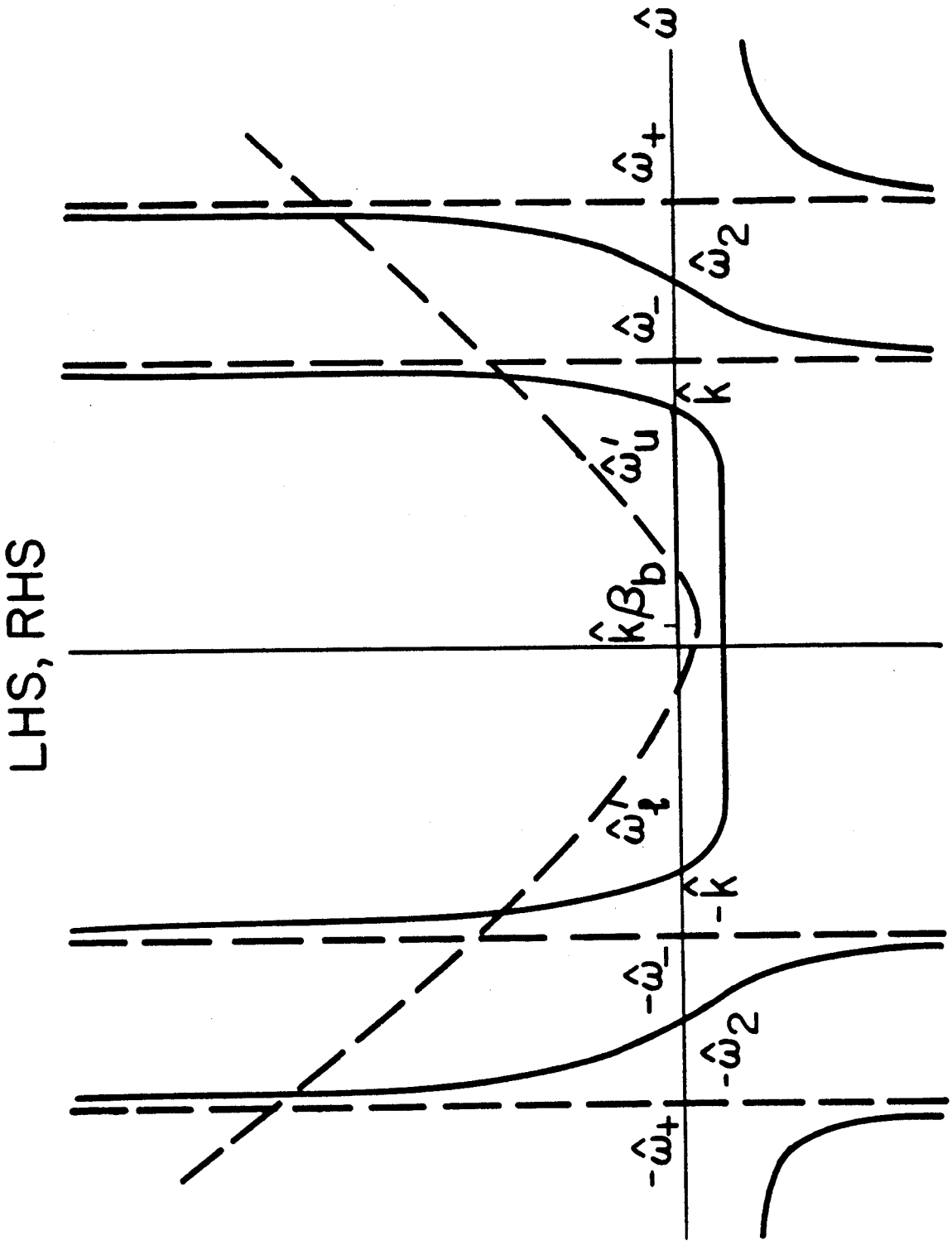
LHS, RHS
$\hat{\omega}$
$\hat{\omega}_+$
$\hat{\omega}_2$
$\hat{\omega}_-$
k
$\hat{\omega}'_u$
$\hat{k}\beta_b$
$\hat{\omega}'_\ell$
$-k$
$-\hat{\omega}_-$
$-\hat{\omega}_2$
$-\hat{\omega}_+$

Fig. 7(a)

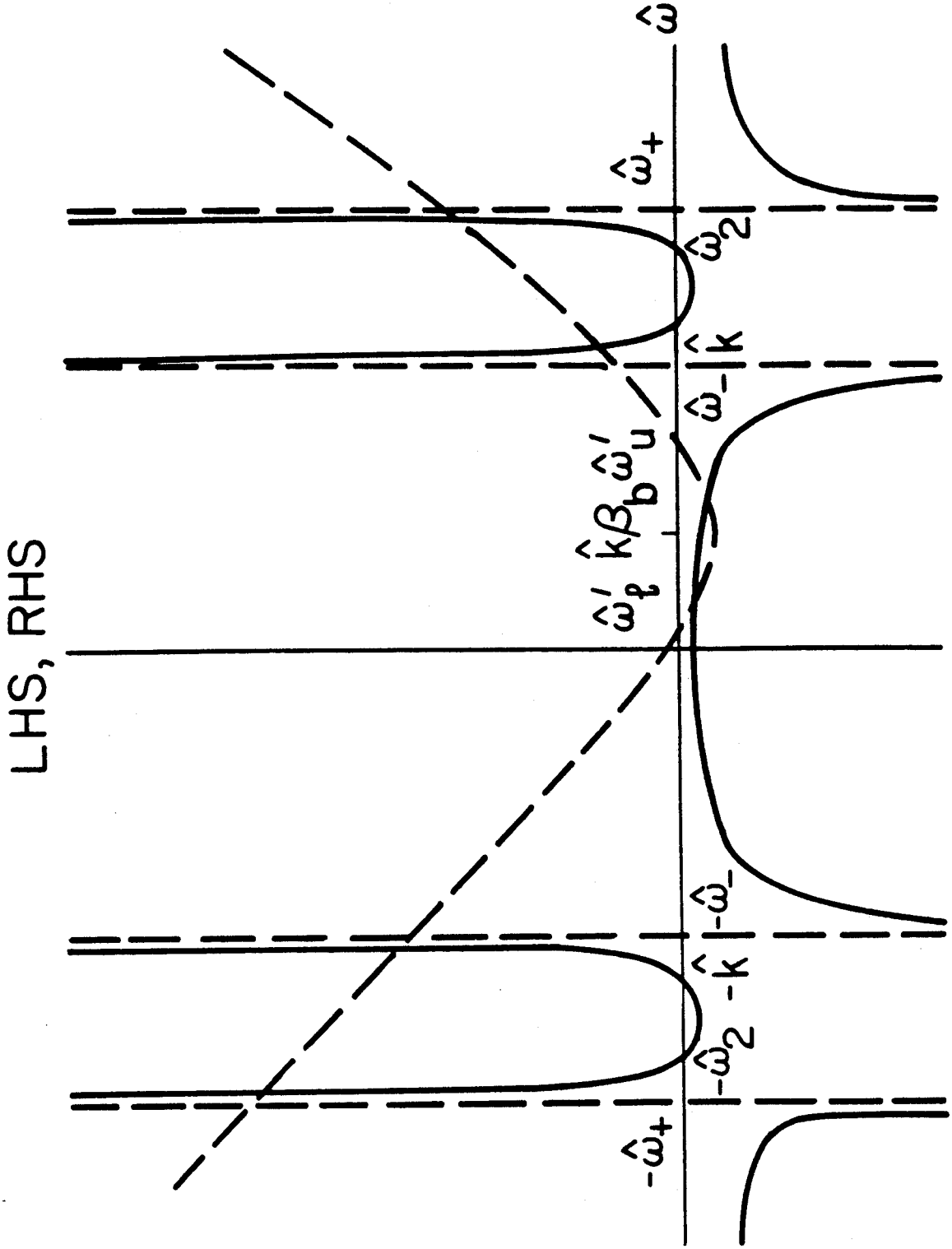
LHS, RHS
$\hat{\omega}$
$\hat{\omega}_+$
$\hat{\omega}_2$
$\hat{k}$
$\hat{\omega}_-$
$\hat{\omega}'_t$ $\hat{k}\beta_b\hat{\omega}'_u$
$-\hat{\omega}_-$
$-\hat{k}$
$-\hat{\omega}_2$
$-\hat{\omega}_+$

Fig. 7(b)

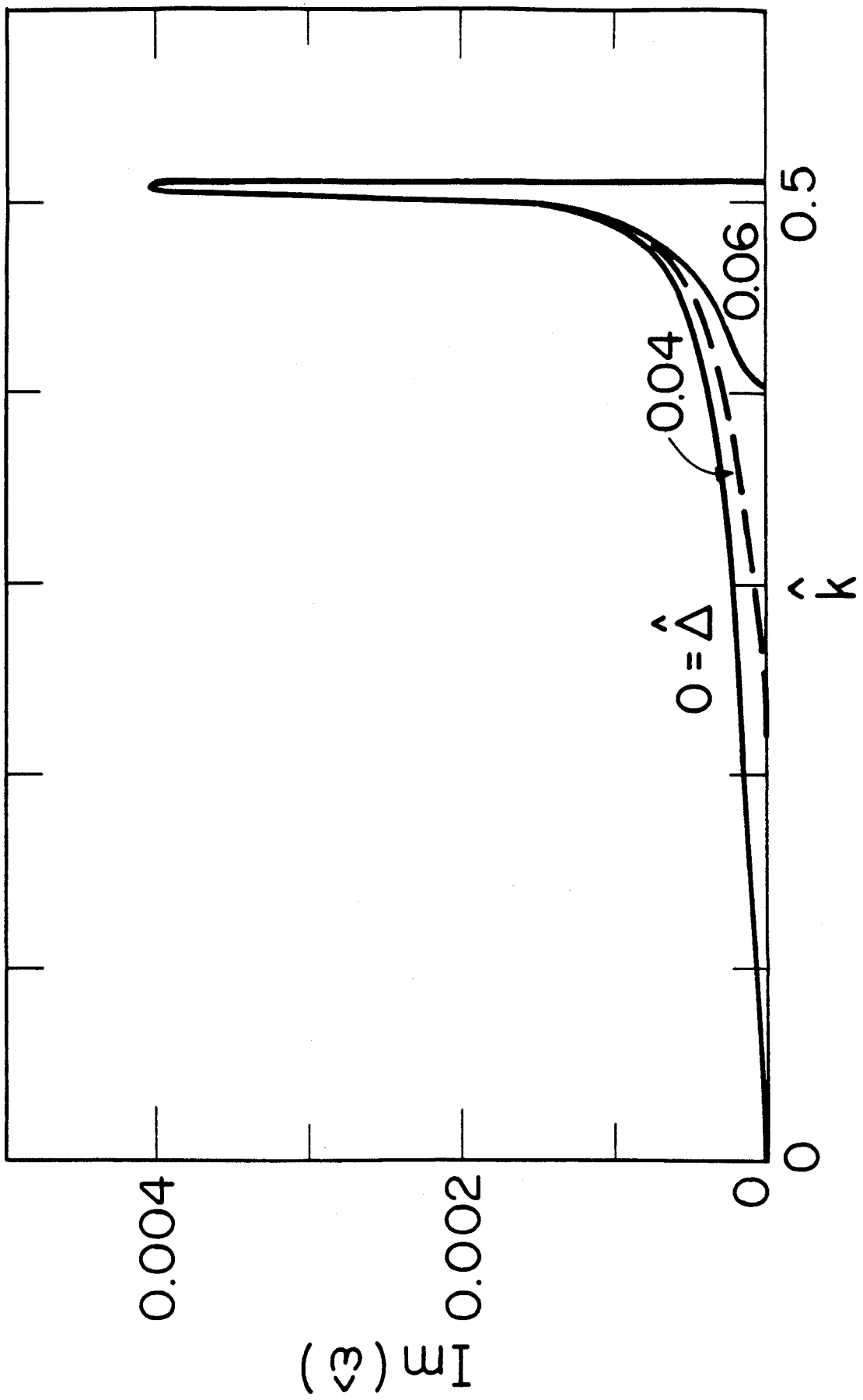

Fig. 8

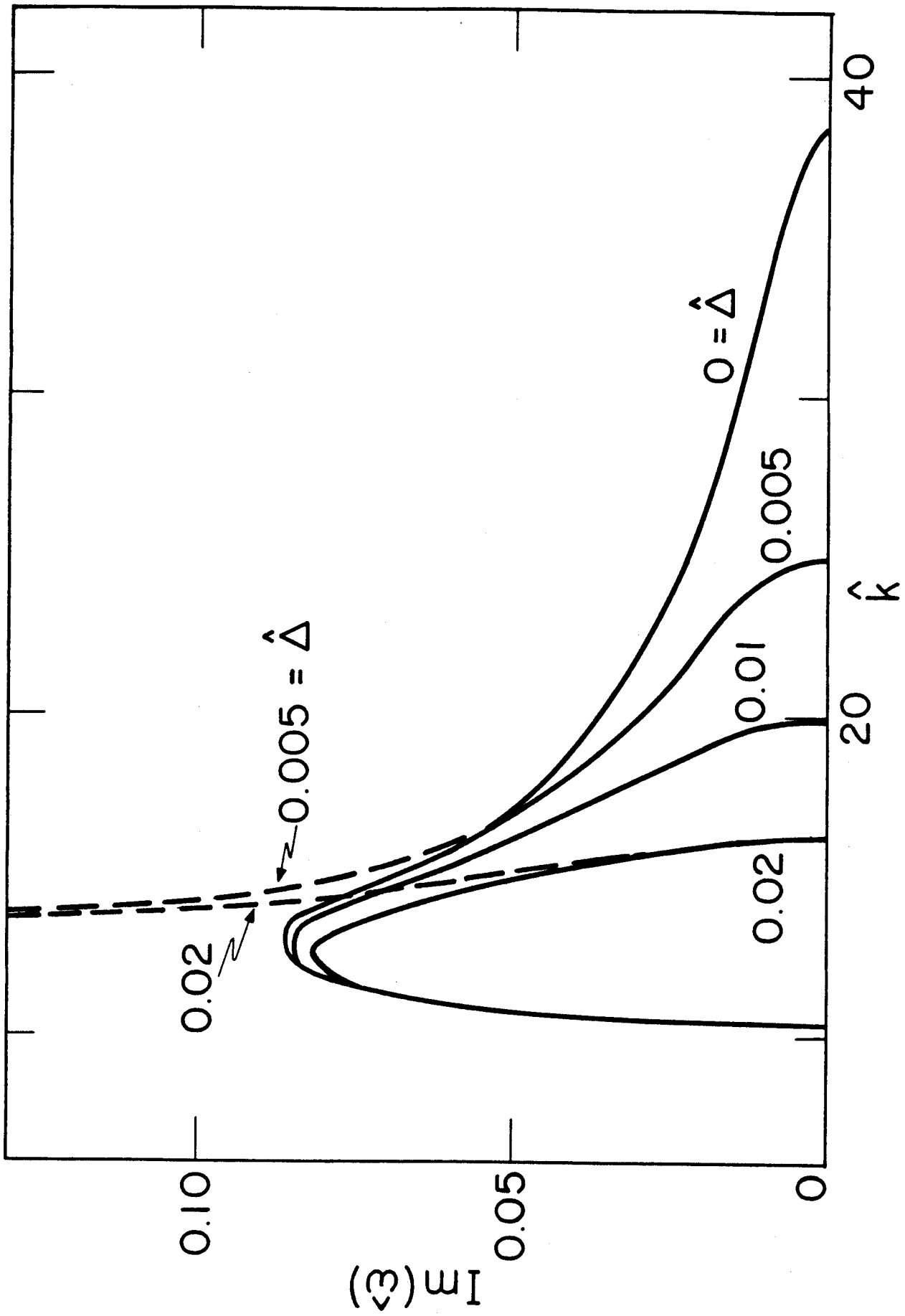

Fig. 9

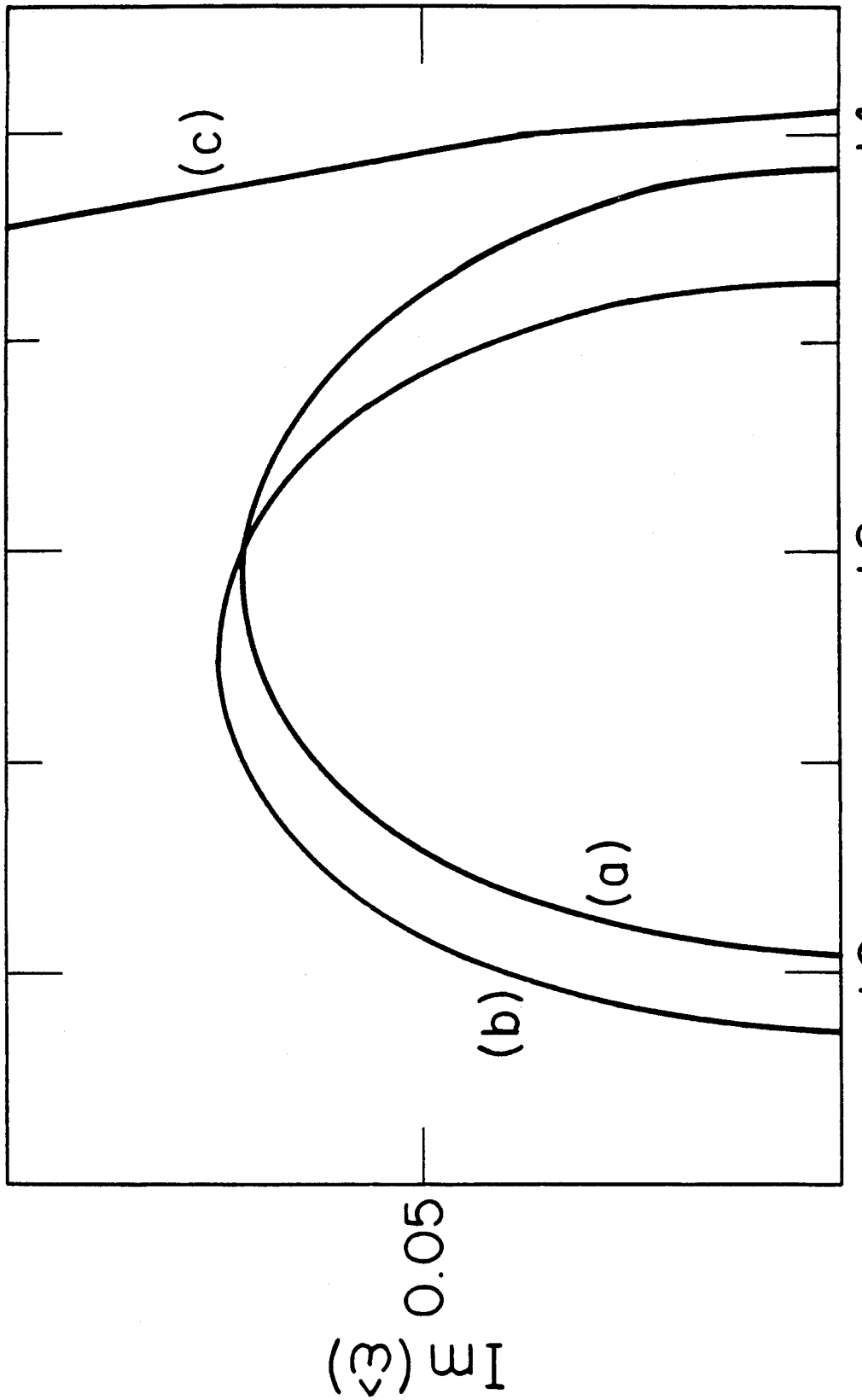

Fig. 10

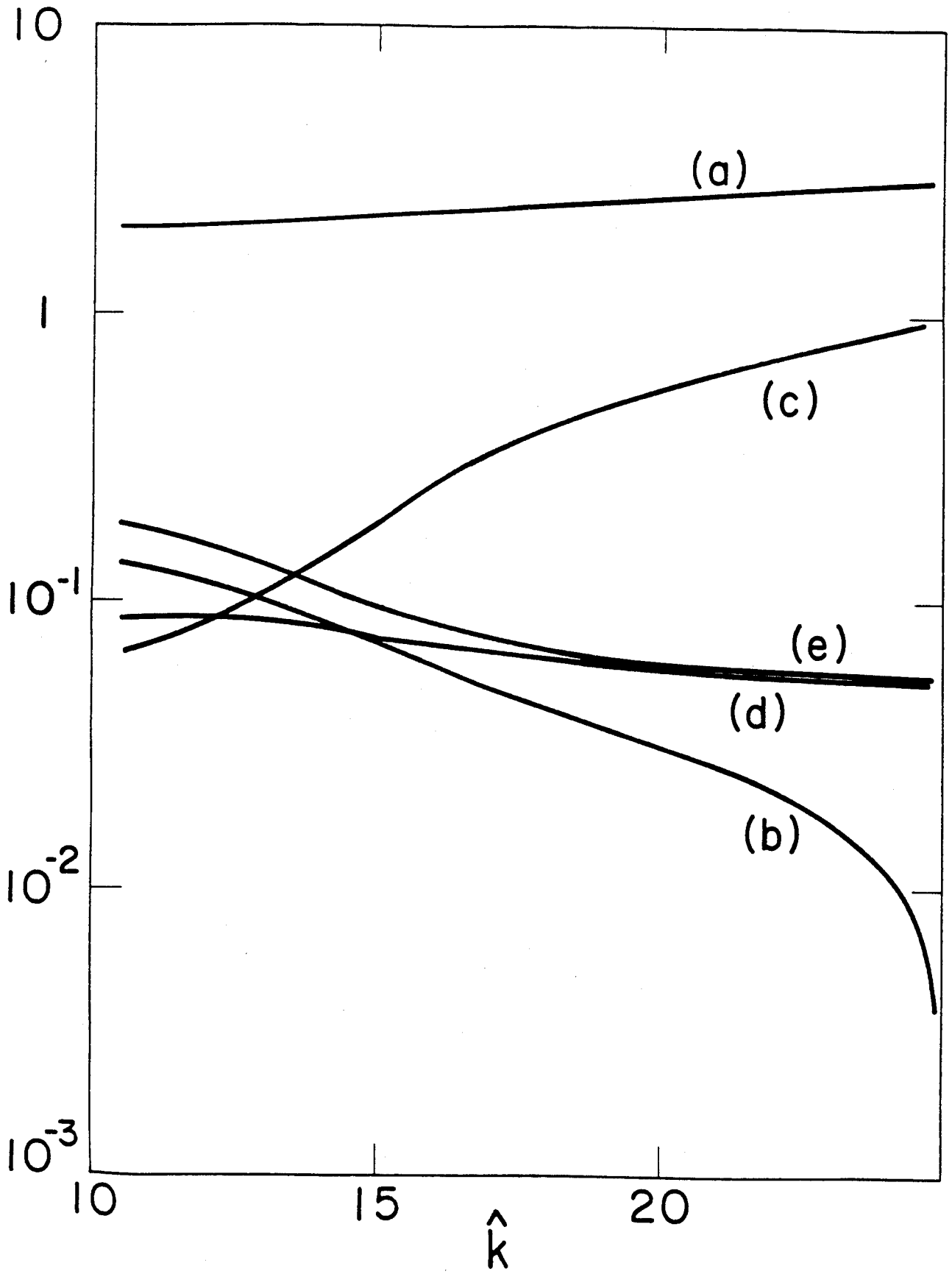

Fig. 11

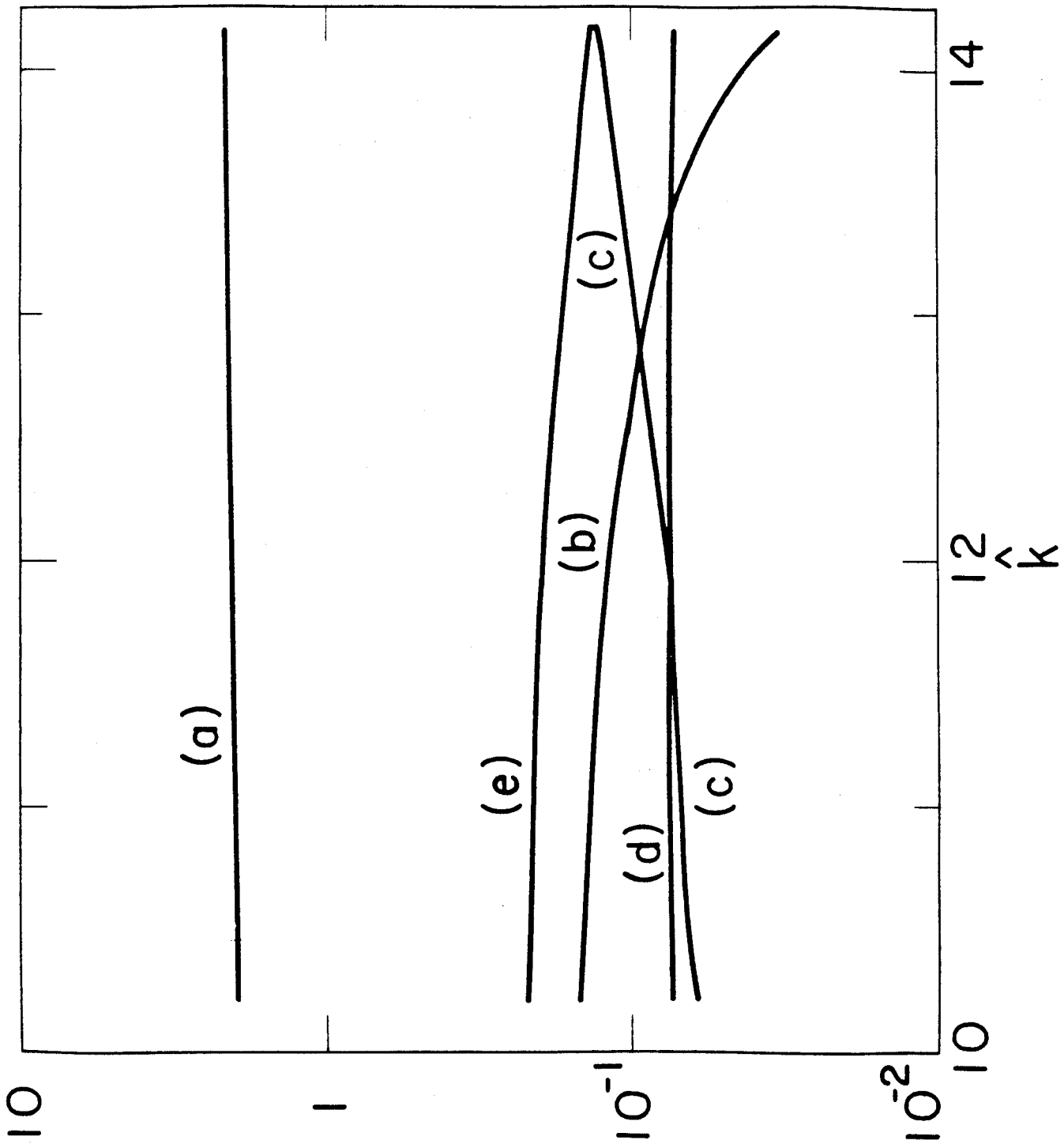

Fig. 12

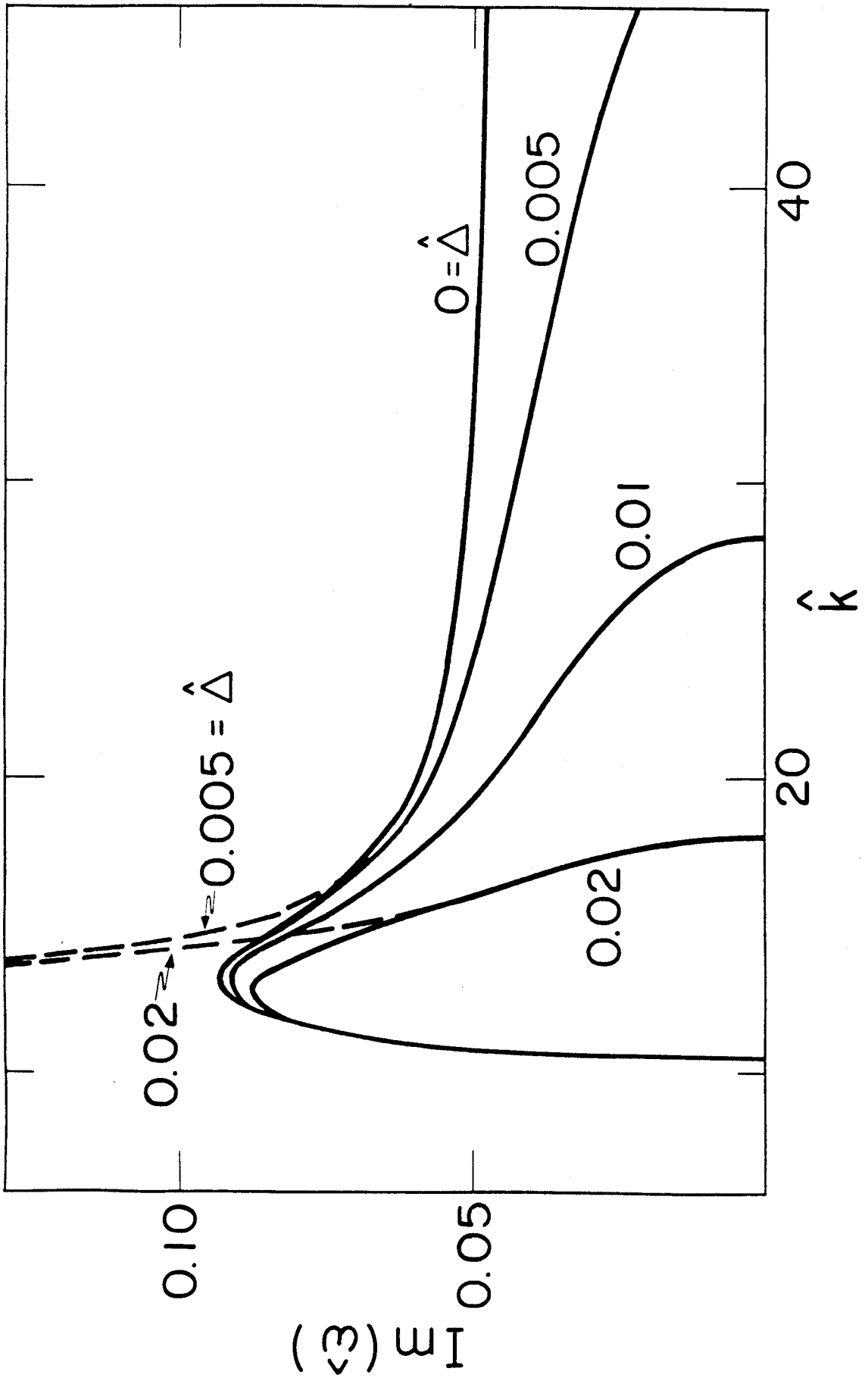

Fig. 13

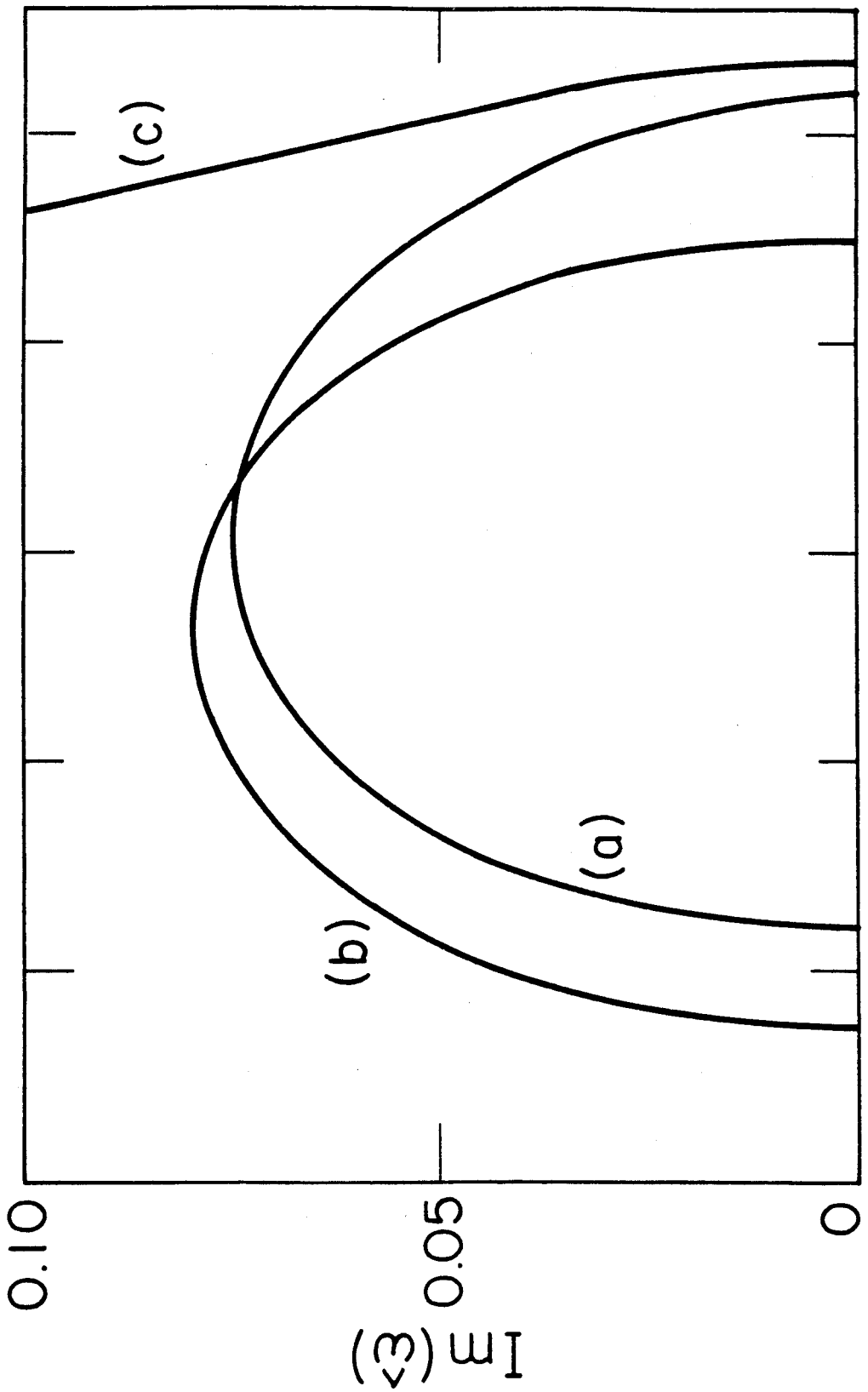

Fig. 14

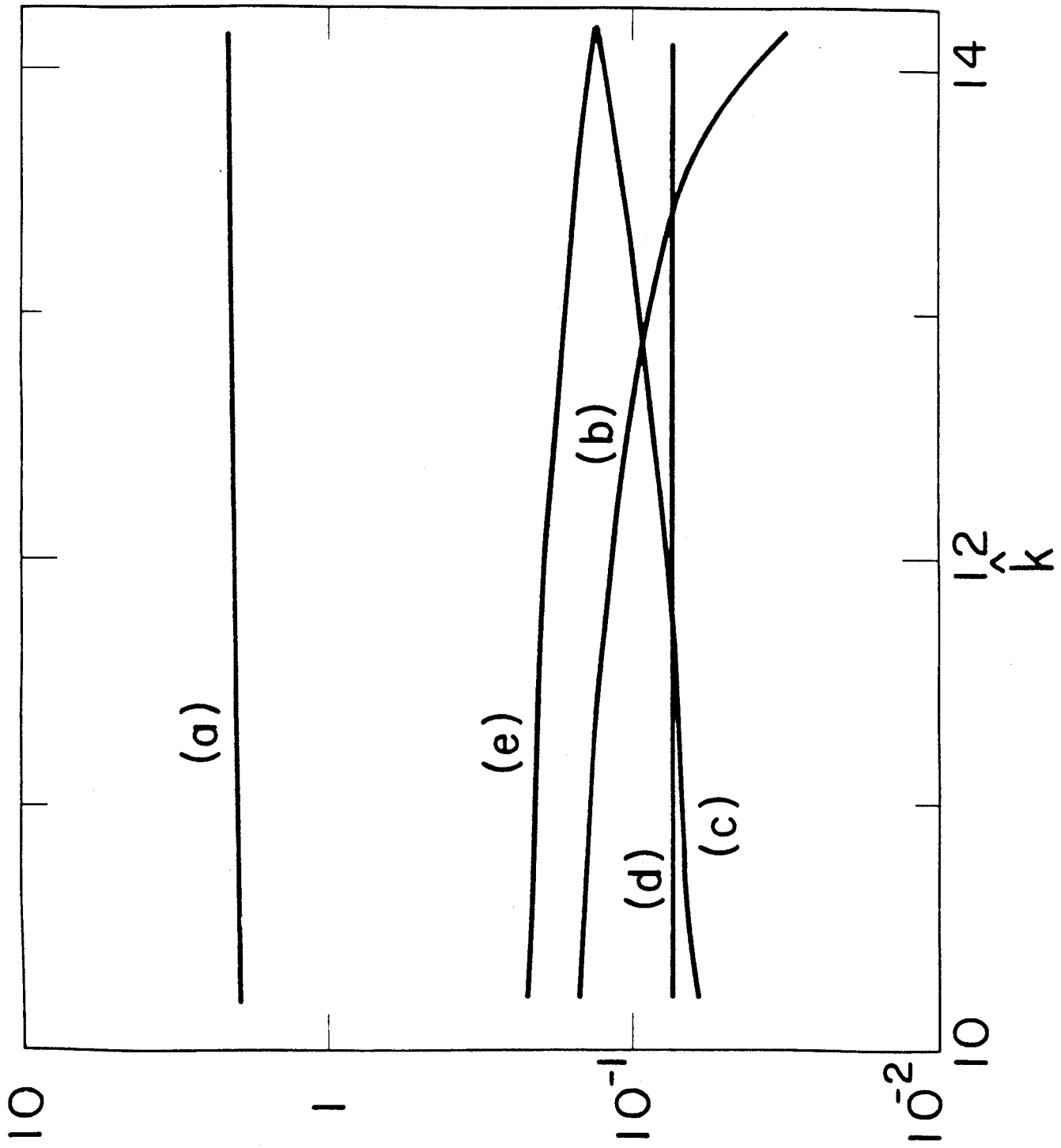

Fig. 15

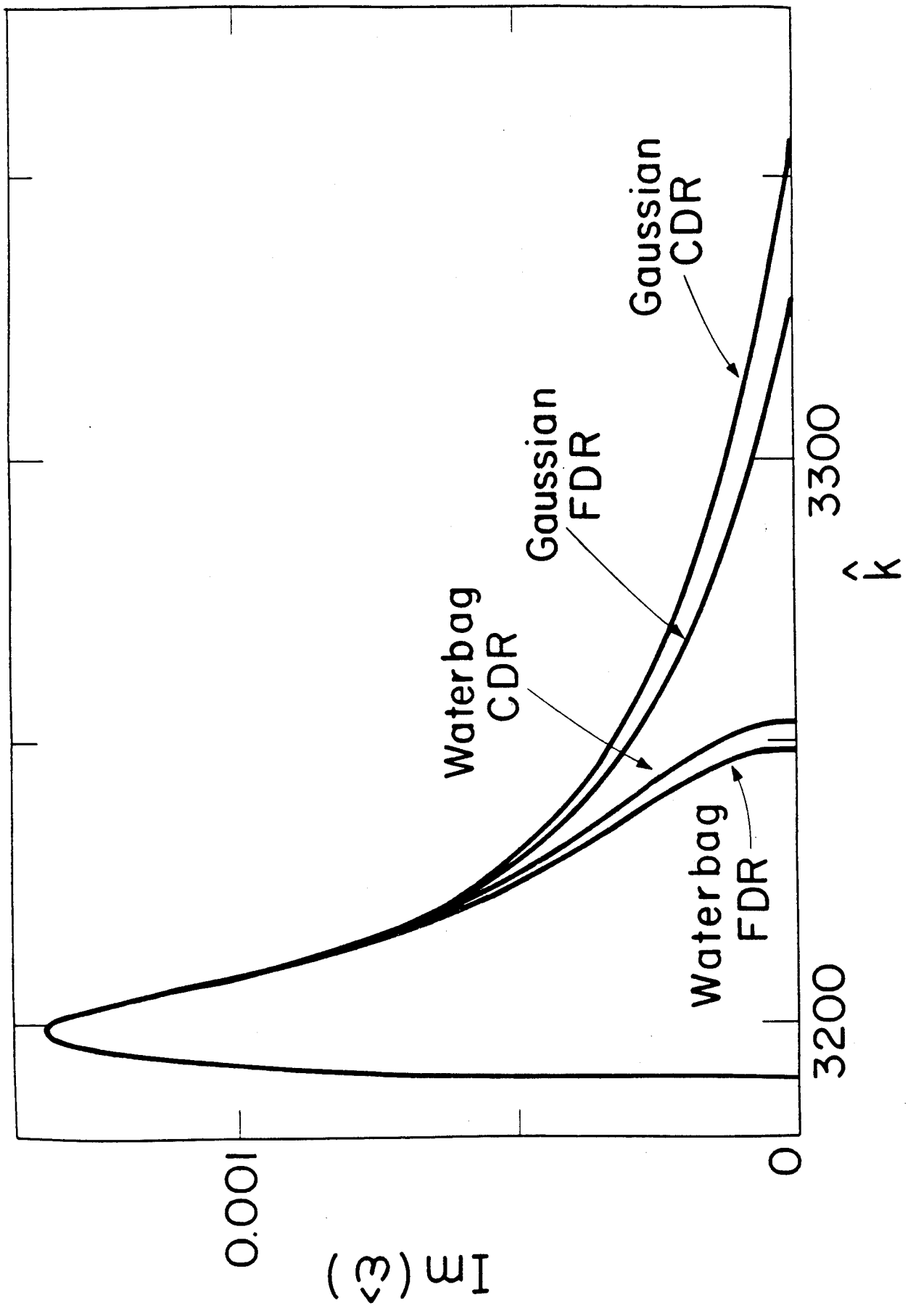
Im(ε)
0.001
0
3200
3300
k̂
Waterbag FDR
Waterbag CDR
Gaussian FDR
Gaussian CDR

Fig. 16

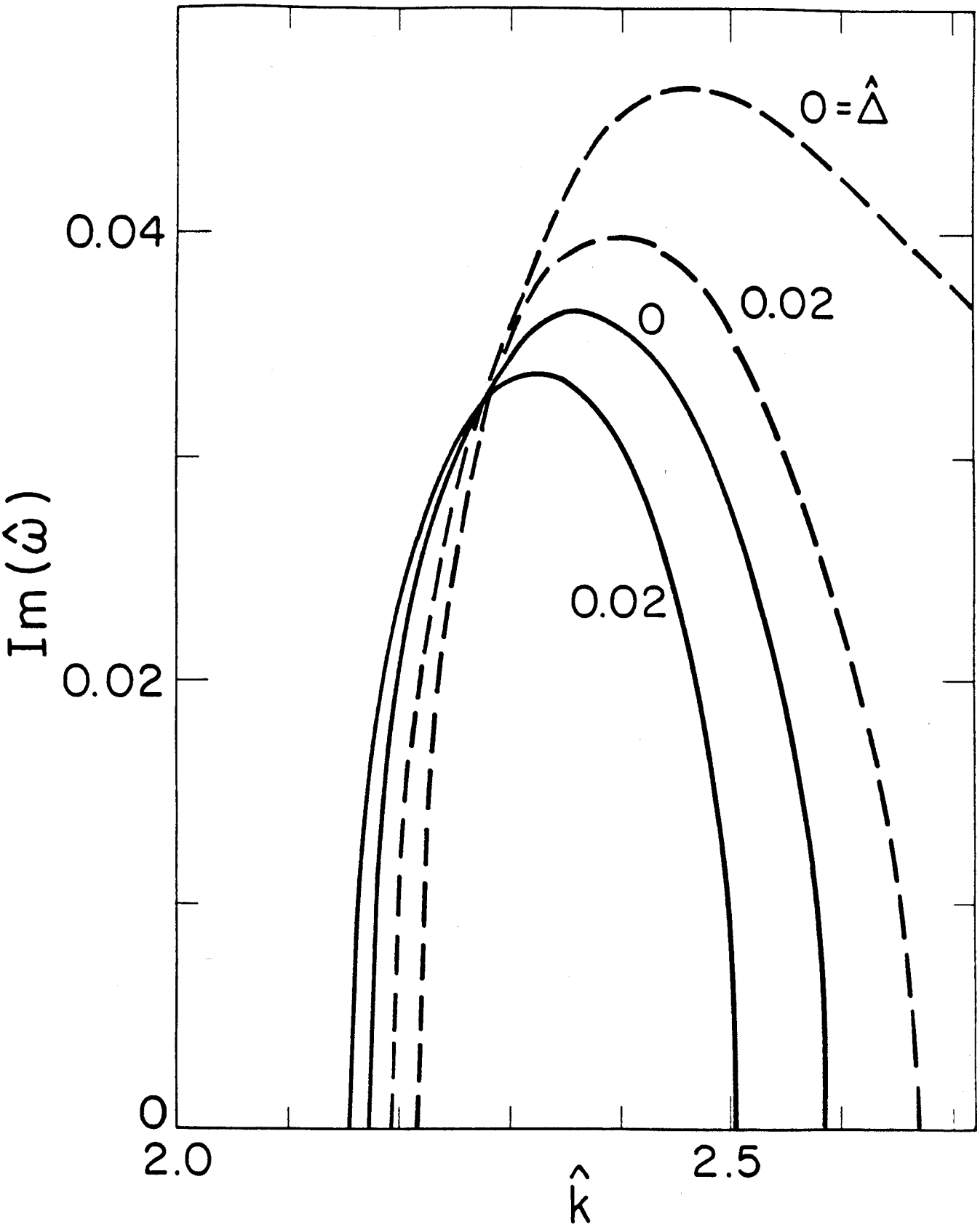

Fig. 17

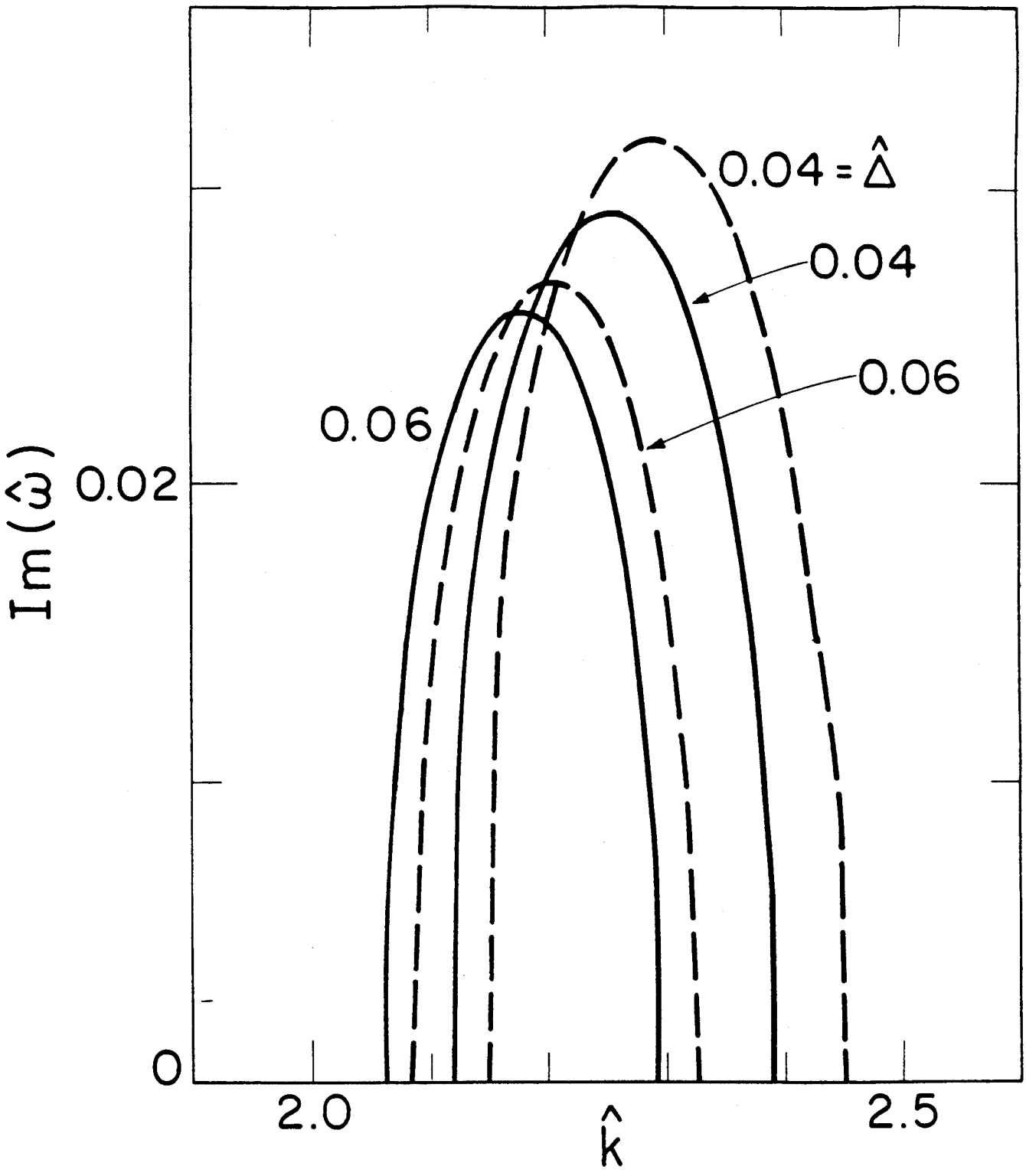

Fig. 18

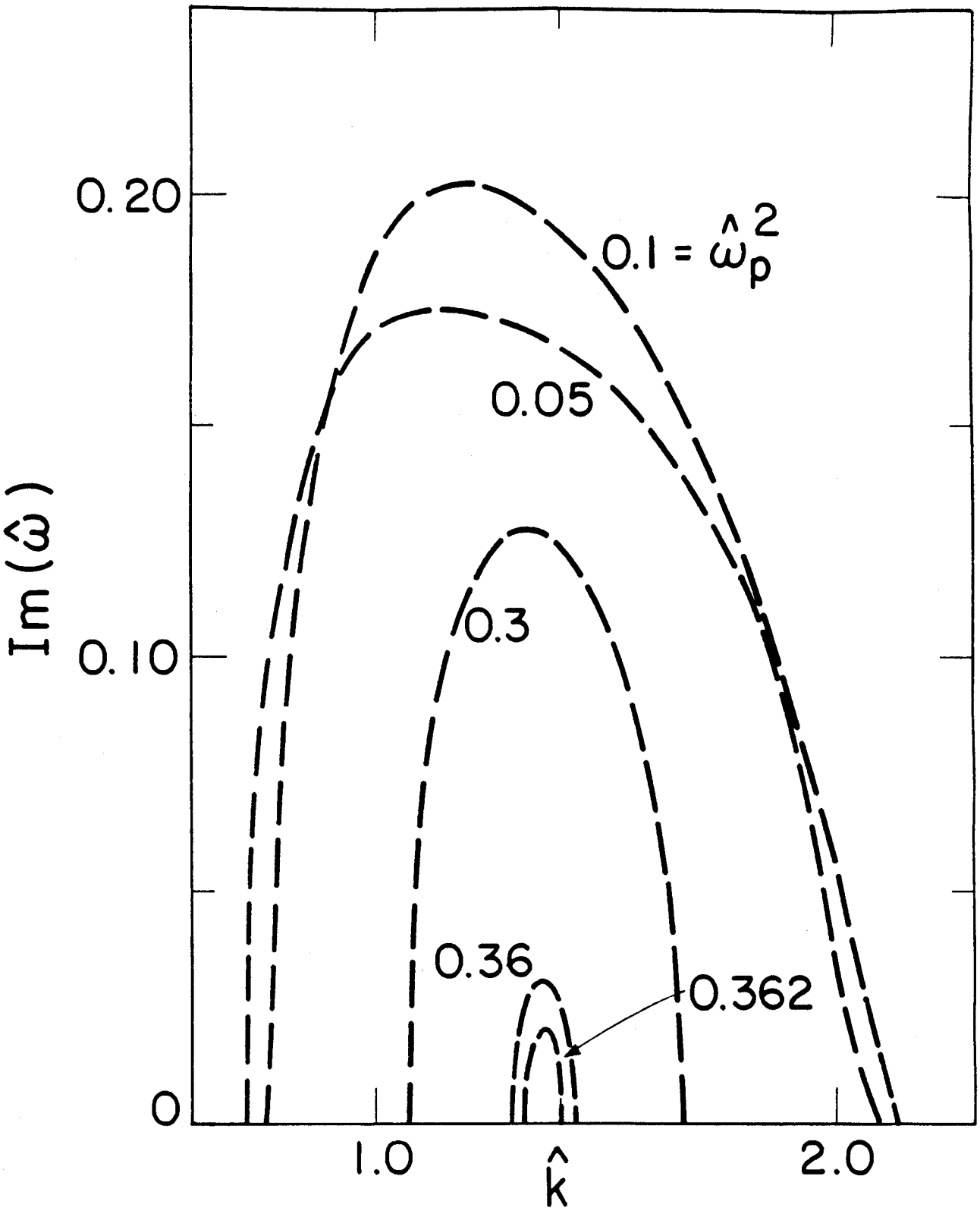

Fig. 19

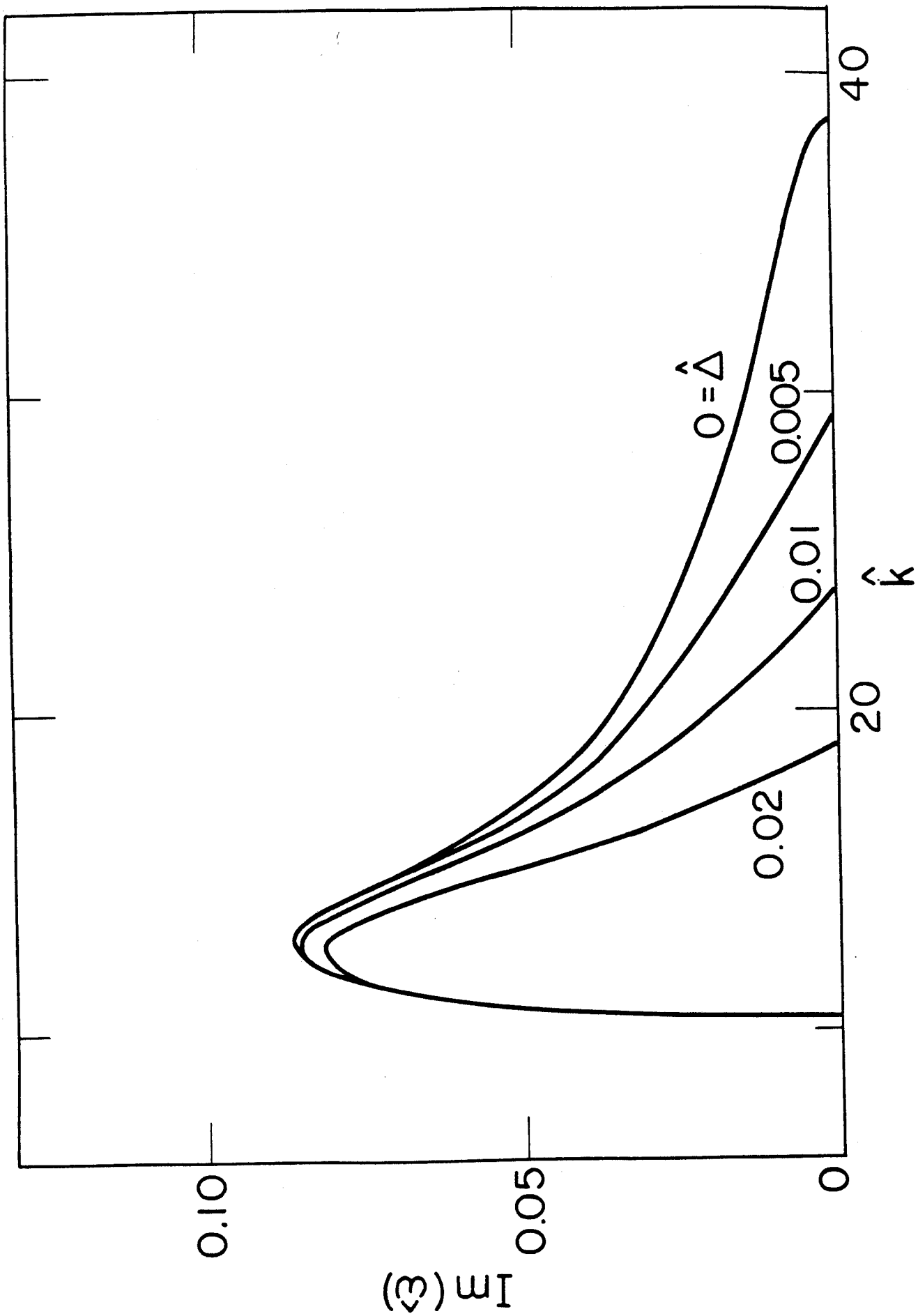

Fig. 20

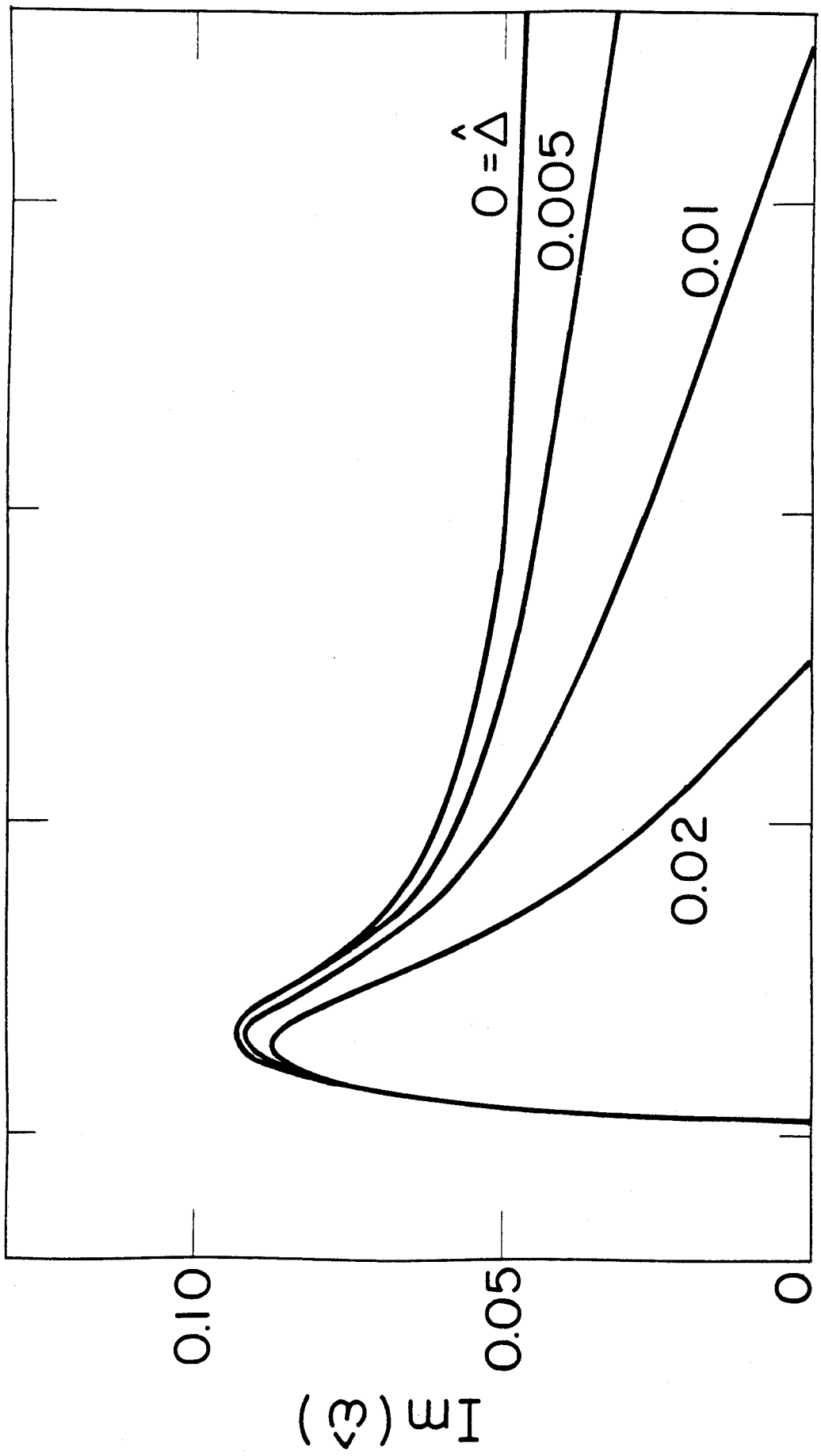

Fig. 21

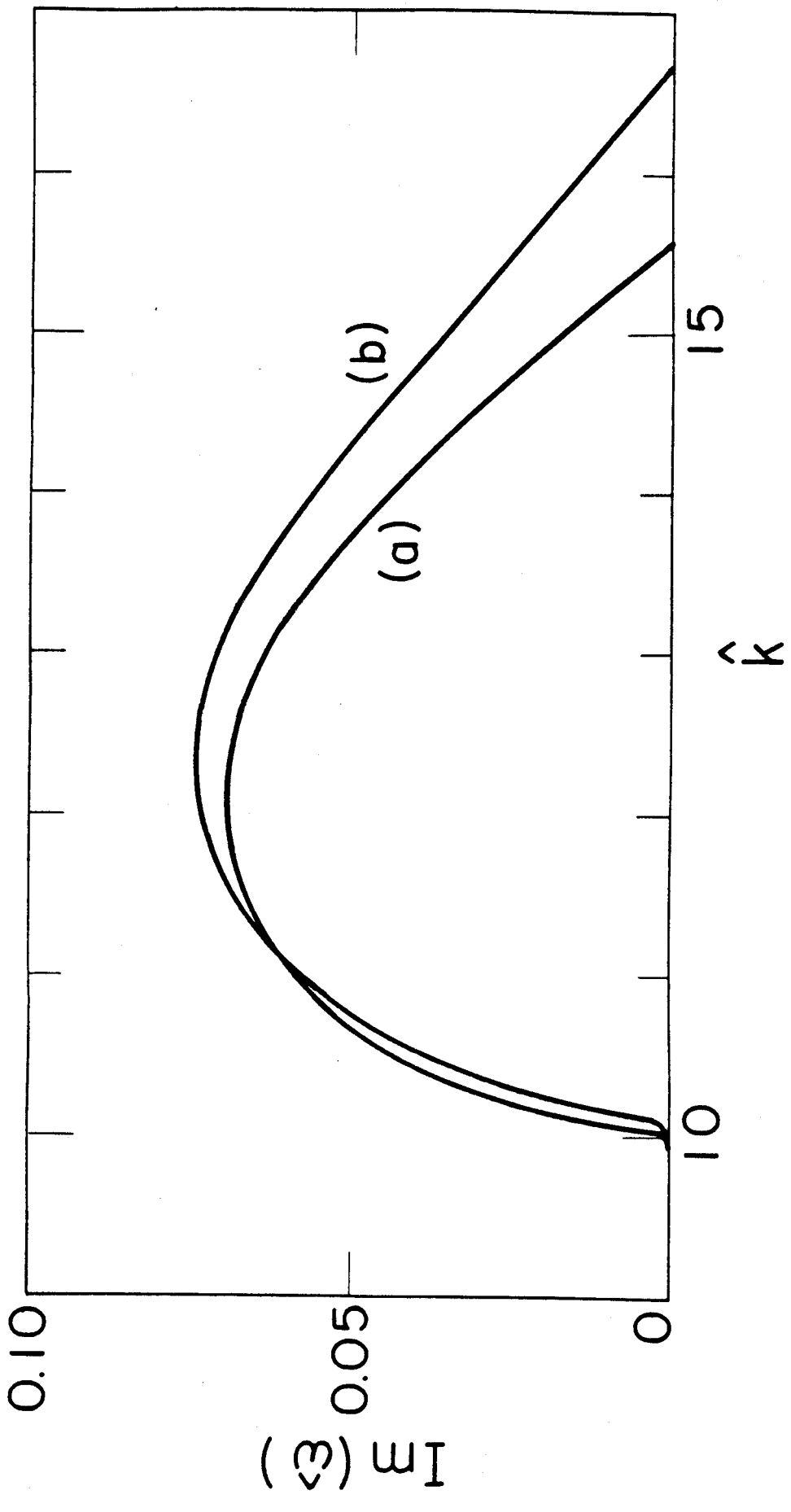

Fig. 22

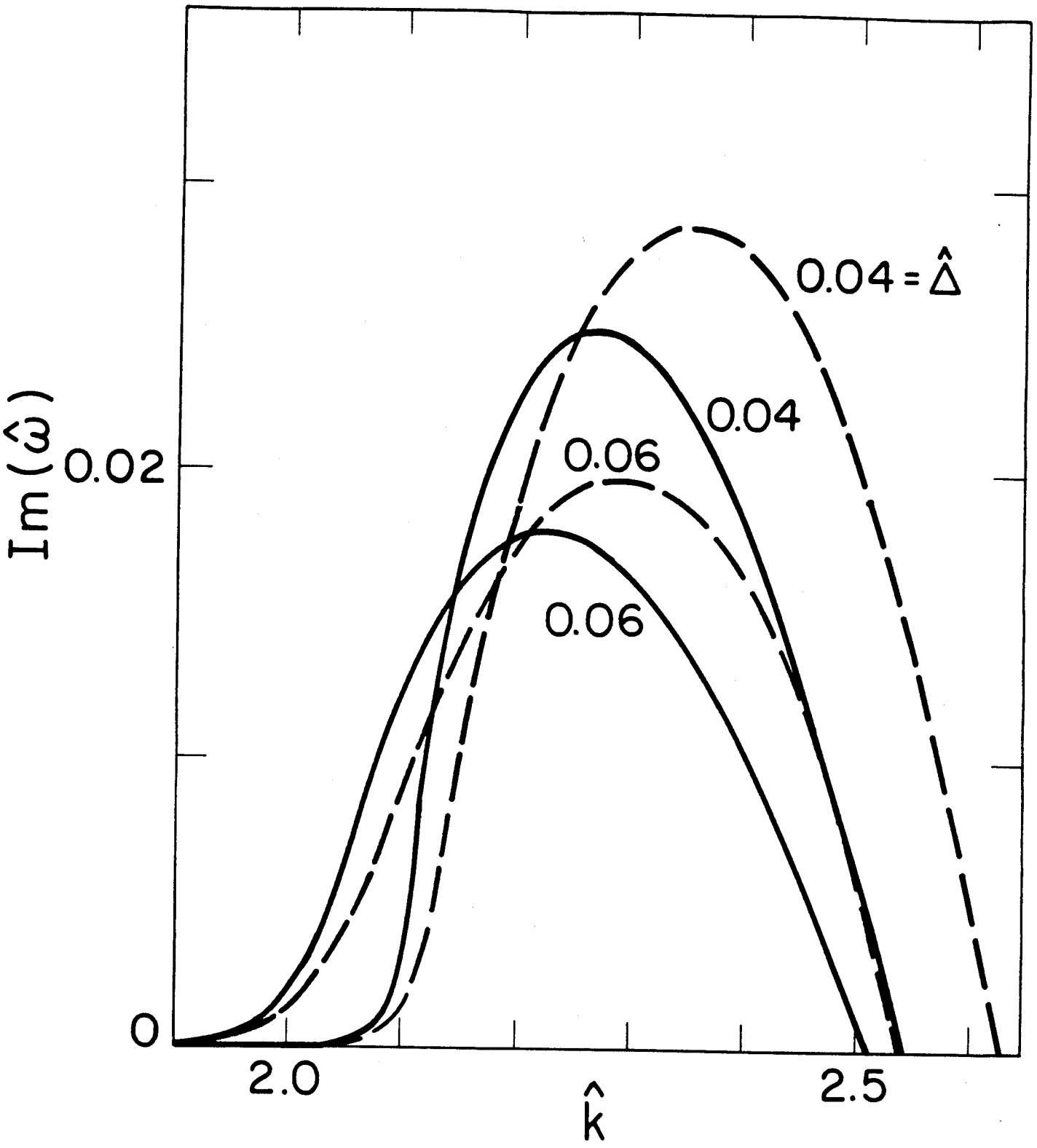

Fig. 23